Accepted Manuscript

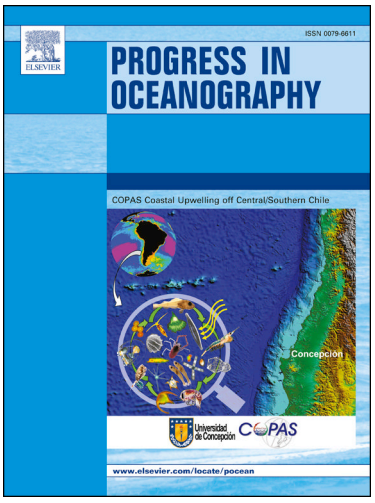

Patterns and drivers of phytoplankton phenology off SW Iberia: a phenoregion based perspective

Lilian Anne Krug, Trevor Platt, Shubha Sathyendranath, Ana B. Barbosa

PII: S0079-6611(18)30082-X
DOI: https://doi.org/10.1016/j.pocean.2018.06.010
Reference: PROOCE 1977

To appear in: *Progress in Oceanography*

Received Date: 31 March 2018
Accepted Date: 25 June 2018

Please cite this article as: Anne Krug, L., Platt, T., Sathyendranath, S., Barbosa, A.B., Patterns and drivers of phytoplankton phenology off SW Iberia: a phenoregion based perspective, *Progress in Oceanography* (2018), doi: https://doi.org/10.1016/j.pocean.2018.06.010

Patterns and drivers of phytoplankton phenology off SW Iberia: a phenoregion based perspective

Lilian Anne Krug[a *], Trevor Platt [b], Shubha Sathyendranath[c], Ana B. Barbosa[a]

[a]University of the Algarve/ Centre for Marine and Environmental Research (CIMA), Campus de Gambelas, 8005-139 Faro, Portugal.

[b]Plymouth Marine Laboratory. Prospect Place, The Hoe, PL1 3DH, Plymouth, Devon, United Kingdom.

[c]National Centre for Earth Observation, Plymouth Marine Laboratory, Prospect Place, The Hoe, PL1 3DH, Plymouth, Devon, United Kingdom

lakrug@ualg.pt, tplatt@dal.ca, ssat@pml.ac.uk, abarbosa@ualg.pt

*Corresponding author. University of the Algarve, Centre for Marine and Environmental Research (CIMA). Campus de Gambelas, 8005-139, Faro, Portugal. Tel: +351 289 800 900 (ext 7372), E-mail address: lakrug@ualg.pt.

Abstract

Phytoplankton patterns, tightly linked to the dynamics of the ocean surface layer and its atmospheric forcing, have major impacts on ecosystem functioning and are valuable indicators of its response to environmental variability and change. Phytoplankton phenology and its underlying drivers are spatially variable, and the study of its patterns, particularly over heterogeneous regions, benefits from a delineation of regions with specific phenological properties, or phenoregions. The area Southwest off the Iberian Peninsula (SWIP, NE Atlantic) integrates a highly complex set of coastal and ocean domains that collectively challenge the understanding of regional phytoplankton phenology and related forcing mechanisms. This study aims to evaluate phytoplankton phenology patterns over the SWIP area, during an 18-year period (September 1997 - August 2015), using an objective, unsupervised partition strategy (Hierarchical Agglomerative Clustering – HAC) based on phenological indices derived from satellite ocean colour data. The partition is then used to describe region-specific phytoplankton phenological patterns related to bloom magnitude, frequency, duration and timing. Region-specific variability patterns in phenological indices and their linkages with environmental determinants, including local ocean physical-chemical variables, hydrodynamic variables and large scale climate indices, were explored using Generalized Additive Models (GAM). HAC analyses identified five coherent phenoregions over SWIP, with distinctive phytoplankton phenological properties: two open ocean and three coastal regions. Over the open ocean, a single, low magnitude and long bloom event per year, was regularly observed. Coastal phenoregions exhibited up to six short bloom events per year, and higher intra-annual and variability. GAM models explained 50 to 90% of the variance of all phenological indices except bloom initiation timing, and revealed that interannual patterns in phytoplankton phenology and their environmental drivers varied markedly among the five phenoregions. Over the oceanic phenoregions, large-scale climate indices (Eastern Atlantic Pattern, Atlantic Meridional Oscillation), mixed layer depth (MLD) and nitrate concentration preceding primary bloom events were influential predictors, reflecting the relevance of nutrient limitation. For the Coastal-Slope, a relatively more light-limited phenoregion, North Atlantic Oscillation and wind speed were more relevant, and bloom magnitude was also positively influenced by riverine discharge. This variable was a significant predictor of bloom frequency, magnitude and duration over the Riverine-influenced region. Over the Upwelling-influenced region, upwelling intensity and mean annual MLD showed stronger partial effects on phytoplankton phenology. Overall, our phenology-based unsupervised approach produced a biologically-relevant SWIP partition, providing an evaluation of the complexity of interactions between phytoplankton and multiple environmental forcing, particularly over coastal areas.

Keywords: phytoplankton phenology; phytoplankton blooms; phytoplankton drivers; partitioning; Ocean Colour.

1 - Introduction

Phytoplankton are the dominant primary producers of marine ecosystems, responsible for about 50% of global primary production (Field et al., 1998), and a key component of the biological carbon pump (Gregg et al., 2003; Cermeño et al., 2008). Phytoplankton growth is mostly controlled by light and nutrient availability and, therefore, tightly linked to the dynamics of the ocean surface mixed layer (Longhurst, 2007; Cloern and Dufford, 2005) and regulated by atmospheric forcing and large scale climate variability patterns (Martinez et al., 2009, 2011, 2016; Boyce et al., 2010; Racault et al., 2012, 2017; Zhai et al., 2013). Over coastal zones, terrestrial nutrient inputs and topographic irregularities increase the complexity of phytoplankton patterns and driving forces (Carstensen et al., 2015; Cloern et al., 2016). Together with top-down controls, these environmental determinants modulate phytoplankton phenology, i.e., their periodically-recurring variability patterns, including the timing and intensity of phytoplankton blooms, short-term events that can represent a substantial fraction of the annual primary production in marine ecosystems (Behrenfeld, 2014; Sallée et al., 2015; Martinez et al., 2016). Phytoplankton phenology patterns, and alterations therein, have large impacts on ecosystem functioning (see review by Ji et al. 2010), affecting the efficiency of carbon transfer to higher trophic levels (Edwards and Richardson, 2004; Barth et al., 2007; Friedland et al., 2016), the recruitment success of economically important fish and invertebrate resources (Platt et al., 2003; Fuentes-Yaco et al., 2007; Koeller et al., 2009; Malick et al., 2015), benthic-pelagic coupling (Nixon et al., 2009), the carbon export efficiency and the depth of remineralization (Lutz et al., 2007). Through such mechanisms, phytoplankton provide a critical connection between environmental changes and ecosystem dynamics and productivity.

Phytoplankton phenology has been the subject of intense research in the last decade, mostly stimulated by the availability of satellite-retrieved surface chlorophyll-a concentration (Chl-a)

and the anticipated climate-induced changes in marine ecosystems (e.g., Platt and Sathyendranath, 2008; Platt et al., 2010; Racault et al., 2012, 2014a; Friedland et al., 2018; Henson et al., 2018). As an integrative environmental science (Schwartz, 2003), phenological studies have evaluated phytoplankton periodic events as well as their interactions with environmental conditions and climatic forcing (e.g., Henson et al., 2006, 2018; Demarcq et al., 2012; Racault et al., 2012; Sapiano et al., 2012; Cabré et al., 2016; Kostadinov et al., 2017). Phytoplankton phenology has usually been synthesized into a set of ecologically relevant indices: the timing, duration and magnitude of bloom events (Platt and Sathyendranath, 2008; Platt et al., 2009, 2010; Racault et al., 2014a). These indices are currently considered key indicators of ecosystem functioning and its response to climate variability and change, at multiple scales (see Platt and Sathyendranath, 2008; Winder and Cloern, 2010; Racault et al., 2014a; Scheffers et al., 2016).

Global (Demarcq et al., 2012; D'Ortenzio et al., 2012; Racault et al., 2012, 2017; Sapiano et al., 2012; Friedland et al., 2018) and regional phenological studies, based on satellite-remote sensing and *in situ* sampling, have reported significant interannual changes in phytoplankton phenology for a wide diversity of marine ecosystems including epipelagic, neritic (e.g., North Atlantic - Harrison et al., 2013; Henson et al., 2010; Land et al., 2014; Martinez et al., 2011; González Taboada and Anadón, 2014; Mediterranean - Lavigne et al., 2013; North Sea - Edwards and Richardson, 2004; North Pacific – Yoo et al., 2008; California Current – Foukal and Thomas, 2014; Arctic and Southern Ocean – Kahru et al., 2010; Ardyna et al., 2014; Soppa et al., 2016; Oziel et al., 2017) and confined or estuarine ecosystems (Wiltshire et al., 2008; Nixon et al., 2009; Kromkamp and van Engeland, 2010; Groetsch et al., 2016; Kahru et al., 2015). However, most interannual changes in phytoplankton phenology and their underlying drivers are spatially variable, even over particular ocean basins (e.g., Yoo et al., 2008; Henson et al., 2010; Kahru et al., 2010; Martinez et al., 2011; Sasaoka et al., 2011; Friedland et al., 2016, 2018) or domains (e.g., Song et al., 2010; Lavigne et al., 2013; Zhao et al., 2013; Foukal and

Thomas, 2014), depending on region-specific properties and factors controlling the initiation, collapse and magnitude of phytoplankton blooms. These results indicate that a proper geographic partitioning of marine ecosystems should be implemented for the investigation of phytoplankton phenology (e.g., Zhao et al., 2013).

Due to their ecological relevance, the shape of phytoplankton climatological seasonal cycles, extracted from Chl-a time series, has been used for objectively partitioning the complex spatial organization of ocean surface into biologically meaningful regions (bioregions, trophic regimes or bloom phenology regimes), at global (D'Ortenzio et al., 2012) or regional scales (D'Ortenzio and Ribera d'Alcalà, 2009; Sasaoka et al., 2011; Foukal and Thomas, 2014; Lacour et al., 2015; Mayot et al., 2015; Ardyna et al., 2017; Eliasen et al., 2017; Krug et al., 2017b). In some cases, phytoplankton phenology indices were used directly as input variables for delineating ocean surface "phenological provinces" or (pheno)regions (see Sasaoka et al., 2011; Xu et al., 2013; Land et al., 2014). Ocean partition represents a relevant strategy to simplify ocean complexity and disentangle the interactions between phytoplankton and multiple environmental determinants, particularly relevant for heterogeneous marine domains, providing a framework for assessing marine ecosystem status and trends, as well as its resilience and vulnerability to climate change (see reviews IOCCG, 2009; Krug et al., 2017a).

The southwest area off the Iberian Peninsula (SWIP; NE Atlantic), located at a transition zone between temperate and subtropical waters, constitutes a highly heterogeneous domain, particularly vulnerable to climate change (Kovats et al., 2014). A wide diversity of processes, including local and large scale oceanic and atmospheric circulation patterns, topographic irregularities, coastal upwelling and continental freshwater outflows, impacts phytoplankton spatial and temporal dynamics (e.g., Navarro and Ruiz, 2006; García-Lafuente and Ruiz, 2007; Prieto et al., 2009; Navarro et al., 2012; Bruno et al., 2013; Goela et al., 2013; Caballero et al., 2014; Sala et al., 2018), promoting the occurrence of distinct regions where phytoplankton are

driven, differently, by specific combinations of physical and climatic environmental drivers (see Krug et al., 2017b). Due to its geographical location (eastern boundary of the North Atlantic basin), SWIP and its complex coastal areas are often overlooked (Follows and Dutkiewicz, 2002; Vargas et al., 2009; Racault et al., 2012; Ferreira et al., 2014) or sparsely resolved (e.g., Siegel et al., 2002; Ueyama and Monger, 2005; Henson et al., 2009; Kahru et al., 2010; Martinez et al., 2011; Demarcq et al., 2012; D'Ortenzio et al., 2012; Sapiano et al., 2012; Land et al., 2014; Racault et al., 2014b, 2017; González Taboada and Anadón, 2014; Cole et al., 2015; Cabré et al., 2016; Friedland et al., 2016, 2018; Zhang et al., 2017) in global or basin-scale phenological analysis. The analysis of phytoplankton phenology over SWIP at a finer, regional-scale resolution, however, has been restricted to the central Gulf of Cadiz area (Navarro et al., 2012). Thus, knowledge on phytoplankton phenology over the SWIP area, its interannual variability and underlying environmental drivers, is still limited.

In this context, our study aims to evaluate phytoplankton phenology patterns over the SWIP area, during an 18-year period (September 1997 - August 2015), using satellite ocean colour data, and to identify underlying environmental determinants. Our specific objectives are: (i) to evaluate the distribution of phytoplankton phenological indices over the study area and period, on a pixel-by-pixel basis; (ii) to partition the highly heterogeneous surface SWIP area into phenoregions using an objective, unsupervised partition based on phenological indices; (iii) to describe region-specific phytoplankton phenological indices and their interannual variability patterns; and (iv) to evaluate region-specific environmental determinants of phytoplankton phenology, including local ocean physical-chemical variables (mixed layer depth, photosynthetically available radiation and dissolved inorganic nutrients), hydrodynamic variables (riverine discharges and coastal upwelling intensity), and large scale climate indices.

2 – Materials and methods

2.1 Study area

SWIP comprises a variety of oceanic and coastal domains. Open ocean domains are interspersed with submarine seamounts and canyons and, over the coast, a 5-35 km wide continental shelf shifts orientation, from meridional to zonal, at Cape São Vicente (CSV). CSV is the northwest limit of the Gulf of Cadiz (GoC), a basin that connects the Mediterranean Sea and the Atlantic Ocean. The main continental influences over SWIP include topographic irregularities, such as prominent capes as CSV, Cape Santa Maria (CSM) and Cape Trafalgar (CT), and the Strait of Gibraltar, which affect coastal circulation dynamics (García-Lafuente et al., 2006; Sala et al., 2018). Freshwater inputs, particularly into the GoC area (e.g., Guadiana and Guadalquivir rivers discharge; Caballero et al., 2014; submarine groundwater discharges; Piló et al., 2018), are relevant local drivers of abiotic conditions and phytoplankton dynamics (Krug et al., 2017b). SWIP, embedded in the Iberian Canary Eastern Boundary Upwelling system, is strongly affected by a seasonal upwelling, promoted by northerly and westerly winds for western and southern coastal areas, respectively (Relvas et al., 2007; Goela et al., 2016a). Offshore circulation over SWIP is affected by mesoscale and submesoscale features including fronts, cyclonic and anti-cyclonic eddies, jets and upwelling filaments (García-Lafuente and Ruiz, 2007; Relvas et al., 2007).

SWIP, along with Southern Europe and Mediterranean, are classified as regions particularly vulnerable to climate change, under effects of increased frequency and intensity of heatwaves, and decline in precipitation and provision of ecosystem services (Kovats et al., 2014). In fact, decadal climate-driven alterations over SWIP were already reported for atmospheric (Trigo, 2006), ocean physical (Varela et al., 2015; Goela et al., 2016a) and biological properties (Horta e Costa et al., 2014; Gamito et al., 2016).

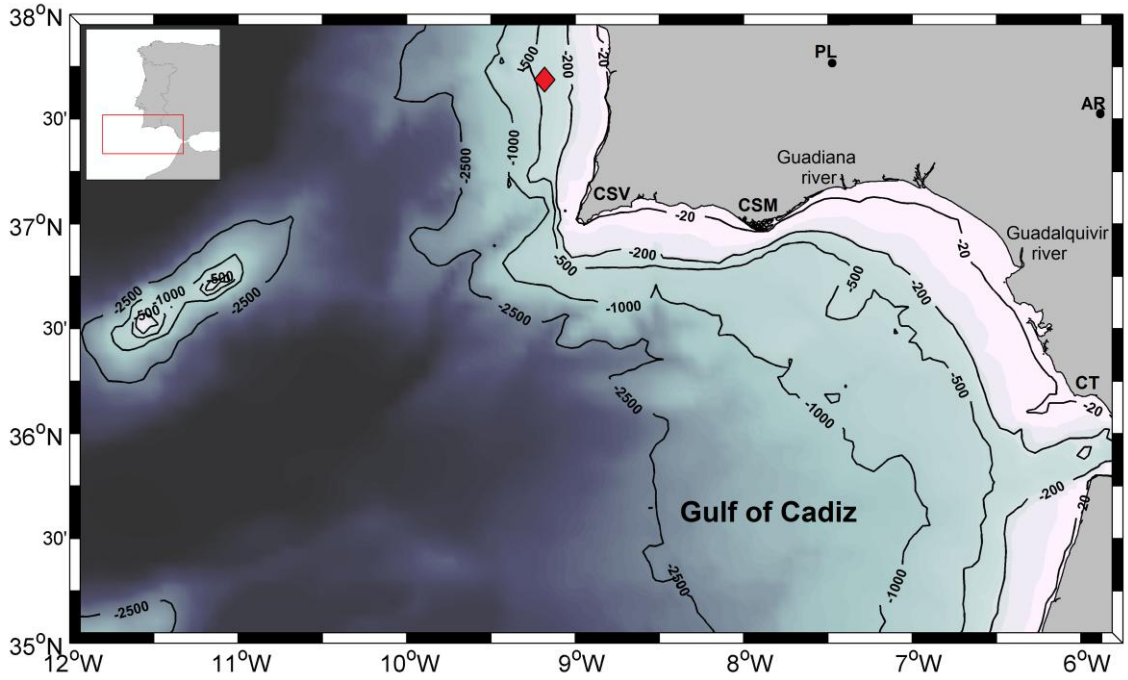

Figure 1 - The southwest area off the Iberian Peninsula (SWIP): bathymetry and main sources of freshwater discharges, the Guadiana and Guadalquivir rivers. CSV, CSM and CT depict the location of prominent topographic features, Cape São Vicente, Cape Santa Maria and Cape Trafalgar, respectively. PL and AR depict the location of Pulo do Lobo and Alcalá del Río hydrographic stations, respectively. Red diamonds shows the position of pixels used for the calculation of Cross Shore Ekman Transport, a wind-based upwelling index. For a colour version of this figure, the reader is referred to the web version of this article.

2.2 Phytoplankton chlorophyll-a concentration

Satellite-derived surface Chl-a from the European Space Agency's Ocean Colour Climate Change Initiative (OC-CCI), at 4 km and 8-day resolution, available at http://www.esa-oceancolour-cci.org/, was used to derive phytoplankton phenological indices over the SWIP area between September 1997 and August 2015 and subsequently used to derive phytoplankton phenological indices. The OC-CCI Chl-a version 3 product uses remote sensing reflectances (R_{RS}) derived from multiple sensors, Sea-viewing Wide Field of View Sensor (SeaWiFS), MODerate-resolution Imaging Spectroradiometer (MODIS-Aqua), MEdium Resolution Imaging Spectrometer (MERIS) and Visible Infrared Imaging Radiometer Suite (VIIRS), which are wavelength synchronized to account for sensor specific centre bands, bias corrected and merged, allowing an enhanced spatio-temporal resolution with respect to the use of single sensors. Moreover, Chl-a values are computed using the merged R_{RS} and

estimated using a blended combination of best-performing algorithms to improve performance in case II waters (Sathyendranath et al., 2016, 2017). Although this OC-CCI product is provided at daily resolution, the 8-day resolution (hereafter weekly) was selected to limit the data gaps and increase accuracy and precision in the calculation of the phenological indices (Cole et al., 2012; Ferreira et al., 2014; Land et al., 2014; Racault et al., 2014b).

The accuracy of satellite-derived Chl-a for the study region and adjacent Atlantic areas was previously assessed during calibration-validation exercises dedicated to different (standard and alternative) bio-optical algorithms and sensors, including SeaWiFS (Navarro and Ruiz, 2006), MERIS (Cristina et al., 2014, 2015, 2016a, 2016b; Nechad et al., 2015; Goela et al., 2016b; Tilstone et al., 2017), MODIS-Aqua (Caballero et al., 2014; Sá et al., 2015) and OC-CCI version 1 products (Sá et al., 2015). Overall, these studies indicated that satellite radiometry provides realistic estimates of *in situ* Chl-a, but usually larger than contemporaneous *in situ* estimates. Higher uncertainty and a systematic overestimation was found for nearshore optically-complex Case II waters. To minimize problems associated with Case II coastal waters, Chl-a was retrieved only for areas outside the 20 m isobath, located at a minimum distance of approximately 4 km from the coastline. All Chl-a values were retained, since unusually high Chl-a values for the study area (> 20 µg L^{-1}; Navarro and Ruiz, 2006; Moita, 2001; Caballero et al., 2014) represented only less than 0.0001% of valid data. Our strategy has not accounted for sub-surface phytoplankton dynamics (e.g., subsurface chlorophyll maxima; Moita, 2001; García-Lafuente and Ruiz, 2007).

2.3 Optical variables

Weekly level-3 mapped mean surface photosynthetically available radiation (PAR) data, at 9 km spatial resolution, were obtained from SeaWiFS (1997-2002) and MODIS-Aqua (2002-2015) products, available at the NASA's Oceancolor portal (https://oceandata.sci.gsfc.nasa.gov/). Weekly level-3 composites of satellite-derived light attenuation coefficient at 490 nm

wavelength (K_{490}), at 4 km spatial resolution, were accessed from ESA's OC-CCI (see section 2.2). Mean PAR intensity in the mixed layer (I_m) was calculated according to Kirk (1986), using PAR vertical attenuation coefficient (K_{PAR}) and euphotic zone depth (Z_{eu}) estimates. K_{PAR} was derived from K_{490} according to Rochford et al. (2001), and Z_{eu}, was defined as the depth at which the irradiance is 1% of incident surface PAR, according to the Lambert-Beer law, assuming a constant attenuation coefficient and optically homogeneous waters (see Krug et al., 2017b for further details).

2.4 Physical and chemical variables

Daily 4-km satellite-derived sea surface temperature (SST) data for the period between September 1997 and December 2010 were obtained from the Sea Surface Temperature Climate Change Initiative (SST-CCI) version 1.0. As OC-CCI, the SST-CCI (http://esa-sst-cci.org/) is a multi-sensor match-up dataset that combines SSTs retrieved from data obtained from the Along Track Scanning Radiometer (ATSR) and Advanced Very-High Resolution Radiometer (AVHRR) series of sensors, creating a gap-free level-4 time series. Daily SST data for the period between January 2011 and August 2015 were retrieved from MODIS-Aqua night time passes, available at NASA's OceanColor portal.

Mixed Layer Depth (MLD) weekly composites were retrieved from the Ocean Productivity group of the Oregon State University (http://www.science.oregonstate.edu/ocean.productivity/index.php), based on three data-assimilating models: Simple Ocean Data Assimilation (SODA), at a 0.5^o spatial resolution (1997-2004); Thermal Ocean Prediction Model based on The Navy Coupled Ocean Data Assimilation system (NCODA/TOPS), at a 1^o spatial resolution (January - May 2005); and Fleet Numerical Meteorology and Oceanography Center model (FNMOC – June 2005 to August 2015), at a 0.25^o spatial resolution. This combination of MLD data was selected in accordance with the preferred MLD sources used in net primary production models of the Ocean Productivity

group. MLD data were adjusted to GEBCO bathymetry (IOC, IHO and BODC, 2003), and maximum MLD values were limited to bathymetry values. The timings of MLD shoaling and deepening (e.g., Lavigne et al., 2013; Shiozaki et al., 2014) were also explored as potential environmental determinants of phytoplankton phenology. For each annual cycle, the timing of MLD shoaling was considered as the week of the year coincident with the MLD maximum. The timing of MLD deepening, considered the week of the year when MLD started to increase significantly, was defined as the time when 10% of the amplitude of the normalized MLD data (minima and maxima on a 0 -1 range) was reached.

Daily sea surface wind speed (W) and its zonal (U) and meridional (V) component fields were obtained from the Blended Sea Winds dataset (BSW) at the National Centers for Environmental Information of NOAA (https://www.ncdc.noaa.gov/data-access/marineocean-data/blended-global/blended-sea-winds), at 0.25^{o} spatial resolution. This product is based on a combination of several scatterometers, standardized across platforms, hence allowing a high quality and more complete temporal and spatial coverage of ocean winds (Zhang et al., 2006). The third power of the wind speed (W) was used as an index of turbulent mixing (W^3) in the upper water column (Elsberry and Camp, 1978).

Concentrations of dissolved inorganic macronutrients (nitrate, NO_3; phosphate, PO_4) and micronutrients (iron, Fe) were obtained from the biogeochemical model reanalysis data provided by the Copernicus Marine Environment Monitoring Service for the Atlantic-Iberian Biscay Irish-Ocean area, for the period February 2002 - December 2014 (Product: IBI_REANALYSIS_BIO_005_003; http://marine.copernicus.eu/). This product, derived from the biogeochemical model PISCES (Pelagic Interaction Scheme for Carbon and Ecosystem Studies), coupled with ocean physics NEMO (Nucleus for European Modelling of the Ocean), is available at a 0.08^{o} spatial resolution and monthly temporal resolution, for 50 depth levels (0.50 m to 5500 m). Validation with World Ocean Atlas climatology showed a good agreement but underestimation of NO_3 and PO_4 over the southern IBI area, which includes SWIP (Dabrowski

et al., 2016). To obtain a more robust estimate of nutrient availability (based on a higher number of data points), in comparison with subsurface level, relevant for phytoplankton, average nutrient concentrations were computed within the first layer, considered as the shallowest depth between MLD and Z_{eu}, for each pixel and time step.

2.5 Upwelling intensity and hydrographic variables

A wind-based upwelling index, the cross-shore Ekman transport (CSET), was used to infer upwelling intensity and patterns during the study period. Weekly CSET was estimated for the west Portuguese coast, positioned at ca. 75 km from the coastline (see Fig. 1), and values were averaged over a 0.75^{o} x 0.75^{o} box, centred at the target site. Due to the N-S coastal orientation, the zonal component of the Ekman transport was used to calculate CSET (Alvarez et al., 2011; Bakun, 1973; see Krug et al., 2017b for further details). Negative CSET values indicate offshore Ekman transport and upwelling-favourable periods; conversely, positive values indicate onshore Ekman transport and downwelling-favourable periods.

Freshwater discharge over the study area is strongly associated with Guadiana and Guadalquivir rivers. Daily Guadiana river discharge (Gdn), measured at the hydrometric station Pulo do Lobo (see Fig. 1), was accessed from the Portuguese Environmental Agency public database (http://snirh.apambiente.pt/). Daily Guadalquivir river discharge (Gdq), measured at the Alcalá del Río station (see Fig. 1), was acquired from the Spanish Regional Water Management Agency (http://www.chguadalquivir.es/saih/).

All environmental variables were re-gridded to the same spatio-temporal resolution of Chl-a data (4-km, 8-day). Data analyses and visualization maps were generated using MATLAB software.

2.6 Large scale climate indices

Six large-scale climate indices were used as indicators of remote forcing over the study area: (i) the Multivariate El Niño Southern Oscillation (ENSO) Index (MEI), a global scale index which monitors ENSO patterns based on six ocean-atmosphere variables over the tropical Pacific (Wolter and Timlin, 2011); (ii) the North Atlantic Oscillation (NAO) Index, a normalized pressure difference between the Azores and Iceland, representative of the dominant mode of climate variability in the north sector of the Atlantic Ocean (Hurrell, 1995); (iii) the Atlantic Multidecadal Oscillation (AMO), an SST-based index related to low frequency variability in SST and themohaline circulation in the North Atlantic (Kaplan et al., 1998); (iv) the Eastern Atlantic Pattern (EA), the second mode of sea-level pressure (SLP) variation in the North Atlantic (Hurrell et al., 2003); (v) the Western Mediterranean Oscillation (WeMO) Index, a barometric ratio between Padua (north Italy), and San Fernando (southwest Spain), representative of low frequency variability patterns of atmospheric circulation over the western Mediterranean basin (Martin-Vide and Lopez-Bustins, 2006); and (vi) the West Europe Pressure Anomaly (WEPA), based on winter (December – March) SLP, which is strongly related to winter wave height variability over the coast of western Europe (Castelle et al., 2017).

Monthly values of the large-scale climate indices were retrieved from diverse sources. MEI, NAO, and AMO indices were accessed at NOAA's Earth System Research Laboratory portal (https://www.esrl.noaa.gov/psd/data/climateindices/list/), EA was acquired at NOAA's Climate Prediction Center website (http://www.cpc.ncep.noaa.gov/data/teledoc/ea.shtml), WeMO was retrieved from the University of Barcelona's Climatology Group website (http://www.ub.edu/gc/en/2016/06/08/wemo/), and WEPA was extracted from supplementary material provided by Castelle et al. (2017). Significant connections between MEI, NAO, AMO, EA and WeMO and phytoplankton variability over SWIP were previously reported by Krug et al. (2017b).

2.7 Data analyses

The general strategy used for partitioning the SWIP area, based on phytoplankton phenology, is summarized in Figure 2. Chl-a time series, available for each study area pixel (n=8570 pixels), covered an 18-year period (n= 828 Chl-a 8-day composites). First, pixel-specific Chl-a time series were organized considering the start point of the annual cycle as the first week of September (week 1; year t) and the end point as the last week of August (week 46; year t+1), i.e., spanning two calendar years. This 12-month delineation period was chosen to follow phytoplankton seasonal variability patterns (see Krug et al., 2017b). Six phenological indices were then computed, for each pixel. A dissimilarity analysis was used to select the set of independent phenological indices that were subsequently used as partitioning variables. An unsupervised classification technique was then used to partition SWIP into regions sharing similar phytoplankton phenology (phenoregions). This phenology-based SWIP partition was later used as a framework to investigate region-specific phenological indices, their interannual variability during the study period, and the underlying environmental determinants of phytoplankton phenology.

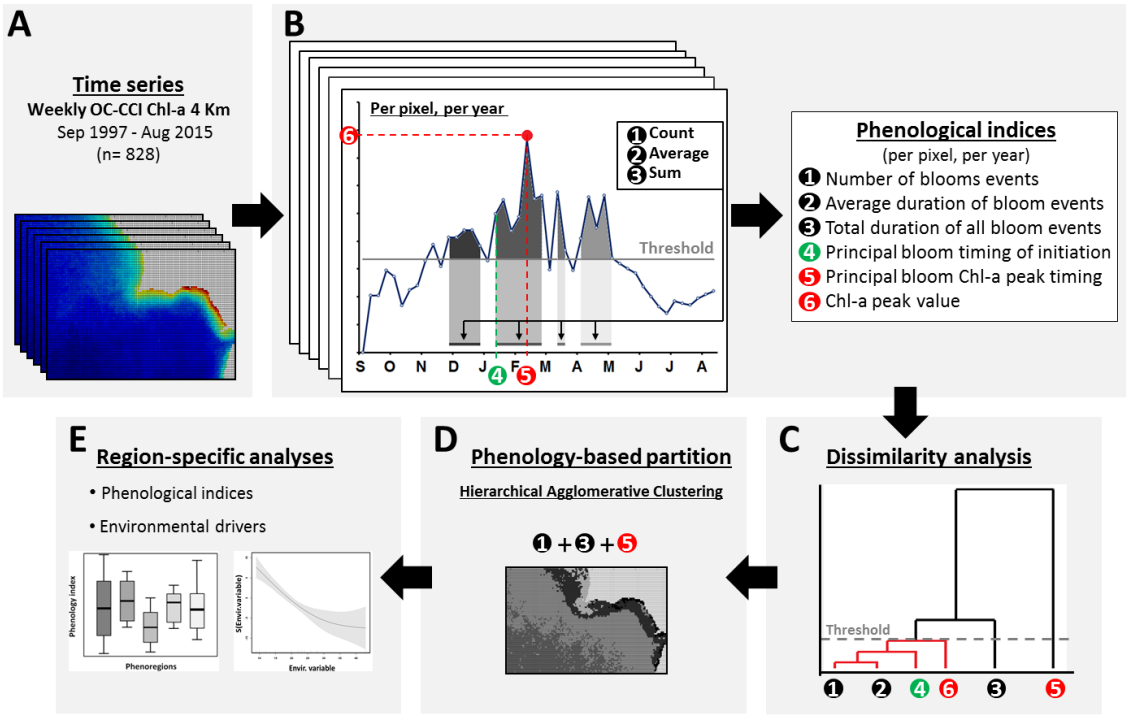

Figure 2 – Flow diagram representing the different steps (A – D) involved in the partition of the area off South West Iberian Peninsula (SWIP) based on phytoplankton phenology during a 18-year period (1997

– 2015). Workflow included: (A) Extraction of the Chl-a time series for SWIP, on a pixel-by-pixel basis; (B) calculation of six phenological indices, on a pixel-by-pixel basis; (C) selection of specific non-redundant phenological indices to be used as partitioning variables; and (D) delineation of phenology-based coherent regions (phenoregions) using an unsupervised objective classification technique (Hierarchical Agglomerative Clustering). Step E represents the analyses of region-specific phenological indices and environmental driving forces for different bloom indices. See text for further details. For a colour version of this figure, the reader is referred to the web version of this article.

2.7.1 Phytoplankton phenological indices

Several phenological indices have been applied to synthesize phytoplankton phenology patterns (see Platt and Sathyendranath, 2008; Platt et al., 2009, 2010), and multiple strategies have also been used to derive specific metrics (see Brody et al., 2013; Ferreira et al., 2014 and references therein; Land et al., 2014; Friedman et al., 2018). Ideally, "a phenology metric should be accurate, precise, and simultaneously sensitive to the underlying environmental processes" (Ferreira et al., 2014). However, several observation-related and analysis-related issues (e.g., missing data, observational noise, temporal resolution, preprocessing, bloom amplitude, phenology metric), introduce errors in the estimates of phytoplankton phenology (Ferreira et al., 2014). These errors or uncertainties associated with phenology metrics usually exhibit a spatial pattern, with smaller values for the latitudes over the study area (Cole et al., 2012; Ferreira et al., 2014; Racault et al., 2014b).

In this study, bloom events were defined as occurrences when Chl-a surpassed the threshold criterion of 5% above the annual local median value (Siegel et al., 2002), at least during two consecutive weeks (Cole et al., 2012; Brody et al., 2013). This biomass-based threshold approach is considered a robust and precise strategy (Ferreira et al., 2014), and widely applied in studies of phytoplankton phenology (e.g., Henson et al., 2009; Racault et al., 2012, 2017; Sapiano et al., 2012; Lavigne et al., 2013). The following phenological indices were estimated on a pixel-by-pixel basis and for each phenoregion, using all detected bloom events (principal and secondary), for each annual cycle, (i) number of bloom events; (ii) total duration of all

bloom events per year; (iii) average duration of bloom events; and (iv) Chl-a peak value. Taking into consideration the principal annual bloom for each pixel or phenoregion (i.e., the events associated with Chl-a maxima for each year), the following phenological indices were also estimated: (v) timing of bloom initiation (first week when Chl-a surpassed the threshold criteria); (vi) bloom peak timing (week of Chl-a peak value within each bloom event); (vii) timing of bloom termination (last week of Chl-a above the threshold criteria); and (viii) bloom duration (time elapsed between bloom initiation and termination) (see Fig. 2). In addition to these eight indices, two other phenological metrics were also derived for each delineated SWIP phenoregion, considering the principal bloom during each year: (ix) duration of the bloom accumulation phase, i.e., time elapsed between bloom initiation and bloom peak; and (x) duration of the bloom deceleration phase, i.e., time elapsed between bloom peak and termination.

2.7.2 Delineation of phenology-based regions off SW Iberia

The climatological average values (18-year period) of six relevant phenological indices, derived for each year on a pixel-by-pixel basis, were tested as potential SWIP partitioning variables: number of bloom events per year, average duration of the bloom events, total yearly duration of the bloom events, timing of the initiation of the main bloom, bloom peak timing, and Chl-a peak value. The value of each index was normalized by subtracting its mean value (18-year) and dividing by its standard deviation. Spearman rank correlation coefficient (r_S) was used to evaluate the strength of monotonic relationships between these phytoplankton phenological metrics (Hauke and Kossowski, 2011), and correlation values ($1-r_s$) were used to build a dissimilarity hierarchical cluster tree (Wilks, 2006). A dissimilarity value of 0.10 was used as a threshold to eliminate strongly correlated, redundant phenological indices. For groups of redundant indices (similarity above 0.90), a single index was selected as a SWIP partitioning variable.

Different delineation methods, based on OCRS, can be applied for ocean surface partition. However, unsupervised learning approaches provide a less biased delineation and more accurate representation of phytoplankton variability (see review by Krug et al., 2017a). In this study, Hierarchical Agglomerative Clustering (HAC) analysis was used to classify SWIP into regions with similar phenological properties (phenoregions). HAC associates objects that are close to each other in an n-dimensional space into the same cluster, using a division that simultaneously minimizes differences between objects of a given cluster and maximizes differences between objects of different clusters, based on Euclidian distance and Ward's linkage (Ward, 1963), respectively (Wilks, 2006). As the number of clusters (i.e., phenoregions) must be defined in advance, HAC analysis was applied multiple times, using a cluster number that varied between 2 and 20. The original data were divided into a training (90%) and a validation (10%) dataset, and used for cross-validation. At each round of the 10-fold cross-validation, HAC was applied to the training dataset and pixels from both training and validation datasets were assigned to a cluster based on the lowest distance from the centroid values. The cross-validation error was computed as the sum of the root mean square deviation between individual pixels of the validation dataset and their respective cluster mean values (centroids). The final cluster number error, calculated as the average error of the 10 cross-validations, was used to determine the optimal number of clusters (phenoregions), defined as the first of three consecutive final error reductions below < 5%, after addition of a further cluster (Fendereski et al., 2014; Oliver et al., 2004).

2.7.3 Region-specific phenological properties, interannual variability patterns and environmental determinants

Phytoplankton phenological metrics for each delineated SWIP phenoregion, and their interannual variability patterns, were investigated during the 18-year study period (1997 -

2015). Region-specific Chl-a time series, based on average Chl-a values and annual Chl-a threshold criteria (5% above the yearly median; Siegel et al., 2002) for each phenoregion, were used to compute the regional phenological metrics (see section 2.7.1). Differences in phenological indices across SWIP phenoregions were tested using the non-parametric Kruskal-Wallis test, an one-way analyses of variance on ranks, and pair-wise comparisons using the Dunn's test (Statistica software, version 10.0). Spearman correlation coefficients (r_s) were used to evaluate the strength of monotonic relationships between phenological indices over each phenoregion. All statistical tests were considered at a 0.05 significance level.

To investigate the environmental drivers underlying phytoplankton phenology over each SWIP phenoregion, the following variables were considered: ocean optical variables (PAR, and I_m), ocean physical variables and related indicators (SST, MLD, MDL:Z_{eu}, timing of MLD shoaling and deepening onsets, W and its components U and V, and W^3), ocean chemical variables (NO_3, PO_4 and Fe), local hydrodynamic variables (CSET, Gdn and Gdq), and large-scale climate indices (MEI, NAO, EA, AMO, WeMO and WEPA). The relationships between phytoplankton phenological indices and environmental variables, for each phenoregion, were evaluated using values of the environmental variables acquired during the conditions preceding the time of bloom initiation (pre-bloom stage) or averaged during specific periods (e.g., winter: December to March; upwelling-favourable period: May to September) or the whole annual cycle (September to August).

Generalized Additive Modelling (GAM) techniques (Wood, 2006) were used to evaluate the linkages between environmental determinants and phenological indices over each SWIP phenoregion. GAMs are a flexible class of statistical models that accommodate linear as well as complex non-linear relationships between a dependent response variable and multiple predictors (for further details see Krug et al., 2017b). The basic GAM model structure is represented by the following equation, where Y represents the response variable, $\propto$ is the

intercept, s_j are nonparametric smoothing functions specifying the partial additive effect of each predictor (X_j), and ε represents a random error term.

$$Y = \propto + \sum_{j=1}^{n} s_j\left(X_j\right) + \varepsilon$$

Response variables, i.e., region-specific phenological indices, and environmental determinants were modelled as cubic spline smoother smoother functions (s). Prior to the analysis, colinearity among environmental determinants was tested using r_s, and variables significantly correlated at $|r_s|>0.70$ were not used as covariates for the same model run (Dormann et al., 2013). Underlying statistical assumptions (homoscedasticity, residuals normality, residual serial dependency) of the GAMs were tested using graphical residual diagnostics and autocorrelation function. Criteria used to select the best-performing models included minimizing the generalized cross-validation (GCV) score, a measure of the predictive error of the model and its complexity related to Akaike's Information Criterion (AIC), and maximizing the level of deviance explained (Wood, 2006; see Krug et al., 2017b for details).

GAMs were also used to decompose temporal variability patterns of phenological indices, Chl-a and environmental variables, over each SWIP phenoregion, into seasonal and interannual components. Due to serial temporal autocorrelation, GAMs were extended to Generalized Additive Mixed Models (GAMM) by including a first order autoregressive correlation structure. Response variables were modelled as a cyclic spline smoother function of time of the year (year-week) and a cubic spline smoother function of time (Wood, 2006; for further details see Krug et al., 2017b). GAM and GAMM analyses were conducted with the "mgcv" library, in R statistical software, version 2.5.1 (R Core Team, 2016). Due to the relatively short time series (18-year), significance at the p-level < 0.10 were also considered. However, the analysis of interannual variability in region-specific phenological indices and underlying environmental drivers, namely climate-related variables, should be interpreted with caution due the

uncertainties associated with the estimates of phenological indices (Cole et al., 2012; Ferreira et al., 2014) and the length of the time series (e.g., typical AMO period: 60-80 years; see Henson et al., 2010, 2016, 2017).

3 – Results

3.1 Phytoplankton phenology off SW Iberia: a pixel-based assessment

Basic statistical information on selected phytoplankton phenological indices over SWIP, extracted on a pixel-by-pixel basis for an 18-year period (1997 - 2015), is summarized in Table 1. Mean spatial distribution of the phenological indices exhibited a substantial spatial variability over the SWIP area, with remarkable cross-shelf gradients, organised with a strong spatial coherency (see Fig. 3). For most indices, maximum variability areas followed approximately the 500 m isobath within most of the GoC area, spreading towards the 1000 m isobath in the vicinity of CSM, and towards the 2500 m isobath near CSV and over the west Portuguese coast (Fig. 3A-E). However, in case of bloom peak timing, cross-shelf gradients were less pronounced over most of the GoC margin (Fig. 3F). For most phenological indices (Fig. 3A, 3B, 3D, 3E), latitudinal gradients were also detected over the oceanic SWIP domains, with a latitudinal discontinuity located at ca. 36.5^{o}N (Fig. 3).

Table 1 – Descriptive statistics of phytoplankton phenological indices over the southwest area off the Iberian Peninsula, estimated for each annual cycle, on a pixel-by-pixel basis, during the period September 1997 - August 2015 (n= 18 years x 8,570 pixels = 154,260). Information includes minimum (Min), maximum (Max) and mean values and standard deviation (SD). *refers to primary blooms, and considers the year starting in January (week of the year 1) and ending in December (week of the year 46).

Phenological index	Min - Max	Mean ± SD
Number of bloom events per year (bloom events.year^{-1})	1 - 9	2.48 ±0.07
Total duration of all bloom events per year (weeks.year^{-1})	5 - 23	18.93 ±0.10
Average duration of bloom events (weeks.bloom^{-1})	2 - 23	11.21 ±0.20

Chlorophyll-a peak value (µg L^{-1})	0.19 - 18.48	0.86 ±0.23
Timing of the bloom initiation* (week of the year)	33 - 29	46.33 ±0.54
Chl-a peak timing* (week of the year)	33 - 30	8.27 ±0.57
Timing of the bloom termination* (week of the year)	34 - 30	13.25 ±0.55

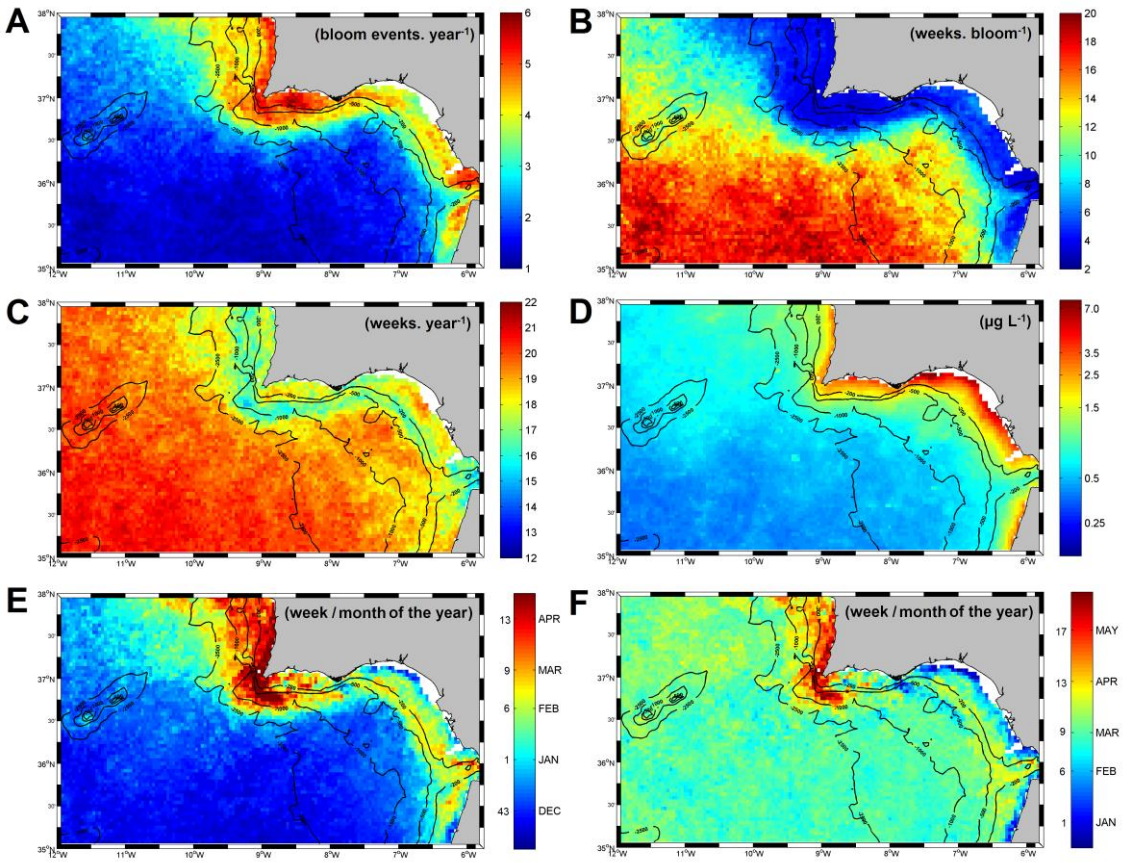

Figure 3 – Distribution of annual mean values of selected phytoplankton phenological indices over the southwest area off the Iberian Peninsula, estimated for each annual cycle, on a pixel-by-pixel basis, during a 18-year period (September 1997 - August 2015): (A) Number of bloom events per year; (B) Average duration of the bloom events; (C) Total duration of all bloom events per year; (D) Chlorophyll-a peak value; (E) Timing of the initiation of the primary bloom; and (F) Chlorophyll-a peak timing. Black lines represent the 200m, 500m 1000m and 2500m isobathymetric contours. For a colour version of this figure, the reader is referred to the web version of this article.

The number of bloom events per year varied from one to two in most of the oceanic SWIP domain, and increased up to six over the Portuguese west coast, CSM and CT area (Fig. 3A). The average duration of phytoplankton blooms showed an opposite pattern, with more

prolonged events over the oceanic domain, average duration varying from eight to 20 weeks, and increasingly greater bloom duration from northern to southern open ocean areas. Over slope and coastal areas, bloom events lasted, on average, two to six weeks (Fig. 3B). The distribution of the total duration of all bloom events during each annual cycle (Fig. 3C) revealed a distinct intermediate area, located along the shelf edge to upper slope (ca. 200 m – 500 m isobaths), with lower values (15 to 16 weeks.year^{-1}), compared with coastal and oceanic SWIP (> 18 weeks.year^{-1}). Chl-a peak values varied, on average, between 0.33 µg L^{-1} and 8.86 µg L^{-1}, with highest values over the continental shelf, especially for the northeastern GoC areas impacted by the freshwater outflow of Guadiana and Guadalquivir estuaries (Fig. 3D). Over the oceanic SWIP area, a latitudinal gradient was also observed, with higher Chl-a peak values north of ca. 36.5^{o}N.

Timings of principal blooms were expressed in week of the year (WOY), considering the year starts in January (WOY 1) and ends in December (WOY 46). The timing of the principal bloom initiation generally showed a northward progression for the open ocean domain (Fig. 3E). Principal blooms initiated earlier, between November and January (WOY: 41-4), for most of the oceanic domain and a narrow coastal fringe area, over the northeastern and southeastern GoC (Fig. 3E). Over most of the shelf and slope areas within GoC, and spreading towards the 2500 m isobath over the Portuguese west coast, the main phytoplankton blooms started, in general, later, between February and March (WOY: 5-9). The area over the west coast and shelf-edge around CSV presented a relatively delayed bloom initiation, usually occurring between April and May (WOY: 13-20). Chl-a peak timing over SWIP showed a more homogeneous spatial distribution, occurring during February-March (WOY: 5-12) for most of SWIP oceanic and coastal domains (Fig. 3F). However, a narrow coastal sector along northeastern and southeastern GoC displayed an anticipated bloom peak (January-February, WOY 1-6), whereas the western Portuguese margin, including the CSV area, displayed a delayed bloom peak (April-May, WOY: 12-19; Fig. 3F).

3.2 Phenology-based partition off SW Iberia

The selection of relevant partition variables to be included in HAC analyses was based on a dissimilarity dendrogram, generated by the inversion of the correlation matrix of the six normalized phenological indices (see section 2.7.2). The indices Chl-a peak timing and total duration of all bloom events per annual cycle presented dissimilarity values above the defined threshold (0.10), whereas the remaining phenological indices showed dissimilarity values below this threshold. As consequence, a single index representative of this group of redundant variables was selected as a partition variable (Fig. S1A). HAC analysis was run several times, each including one of these highly correlated redundant indices, in tandem with the two dissimilar indices. Based on a higher spatial coherence of the resulting SWIP classifications (data not shown), the index number of bloom events per annual cycle was selected. The input dataset, representative of phytoplankton phenology over the SWIP area was, therefore, based on three phenological indices: Chl-a peak timing, total duration of all bloom events per year, and number of bloom events per year. Cross-validation errors associated with HAC analyses, estimated using a number of clusters (i.e, phenoregions) varying between 2 and 20, indicated that phytoplankton phenology over the SWIP area was optimally represented by five distinct phenoregions, with similar phytoplankton phenology patterns (Fig. S1B).

The five delineated phenoregions over SWIP were organized coherently over the study area (Fig. 4A). The open ocean SWIP domain was predominantly associated with two regions: the SW Oceanic phenoregion, located over the southwestern SWIP oceanic domain, and the Oceanic phenoregion, covering most of the open ocean area over the GoC (depth > 500m) and the northwestern SWIP area (depth > 2500m). A single region was delineated over the SWIP continental margin, the Coastal-Slope phenoregion, which covered most of the coastal and slope areas. Notable exceptions were the west Portuguese coast and CSV area, covered by the

Upwelling-influenced phenoregion, and the nearshore areas over the northeastern and southeastern GoC, covered by the River-influenced phenoregion (Fig. 4A).

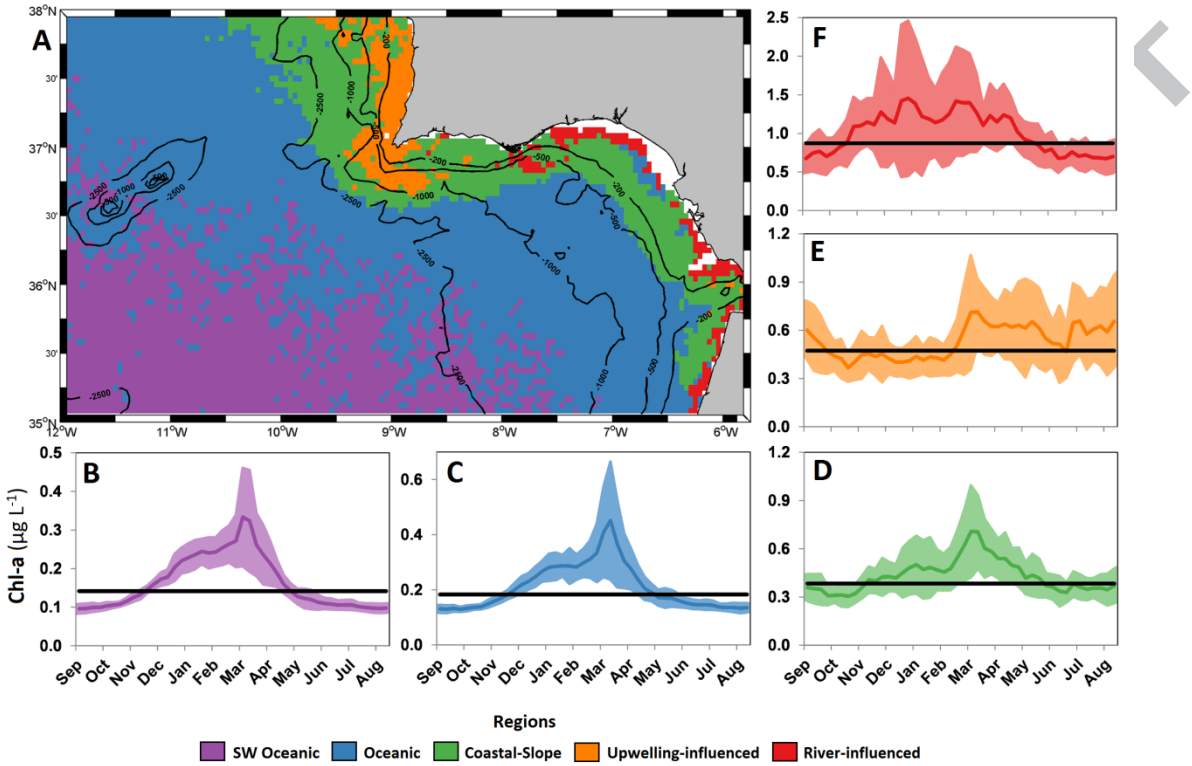

Figure 4 – Partition of the southwest area off the Iberian Peninsula (SWIP) into phenoregions based on phytoplankton phenological indices (number of bloom events per year, Chl-a peak timing and total duration of all bloom events per year), for the period between September 1997 and August 2015. (A) Spatial distribution of the five SWIP phenoregions. (B-F) Weekly-based phytoplankton climatological seasonal cycles, with mean chlorophyll-a (Chl-a) values (coloured lines) ± 1 standard deviation (shaded coloured areas) for each phenoregion: (B) SW Oceanic, (C) Oceanic, (D) Coastal-Slope, (E) Upwelling-influenced and (F) River-influenced regions. Thick, black horizontal lines (B-F) represent the average annual Chl-a threshold criteria (5% above the yearly median) used to define a phytoplankton bloom for each phenoregion. Note different y-scales used for panels B to F. For a colour version of this figure, the reader is referred to the web version of this article.

3.3 Phytoplankton phenology off SW Iberia: a phenoregion-based assessment

Chl-a variability patterns during the 18-year study period (see complete Chl-a time series for each phenoregion in Figs. S2-S3) and weekly-based annual climatologies (Fig. 4B-F) varied across SWIP phenoregions. Both the SW Oceanic and Oceanic phenoregions presented low amplitude unimodal annual cycles.

Phytoplankton bloom period occurred between November and May, for both oceanic phenoregions, with Chl-a maxima (0.34 - 0.41 μg L^{-1}) during February-March (Fig. 4B-C). The three coastal phenoregions presented higher Chl-a variability, longer periods with Chl-a above the threshold criteria, and blooms occurred during different periods of the year (Figs. 4D-F, S2-S3). The Coastal-Slope phenoregion (Fig. 4D) showed a unimodal annual cycle, with Chl-a above the threshold between November and June, and Chl-a peak values (0.71 μg L^{-1}) during March. The Upwelling-influenced phenoregion presented a quasi-bimodal annual cycle, with two distinct periods of Chl-a above the threshold criterion, February-June and June-September (Fig. 4E), and Chl-a peak values occurred during March (0.71 μg L^{-1}) and July (0.65 μg L^{-1}). The River-influenced phenoregion (Fig. 4F) presented a unimodal annual cycle, with Chl-a above the threshold between October-May, and Chl-a peak values between December and February (ca. 1.45 μg L^{-1}). At the interannual scale, Chl-a showed significant patterns only over the open ocean phenoregions, with strong linear increasing tendencies for both SW Oceanic and Oceanic regions ($p<0.001$; data not shown).

A total of 245 phytoplankton bloom events were identified over the five SWIP phenoregions during the 18-year study period, including 90 principal blooms and 155 secondary blooms mostly detected over the coastal phenoregions (Fig. 5A; see complete Chl-a time series, with identification of each bloom event, in Fig. S3). Secondary blooms represented between 70% and 77% of the bloom events detected over the River- and Upwelling-influenced regions, respectively. In respect of phytoplankton phenology, a significant distinction between open ocean (SW Oceanic and Oceanic) and coastal (Coastal-Slope, Upwelling- and River-influenced) phenoregions was detected for all phenological indicators (Fig. 5), except the total duration of all bloom events per year (20-24 weeks; Fig. 5B) and timing of bloom termination (Figs. 5I,5L). Chl-a peak values increased along the ocean-coastal gradient (Fig. 5C), with mean values ranging between 0.35 and 2.00 μg L^{-1} for the SW Oceanic and River-influenced phenoregions, respectively.

SW Oceanic and Oceanic phenoregions usually showed a single prolonged (20-21 weeks) bloom event per year (Figs. 5A and 5D). Over the coastal phenoregions, bloom frequency was higher but highly variable, with from one up to seven events per year (Figs. 5A), and principal bloom duration varied from four to 25 weeks (Fig. 5D). Additionally, the duration of bloom accumulation phase (Figs. 5E) was significantly longer over the open ocean (*ca*. 15 weeks) in comparison with coastal phenoregions (*ca*. four to eight weeks). However, the duration of the bloom deceleration phase was similar among all phenoregions (*ca*. 5 to 8 weeks), except for the Upwelling-influenced region, which exhibited a shorter duration (*ca*. 2-3 weeks; Fig. 5F). Interestingly, the principal bloom event over open ocean phenoregions showed an accumulation phase significantly longer than the deceleration phase ($p<0.01$), whereas over coastal phenoregions the durations of these bloom phases were similar (Fig. 5E-F).

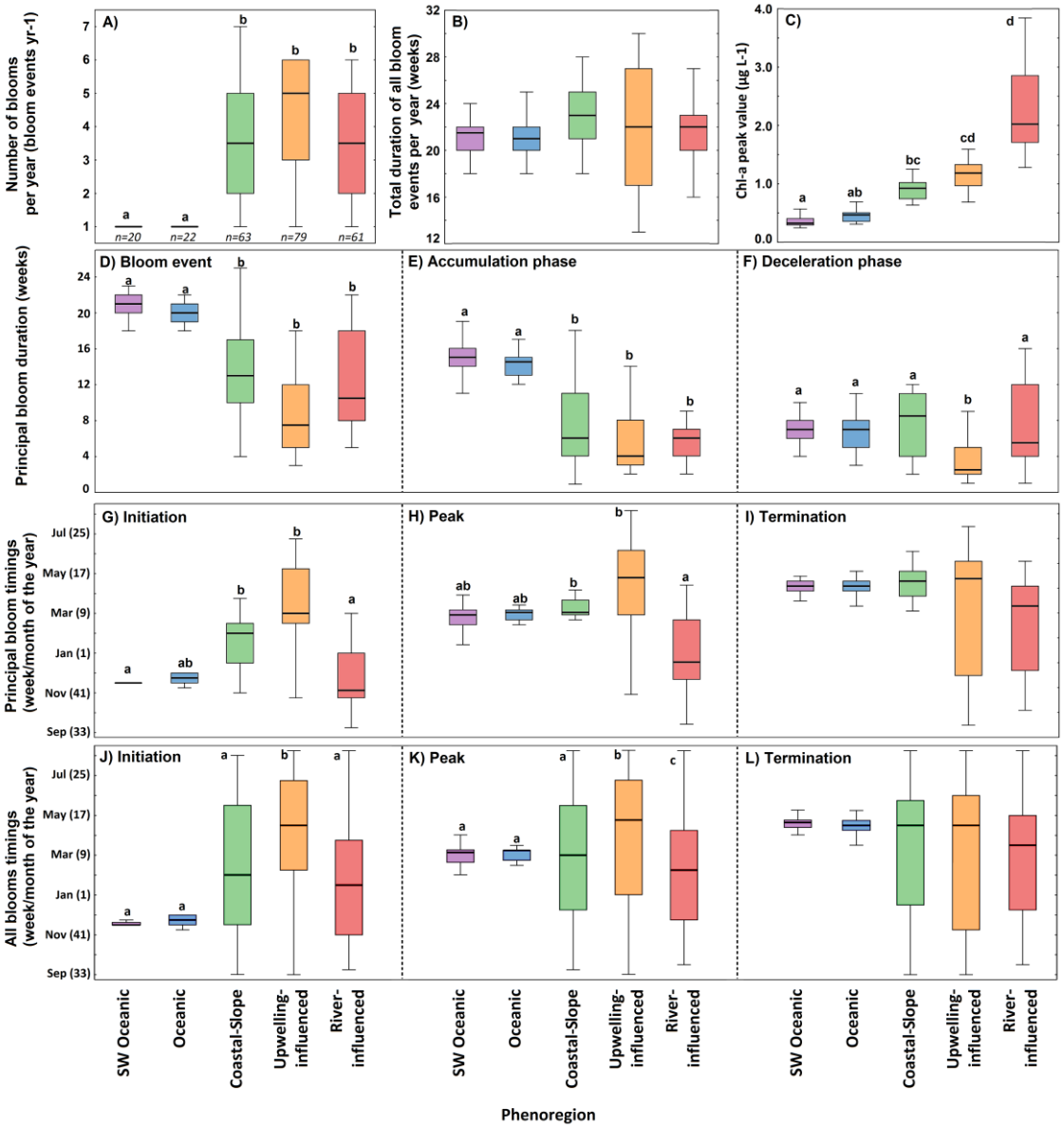

Figure 5 – Phytoplankton phenological metrics for the five phenoregions delineated off SW Iberia, estimated for each annual cycle during the period 1997 to 2015 (See Fig. 4 for region location and colour code). (A) Number of bloom events per year; (B) Total duration of all bloom events per year; and (C) Chlorophyll-a peak value. Considering only the principal blooms: (D) Duration of the bloom event, (E) duration of the bloom accumulation phase, (F) duration of the bloom deceleration phase, (G) Timing of bloom initiation; (H) bloom peak timing; and (I) Timing of bloom termination. Considering the average values for all bloom events (principal and secondary): (J) timing of bloom initiation; (K) bloom peak timing; and (L) timing of bloom termination. Median values are represented by the lines within the boxes, 25th to 75th percentiles are denoted by box edges and non-outlier limits are denoted by whiskers. For each phenological index, different lowercase letters over the bars represent significant differences across phenoregions ($p<0.05$). The number of blooms events identified during the study period for each phenoregion (n) is shown, in italics, in panel A. For a colour version of this figure, the reader is referred to the web version of this article.

The timings of initiation, peak and termination of the principal bloom over the open ocean and Coastal-Slope phenoregions were less variable than over the Upwelling- and River-influenced

phenoregions (Figs. 5G-I). For SW Oceanic and Oceanic phenoregions, the principal bloom initiated around November (WOY: 42-43), during the MLD deepening phase (4.2±3.2 weeks after the onset of MLD deepening), peaked during March (WOY 9), 2.8±3.2 weeks after the onset of MLD shoaling, and terminated during April (WOY 13). Only a minor proportion of the principal oceanic blooms, 11 to 17% for SW Oceanic and Oceanic regions, respectively, effectively terminated during the MLD deepening stage. In comparison with open ocean, over the River-influenced phenoregion principal bloom timings were statistically similar, but more variable (Fig. 5G-I). In fact, 17% of the principal bloom events initiated before the onset of MLD deepening, and 17% of the events initiated during the MLD shoaling phase. For Coastal-Slope and Upwelling-influenced phenoregions, principal blooms initiated (average: February, WOY 8; 15.6±9.4 weeks after MLD deepening onset) and peaked (average: April, WOY 12; 6.9±9.1 weeks after MLD shoaling onset) significantly later than in River-influenced region, and no differences were detected in termination timing across phenoregions. Over the Coastal-Slope phenoregion, 38.9% of the principal bloom events (seven) initiated during the MLD shoaling, mostly before April. For the Upweling-influenced region, a higher proportion of principal bloom events were initiated during the MLD shoaling stage (13 events, 72.2%), with around half (six) of these events initiated during the upwelling favourable period (May – September).

The phenological indices derived using all phytoplankton bloom events occurring each year, including principal and secondary blooms, also revealed a higher variability over the coastal phenoregions (Figs. 5J-L; see full Chl-a time series and bloom events in Fig. S3). Over the Upwelling-influenced phenoregion, 59.0% of the secondary bloom events (36 events) were initiated during the upwelling-favourable period, whereas this value was significantly lower for the Coastal-Slope region (44.4%, 20 events).

Several significant relationships among the phenological indices were detected for the SWIP phenoregions. During the 18-year study period, the number of bloom events per year was

negatively correlated with the duration of principal blooms over all three coastal phenoregions ($-0.84 \leq r_s \leq -0.66$, $p<0.01$). Principal bloom duration was also positively correlated with the duration of both accumulation and deceleration phases over all coastal phenoregions ($0.53 \leq r_s \leq 0.86$, $p< 0.01$). Further, over the Coastal-Slope phenoregion, the timing of bloom initiation was negatively correlated with bloom duration ($r_s=-0.78$, $p<0.001$) and Chl-a peak value ($r_s=-0.47$, $p<0.05$). Over the oceanic phenoregions, the durations of the bloom accumulation and deceleration phases were inversely correlated ($r_s = -0.72$, $p<0.01$).

Interannual variability of the phytoplankton phenological indices was inspected using GAMM analysis. Marginally significant ($p<0.10$) and/or significant ($p<0.05$) interannual trends were detected for all SWIP phenoregions, with the exception of the Oceanic region (Fig. S4; Table S1). Over SW Oceanic phenoregion, the duration of the principal bloom ($p<0.10$) and its accumulation phase ($p<0.001$), and Chl-a peak timing ($p<0.001$) showed significant non-linear trends, with two periods of increasingly prolonged bloom accumulation and delayed bloom peaks before 2003 and after 2007. For the Coastal-Slope phenoregion, both the total duration of all bloom events per year and the duration of the principal bloom displayed weak linearly-increasing trends ($p<0.10$). Over the Upwelling-influenced phenoregion, the duration of the bloom deceleration phase showed a strongly significant linear increase during the study period. For the River-influenced phenoregion, the total duration of all bloom events per year displayed a marginally significant non-linear trend ($p<0.10$), increasing linearly after ca. 2007. Moreover, the timings of the principal bloom initiation and termination exhibited a marginally significant linear increasing delay during the study period ($p<0.10$), whereas Chl-a peak timing showed a significant non-linear increase ($p<0.05$), with a generalized increasing delay until ca. 2007, and a subsequent stabilization (see Fig. S4, Table S1).

3.4 Region-specific drivers of bloom phenology off SW Iberia

The study period encompassed a high variability in large-scale climate and local hydrodynamic forcings (see complete time series in Figs. S5-S6). All physical, optical and chemical ocean variables showed highly significant seasonal patterns, over all phenoregions ($p<0.001$; data not shown). In respect to interannual patterns, CSET exhibited a linear declining trend ($p<0.05$), i.e. an upwelling intensification. Further, increasing trends in W, mostly linear, were detected over all phenoregions (Oceanic and SW Oceanic, $p<0.05$; Coastal-Slope and River-influenced, $p<0.01$; Upwelling-influenced, $p<0.001$). V showed a linear declining trend over open ocean ($p<0.05$) and Upwelling-influenced ($p<0.01$) phenoregions but a non-linear increasing tendency over the River-influenced phenoregion ($p<0.01$). No significant interannual tendencies were detected in case of U or SST. Linear increasing trends in MLD were detected over Coastal-Slope ($p<0.001$) and Upwelling-influenced regions ($p<0.01$). Moreover, significant interannual linear increasingly delays in the onset timing of MLD deepening (SW Oceanic region, $p<0.05$; Oceanic region, $p<0.001$) and MLD shoaling (Upwelling-influenced region, $p<0.05$; River-influenced and Coastal-Slope regions, $p<0.01$; Oceanic region, $p<0.001$) were also observed (data not shown). PAR exhibited non-linear monotonic increasing trends for all phenoregions ($p<0.01$), and I_m interannual patterns ranged from a significant linear decline over the Coastal-Slope ($p<0.01$) and Upwelling-influenced regions ($p<0.001$), to non-linear increases (SW Oceanic, $p<0.05$) or declines (River-influenced region, $p<0.001$). In case of nutrients, a consistent linear increasing trend in NO_3 was observed for most phenoregions ($p<0.01$), except the Upwelling-influenced region.

The physical conditions observed at the time of the principal bloom initiation, specifically MLD and I_m, were less variable over the open ocean regions. Mean (± 1SD) MLD values at the week of the principal bloom initiation ranged between 31.1±16.0 and 77.5±45.1 m, for River-influenced and Coastal-Slope phenoregions, respectively, and was significantly lower for the

former region ($p<0.05$). Mean I_m values at the week of the principal bloom initiation fluctuated between 27.0±8.1 and 69.1±72.2 µmol photons m^{-2} s^{-1}, over the Oceanic and the Upwelling-influenced phenoregions, respectively, and no differences were detected across phenoregions. SST (17.5±1.9 – 19.2±2.5 ^{o}C), U (0.8±3.7 – 2.7±2.5 m s^{-1}), and W (7.8±1.6 – 8.7±1.3 m s^{-1}) conditions observed at the time of bloom initiation were similar across phenoregions. V, however, was significantly higher over the Upwelling-influenced phenoregion (-5.0±2.8 m s^{-1}) in comparison with other regions. Mean concentrations of NO_3, PO_4, and Fe at the time of the principal bloom initiation ranged between 0.027±0.024 - 1.069±0.872 µM, 0.014±0.005 – 0.087±0.056 µM and 0.449±0.050 – 1.419±0.151 nM, respectively, and higher values were detected over coastal phenoregions ($p<0.05$).

GAM analysis was used to explore region-specific linkages between environmental determinants and selected phenological indices associated with principal blooms (Chl-a peak value, duration, timing of initiation and peak timing) and, in case of non-oceanic phenoregions, with the number of bloom events per year. Statistical information for the best performing models is detailed in Table S2, the partial effects of each predictor on the anomaly of selected phenological indices are depicted, for each phenoregion, in Figs. 6-10, and a summary of all models, including relevant predictors and model predictive power, is presented in Table 2. Models predicting the phenological indices over each SWIP phenoregion showed a relatively high predictive skill, explaining between 50 and 90% of the variance of all indices except bloom initiation timing, but the significance and partial effects of each predictor varied across indices and phenoregions (see Tables 2 and S2, Figs. 6-10). Globally, EA, AMO and NO_3 were more influential predictors over the oceanic phenoregions, NAO and W were more relevant over the Coastal-Slope region, CSET and MLD_Y showed stronger partial effects over the Upwelling-influenced region, and riverine discharge was more influential over the Riverine-influenced region (see Table 2).

Table 2 – Summary of best performing generalized additive models (GAMs) used to predict phenological indices for specific phenoregions off SW Iberia, during the period 1997-2015, with indication of model explanatory power (MEP, as % variance explained) and environmental predictors, shown in descending order of relevance. Symbols $^{'}$, *, **, *** indicate p-value <0.10, <0.05, <0.01 and <0.001, respectively. Environmental variables include large-scale climate indices (AMO – Atlantic Multidecadal Oscillation; EA – Eastern Atlantic Pattern; MEI – Multivariate ENSO Index; NAO – North Atlantic Oscillation; WeMO – Western Mediterranean Oscillation), local hydrodynamic variables (CSET - cross shore Ekman transport off the western Portuguese coast; Gdn – Guadiana river discharge; Gdq – Guadalquivir river discharge), MLD_Y – annual average of mixed layer depth; MLD_{Max} – maximum annual value of mixed layer depth, and average environmental conditions preceding the initiation of the principal bloom for MLD – mixed layer depth; PAR – surface photosynthetically available radiation; NO_3 – nitrate concentration averaged within the first layer; SST – sea surface temperature; W – wind speed; V – meridional wind speed. Subscripts Y, W and S associated to predictors indicate annual, winter and upwelling-favourable season (May-September) averages, respectively. See Fig. 4 for region location, Figs. 6-10 for partial effects of individual predictors and Table S2 for detailed statistics.

Phenoregion/Phenological index	MEP (%)	Predictors
SW Oceanic phenoregion		
Chl-a peak value	90	EA_W^{**}, NO_3^{*}, MLD_{Max}^{*},V'
Principal bloom duration	63	AMO_Y^{**}, MEI_Y^{*}, NO_3^{*}
Principal bloom timing of initiation	37	PAR^{*}
Principal bloom peak timing	70	SST^{**}, W^{*}
Oceanic phenoregion		
Chl-a peak value	86	EA_W^{**}, NO_3^{*}
Principal bloom duration	95	NO_3^{**}, MLD'
Principal bloom timing of initiation	98	NO_3^{***}, MLD^{**}, EA_W^{*}
Principal bloom peak timing	77	MLD_W^{**}
Coastal-Slope phenoregion		
Number of blooms per year	58	W^{**}, NAO_W^{*}
Chl-a peak value	73	NAO_Y^{**}, Gdn_W^{**}, W'
Principal bloom duration	65	**M1** – SST^{**}, W^{**}; **M2** – $Initiation^{***}$
Principal bloom timing of initiation	47	NAO_Y^{*}, W^{*}
Principal bloom peak timing	86	W^{***}
Upwelling-influenced phenoregion		
Number of blooms per year	83	MLD_Y^{**}, V^{**}, SST^{**}
Chl-a peak value	73	MLD_Y^{***}, SST^{**}, $CSET_S^{**}$
Principal bloom duration	57	$CSET_Y^{*}$, SST^{*}
Principal bloom timing of initiation	30	$CSET_Y^{*}$
Principal bloom peak timing	50	$CSET_Y^{*}$
River-influenced phenoregion		
Number of blooms per year	79	NAO_W^{***}, Gdn_Y^{*}, MLD_Y^{*}, $WeMO_W^{'}$
Chl-a peak value	71	Gdq_W^{**}, PAR^{*}
Principal bloom duration	83	Gdq_W^{***}, MLD_Y^{**}

Over the SW Oceanic phenoregion, large scale climate indices (EA, AMO, MEI), MLD_{Max} and pre-bloom conditions were identified as predictors of the phenological indices (Fig. 6). The combined partial effects of EA_W, NO_3, MLD_{Max} and V explained 90% of the variance in Chl-a peak value, and EA_W and NO_3 represented the most influential predictors, showing negative

quasi-linear and positive linear influences, respectively. Maximum Chl-a peak values were associated with years of (high) negative EA_W, high NO_3 periods preceding the bloom onset stage, intermediate MLD_{Max} (ca. 160-200 m) and strong northerly winds (Fig. 6). AMO_Y was the most relevant predictor of bloom duration, showing a linear negative partial effect, and MEI represented a minor predictor with non-linear influences and a positive partial effect at intermediate levels (ca. -0.5 and 0.5). PAR was the only predictor of the timing of bloom initiation, showing a moderate non-linear influence and reduced predictive power. In case of bloom peak timing, SST preceding bloom initiation was the most influential predictor, showing complex non-linear effects and values below ca. 18.3 ^{o}C associated with positive anomalies in bloom peak timing (delayed Chl-a peak). W represented a minor predictor of bloom peak timing, with linear positive influences (Fig. 6).

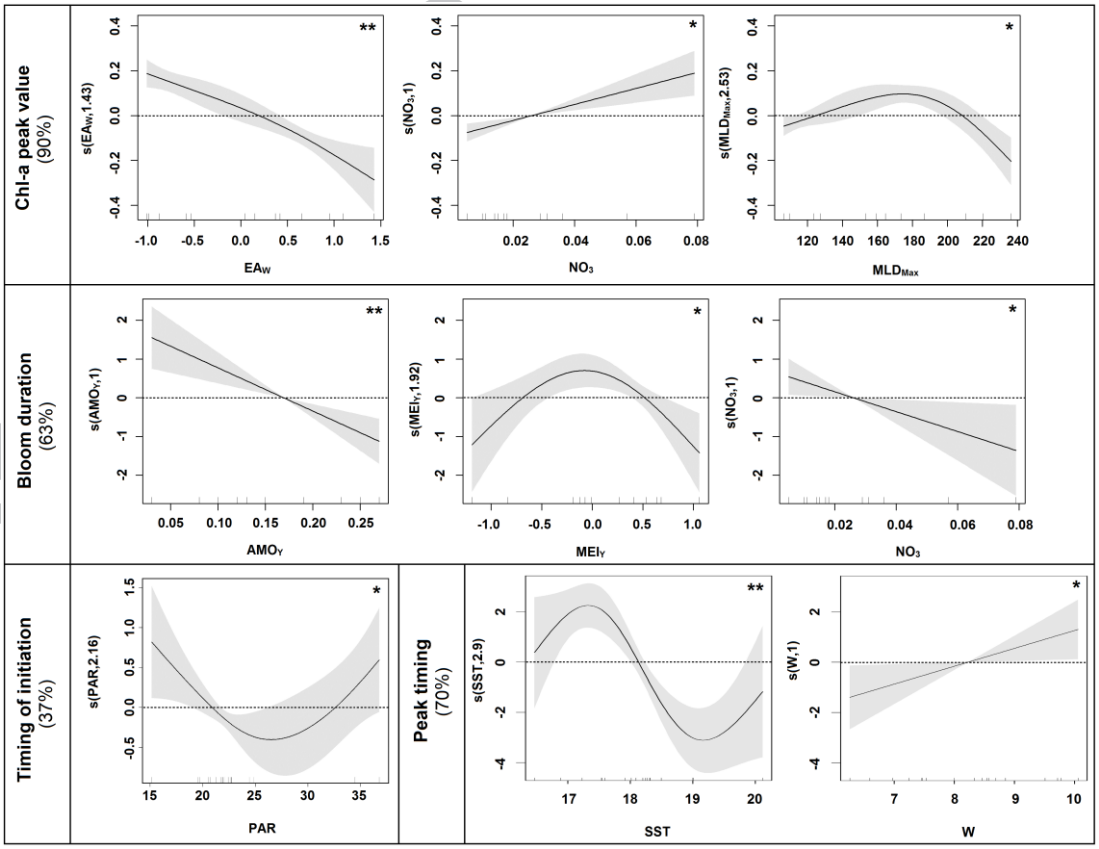

Figure 6 – Partial effects of individual environmental predictors on phenological indices over the SW Oceanic phenoregion, derived from the best performing generalized additive model (GAM). For each phenological index (model), the model explanatory power (as % of the variance explained) is shown in

brackets (after index designation); individual predictor plots are organized in descending order of their explanatory power, and the significance level (p-value) of each predictor is denoted by asterisk symbols (top right), where ‘, *, **, *** indicate p-value <0.10, <0.05, <0.01 and <0.001, respectively. For each plot, predictor values are represented on the x-axis, and short vertical lines indicate the exact predictor observations. Values on the y-axis represent the partial effects that the specific predictor has on the anomaly of the phenological index, holding the remaining predictors constant. On the y-axis, numbers in parentheses represent the effective degrees of freedom (edf), indicative of the smoothness of each function. Values of edf equal to 1 represent a linear effect of the predictor and values higher than 1 indicate progressively stronger non-linear effects. Solid lines indicate the smoothed non-parametric trends, and grey shaded areas designate the point-wise 95% confidence intervals. Regions where the 95% CI bands enclose the x-axis line indicate no significant effects of the predictor. At each stage, the value of the dependent variable (phenological index) is given by the sum of the partial effects of all predictors plus a constant. (See Table 2 for environmental variables abbreviations and S2 for detailed statistics).

Over the Oceanic region, EA_W and NO_3 preceding bloom onset were also the most relevant predictors of Chl-a peak value. In contrast with the SW Oceanic region, NO_3 effects were non-linear, and positive for NO_3 below ca. 0.4 µM. Higher Chl-a peak values were therefore associated with years of high negative EA_W and intermediate NO_3 values (Fig. 7). NO_3 and MLD conditions preceding bloom onset were significant predictors of bloom duration. NO_3 partial effects were significant and negative above a threshold of ca. 0.4 µM (shorter blooms) and MLD effects, less significant, were positive during periods of MLD higher than ca. 60 m. For the timing of bloom initiation, NO_3 and MLD preceding bloom onset were the most influential predictors. The former showed highly significant non-linear effects, positive (delayed bloom initiation) for NO_3 higher than 0.4 µM, and MLD and EA_Y presented minor linear positive influences on bloom initiation. MLD_W was the single predictor of bloom peak timing over this phenoregion, showing complex non-linear influences, mostly positive for years of MLD_W higher than ca. 100 m (Fig. 7).

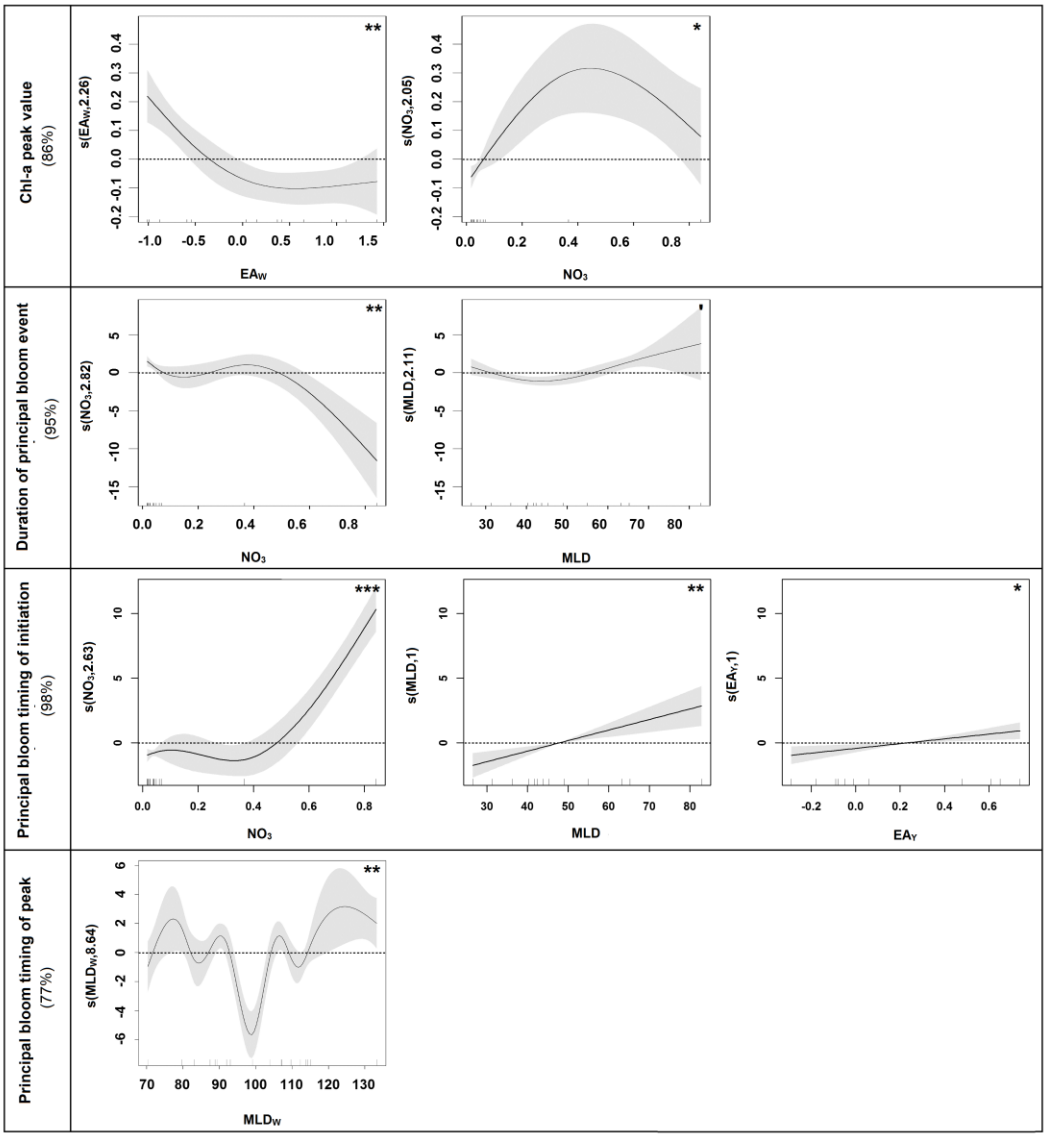

Figure 7 – Partial effects of individual environmental predictors on phenological indices over the Oceanic phenoregion, derived from the best performing generalized additive model (GAM). See caption of Figure 6 for further details.

Over the Coastal-Slope phenoregion, NAO and W preceding bloom initiation were the most influential predictors affecting all (W) or most (NAO) phenological indices (Fig. 8). W showed a negative linear influence on the number of blooms per year, and NAO_W presented positive effects during negative NAO years. For Chl-a peak value, NAO_Y and Gdn_W were the most relevant predictors, exerting linear negative and positive effects, respectively; high Chl-a peak values were therefore associated with years of high negative NAO and high riverine discharge. W showed minor influences, with positive effects under W < ca. 7.5 m s^{-1}. SST and W preceding

bloom initiation were significant predictors of bloom duration, both showing linear to quasi-linear positive effects on this index (see Bloom duration M1, Fig. 8). However, over the Coastal-Slope phenoregion, timing of bloom initiation was a best predictor of bloom duration (see Bloom duration M2, Fig.8). For the timing of bloom initiation, NAO_Y and W were significant predictors, showing moderate linear positive and negative influences, respectively. W was the single predictor of bloom peak timing over this phenoregion, showing complex non-linear influences; negative anomalies in this index were mostly associated with years of extreme values of W preceding principal bloom initiation (Fig. 8).

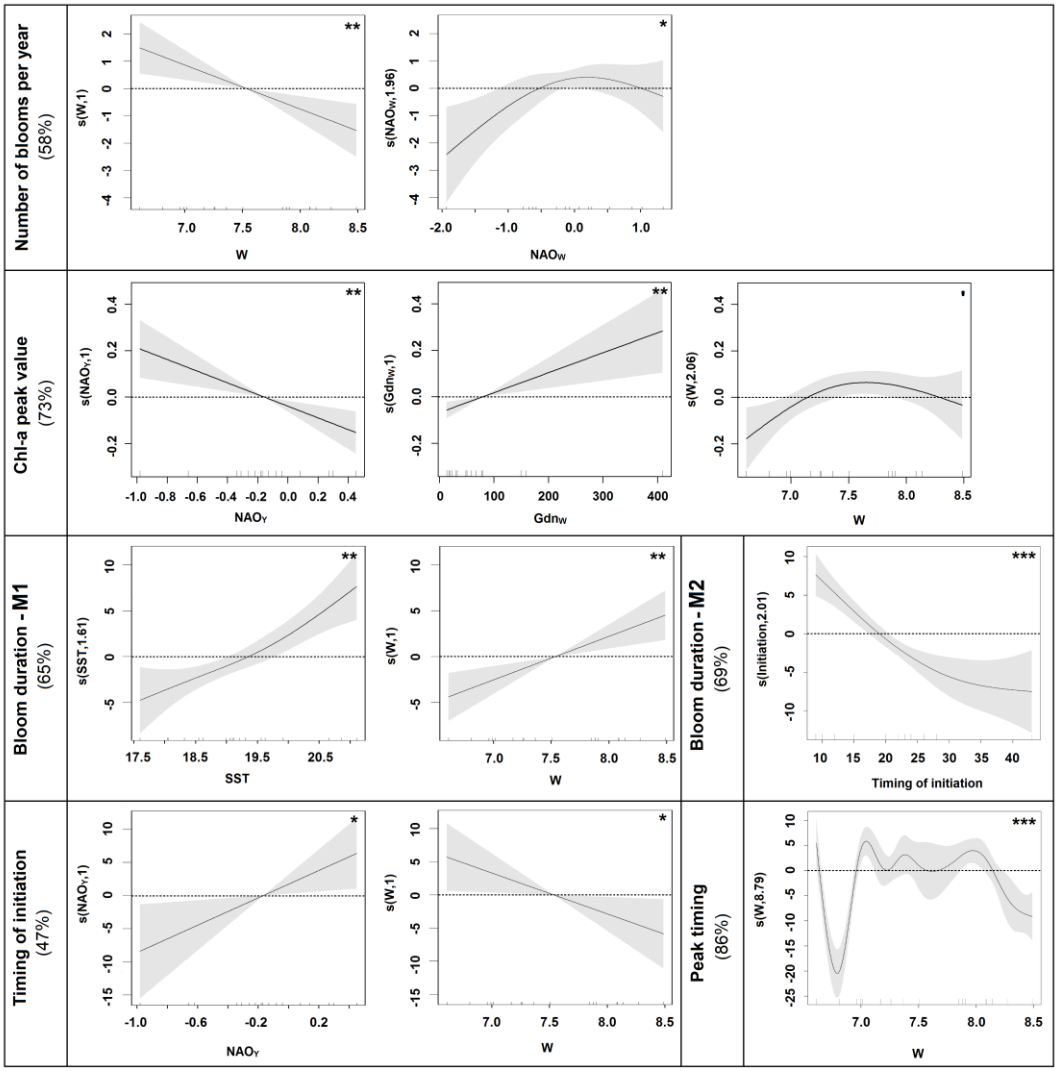

Figure 8 – Partial effects of individual environmental predictors on phenological indices over the Coastal-Slope phenoregion, derived from the best performing generalized additive model (GAM). See caption of Figure 6 for further details.

Over the Upwelling-influenced region, the number of bloom events per year was predicted using a combination of MLD_Y, V and SST (Fig. 9). MLD_Y and V showed linear opposing influences, negative and positive, respectively, while SST showed a positive influence below ca. 19.5 ^oC. For Chl-a peak value, SST and $CSET_S$ showed linear to quasi-linear negative effects while MLD_Y, the most influential predictor, presented mostly positive influences for MLD higher than ca. 43 m. Higher Chl-a peak values were associated with years of high MLD_Y, strong upwelling intensity during the upwelling favourable period (negative $CSET_S$), and low SST values preceding the initiation of the principal bloom. In case of bloom duration, $CSET_Y$ and SST were the most relevant predictors; SST showed negative linear effects and $CSET_Y$ exhibited non-linear effects, negative for $CSET_Y$ higher than ca. -400 $m^3 s^{-1} km^{-1}$ coastline. $CSET_Y$ was also the single predictor of bloom initiation and peak timings, showing non-linear effects on these indices. Years with intermediate annual average upwelling intensities (-400 < $CSET_Y$ <-300 $m^3 s^{-1} km^{-1}$ coastline) were generally associated with a moderate delay in bloom initiation and peak timing, and extreme upwelling intensities ($CSET_Y$ < ca. -500 $m^3 s^{-1} km^{-1}$ coastline) were related with earlier Chl-a peak values (Fig. 9).

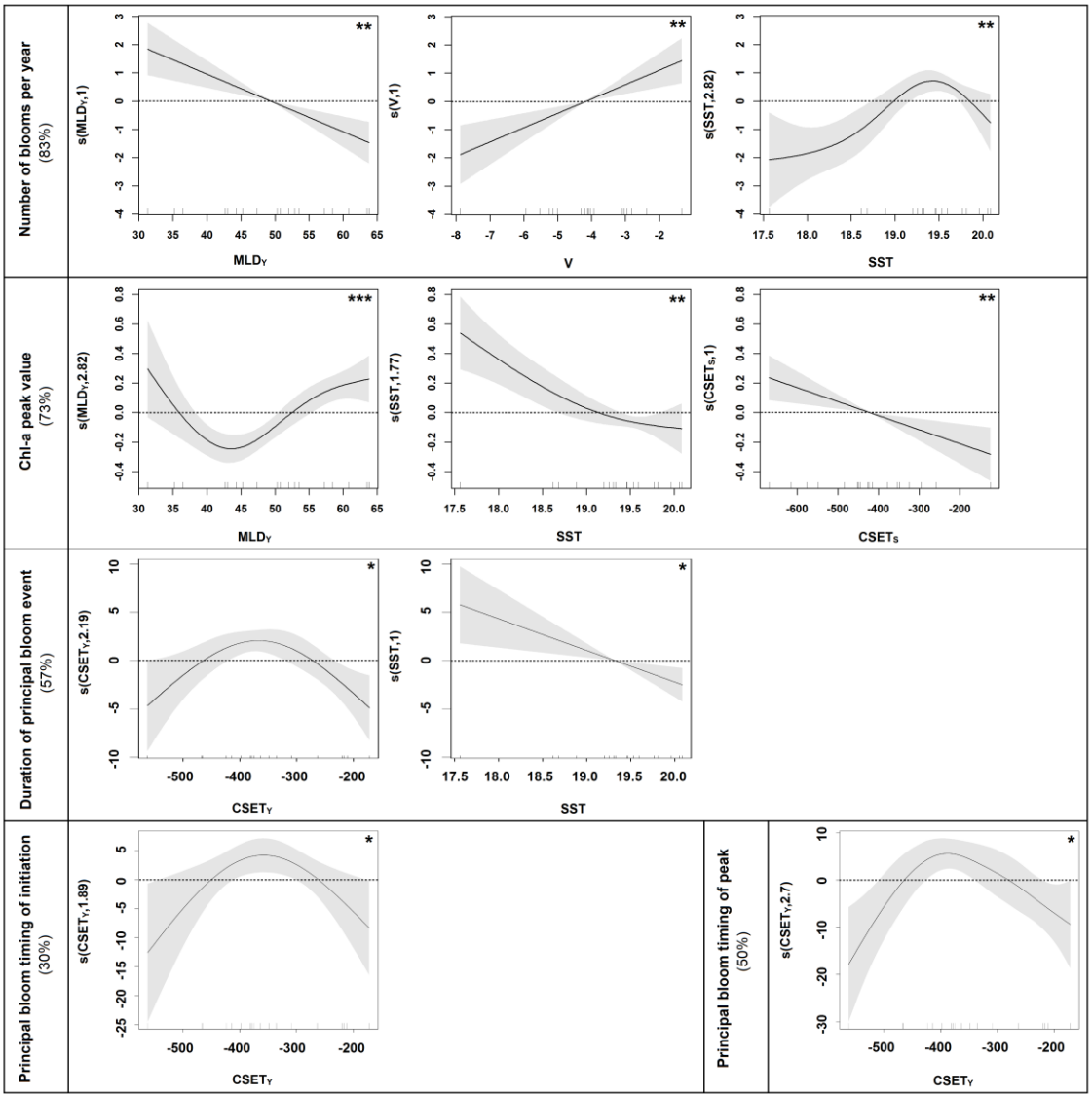

Figure 9 – Partial effects of individual environmental predictors on phenological indices over the Upwelling-influenced phenoregion, derived from the best performing generalized additive model (GAM). See caption of Figure 6 for further details.

Over the River-influenced phenoregion, riverine discharge was a significant predictor of most phenological indices. NAO_W was the most influential predictor of the number of blooms per year over this region, showing a linear positive effect. Partial effects of Gdn_Y and MLD_Y on this index were minor and non-linear, positive for Gdn_Y above ca. 75 m^3 s^{-1} and MLD_Y below ca. 23m (Fig. 10). For Chl-a peak value, Gdq_W was the most significant predictor, with a non-linear positive influence, and PAR showed minor negative linear effects on this index. In case of bloom duration, Gdq_W and MLD_Y were identified as the most influential predictors, showing

non-monotonic effects. Gdq_W values lower than ca. 750 m^3 s^{-1} showed positive effects on bloom duration (negative effects for higher values), and MLD_Y values lower than ca. 25 m showed negative effects on this index (Fig. 10). No significant predictive models were derived in case of bloom initiation and peak timings over the River-influenced phenoregion.

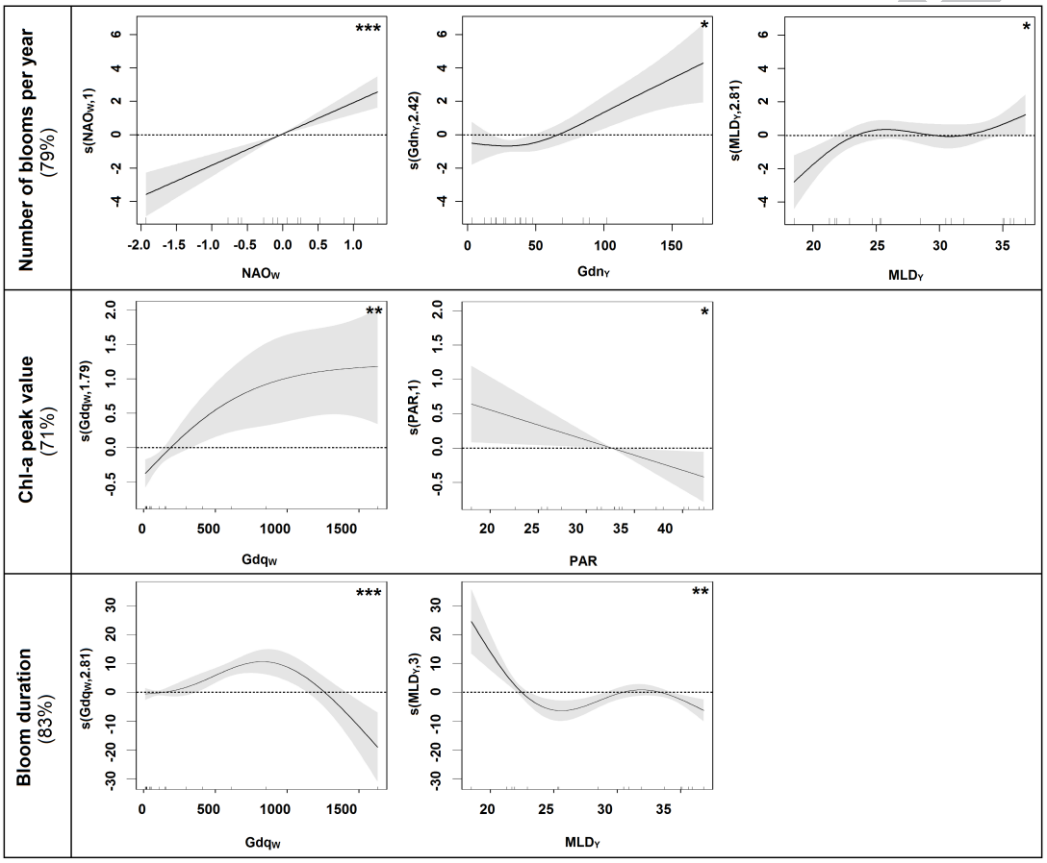

Figure 10 – Partial effects of individual environmental predictors on phenological indices over the River-influenced phenoregion, derived from the best performing generalized additive model (GAM). See caption of Figure 6 for further details.

4 - Discussion

An 18-year time series of OCRS Chl-a was used to evaluate phytoplankton phenological patterns over the SWIP area, and subsequently applied as the basis for an unsupervised, objective partition of the study area. In addition to the multiple potential applications associated with the delineation of ecosystem partitions (e.g., biogeochemical modelling,

marine spatial planning, ecosystem-based management; see review by Krug et al., 2017a), this SWIP partition was specifically used as a framework for discriminating the environmental drivers of phytoplankton phenology over a complex marine domain. Most phytoplankton global and regional phenology studies have addressed indices related to the principal annual bloom event (e.g., spring bloom), including bloom magnitude, timing and duration (e.g., Henson et al., 2006, 2010, 2018; Racault et al., 2012; Sapiano et al., 2012; Soppa et al., 2016; Kostadinov et al., 2017; see Friedland et al., 2016, 2018). The number of studies evaluating multiple bloom events per year, usually two (e.g., spring and autumn blooms; Winder and Cloern, 2010; Martinez et al., 2011; Sapiano et al., 2012; Chiswell et al., 2013; González Taboada and Anadón, 2014; Land et al., 2014; Racault et al., 2015, 2017; Friedland et al., 2016) is, in fact, limited. Over complex coastal marine domains, such as upwelling-influenced areas with multiple bloom events per year (Foukal and Thomas, 2014), a more penetrating analysis of phytoplankton phenology is required. In the present study, in addition to the indices associated to principal blooms, other indices were used, including the number of bloom events and the total duration of all events per year, as a way to enhance the comprehensive understanding of the processes shaping phytoplankton phenology, and their responses to environmental variability and change (Vargas et al., 2009). Our strategy delineated phenoregions over the SWIP domain, with distinct phenological indices and variable interannual trends and interactions with environmental variables, enhancing the advantage of a partition-based strategy to investigate phytoplankton phenology over heterogeneous regions (Zhao et al., 2013; Foukal and Thomas, 2014; Henson et al., 2018). Morever, the use of GAM analyses allowed the identification of relevant predictors of phytoplankton phenology, incorporating multiple, linear and complex non-linear, linkages between phenological indices and environmental determinants.

4.1 Phenology-based partition of the marine domain off SW Iberia

Our phenology-based static partition objectively delineated five regions over the SWIP area, including two over the oceanic domain and three phenoregions over the coastal and continental slope areas. This partition contrasts with global scale partitions, which subjectively imposed pre-defined rectilinear boundaries over the study region (e.g., Sherman, 1994; Longhurst, 2007; Spalding et al., 2007, 2012; see review by Krug et al., 2017a). The phenology-based partition showed a remarkable spatial coherency, with clear coastal-offshore and latitudinal gradients. These gradients were also visible in previous unsupervised partitions, including the macroscale dynamic classification of the European seas (Hoepffner and Dowell, 2005), and the static (Krug et al., 2017b) and dynamic mesoscale SWIP partitions (Krug et al., 2018). The number of phenoregions was lower than the number of dynamic abiotic-based environmental provinces (up to 12; Krug et al., 2018), and static regions based on EOF dominant modes of Chl-a variability (nine; Krug et al., 2017b), previously reported for the study area. Likewise, compared with the results of our study, a higher number of coastal regions (four) was identified in partition studies addressing the GoC (Navarro and Ruiz, 2006; Muñoz et al., 2015).

Our phenology-based partition clearly delimited the SWIP region with strongest upwelling intensity (Relvas et al., 2007), the Upwelling-influenced phenoregion, where upwelling patterns strongly modulate abiotic variables, phytoplankton biomass and annual cycles (Navarro and Ruiz, 2006; Goela et al., 2014; Krug et al., 2017b, 2018). The SWIP region with strongest influence of riverine discharges (Vargas et al., 2003; García-Lafuente et al., 2006; Caballero et al., 2014) was also differentiated, as the River-influenced phenoregion. Previous unsupervised partitions of the SWIP area also reflected the influence of coastal upwelling and riverine discharges (Navarro and Ruiz, 2006; Muñoz et al., 2015; Krug et al., 2017b, 2018). Over the ocean domain, our unsupervised objective partition differentiated the southwesternmost

area (SW Oceanic) from the other oceanic areas (Oceanic phenoregion) (Fig. 4). These open ocean sectors were also differentiated in previous SWIP partitions, based on Chl-a (Krug et al., 2017b) and abiotic variables (Krug et al., 2018). The former sector was previously associated with "low to very low Chl-a" (Hoepffner and Dowell, 2005), consistent with the oligotrophic nature of the eastern North Atlantic Subtropical Gyre province (Longhurst, 2007; Teira et al., 2005).

4.2 Phytoplankton phenological patterns off SW Iberia

During this 18-year study period, phytoplankton phenology patterns showed striking differences between open ocean and coastal phenoregions (see Fig. 3), with increasing variability over the latter (Figs. 4 and 5). Despite the significant differences in the number of bloom events per year and bloom duration between open ocean and coastal phenoregions (Figs. 5A and 5D), the duration of all blooms events per year was similar across phenoregions (Fig. 5B). This similarity indicates that the environmental conditions that promote positive phytoplankton net growth rates (i.e., biomass accumulation) are more sustained over the open ocean and more intermittent over coastal areas. Indeed, coastal areas are highly-heterogeneous transition zones (Cloern and Jassby, 2008; Winder and Cloern, 2010), with strong physical and chemical variability at short temporal scales, naturally imposed by the proximity with terrestrial sources and topographic irregularities, including riverine plumes, coastal upwelling events, and mesoscale circulation features (García-Lafuente and Ruiz, 2007; Relvas et al., 2007; Criado-Aldeanueva et al., 2009; Caballero et al., 2014).

Over the open ocean SWIP phenoregions, phytoplankton presented a unimodal annual cycle, and bloom events (ca. 1 $year^{-1}$) were prolonged (ca. 18-23 weeks), typically initiated around November, peaking in March and terminating in April. These phenological properties, including

the absence of secondary autumn blooms, were consistent with those usually reported in global (Kahru et al., 2010; Cole et al., 2012; D'Ortenzio et al., 2012; Racault et al., 2012; Sapiano et al., 2012; Cabré et al., 2016) and basin-scale phenological studies which included the SWIP area (Siegel et al., 2002; Ueyema and Monger, 2005; Henson et al., 2009; Brody et al., 2013; Ferreira et al., 2014; Land et al., 2014; González Taboada and Anadón, 2014). Yet, some studies reported delayed bloom initiation and shorter primary blooms for the oceanic SWIP area (Friedland et al., 2016, 2018). Over open ocean phenoregions, blooms mostly initiated during the MLD deepening stage (ca. one month after MLD deepening onset timing), some blooms even terminated during this period, and mostly peaked during the MLD shoaling phase. I_m values at the time of bloom initiation (2.33±0.70 mol photons m^{-2} d^{-1}), usually interpreted as phytoplankton compensation irradiance, were consistent with published values of community compensation irradiance (ca. 1.0 - 3.6 mol photons m^{-2} d^{-1}; Siegel et al., 2002; Henson et al., 2006; Zhao et al., 2013). Despite decreasing PAR, photoperiod and I_m values during the MLD deepening stage, light conditions during this period were sufficient for exploitation by phytoplankton of the new supply of nutrients entrained into the euphotic zone, leading to late winter-spring blooms. These events have been typically reported for subtropical regions, and interpreted as a sign of nutrient limitation (Follows and Dutkiewicz, 2002; Siegel et al., 2002; Longhurst, 2007). Conversely, over temperate and sub-polar regions (Henson et al., 2009; Lacour et al., 2015; Martinez et al., 2011; González Taboada and Anadón, 2014; Sallée et al., 2015), delayed spring blooms, usually initiated during the MLD shoaling phase, are interpreted as a sign of light limitation, in accordance with the critical depth hypothesis (Sverdrup, 1953).

Even if, from a bottom-up perspective, MLD deepening could effectively increase nutrient availability promoting bloom initiation, our data set does not allow the rejection of other alternative bloom initiation hypothesis (see reviews by Fischer et al., 2014; Franks, 2014; Chiswell et al., 2015; Cole et al., 2015 and references therein), including the critical turbulence

hypothesis (Huisman et al., 1999), eddy-driven stratification hypothesis (Mahadevan et al., 2012) and the disturbance-recovery hypothesis (Behrenfeld, 2010; Boss and Behrenfeld, 2010; Behrenfeld et al., 2013). The loss-driven hypothesis could support the initiation of phytoplankton blooms over these phenoregions (see Navarro et al., 2012; Krug et al., 2017b). Subsequent Chl-a increase and peak-values during the MLD shoaling phase probably reflect the effects of light-stimulation on phytoplankton instantaneous growth rates (e.g., Sverdrup, 1953; Behrenfeld and Boss, 2014; Itoh et al., 2015). However, thoroughly testing the different hypotheses underlying bloom initiation, including the critical depth hypothesis (Sverdrup, 1953), would effectively require the measurement of short-term variability in vertical gradients of turbulence, which could allow the differentiation between the thoroughly mixed top layer (surface turbulent layer) and MLD derived from hydrographic data (see Franks, 2014), and *in situ* growth and mortality rates of phytoplankton.

Over the Coastal-Slope phenoregion, Chl-a also presented a unimodal annual cycle but bloom duration (2-25 weeks), number of bloom events per year (1-7 events $year^{-1}$) and timing of bloom initiation were highly variable. Compared with open ocean phenoregions, bloom initiation was delayed over the Coastal-Slope region, as also reported for other marine domains (e.g., Liu et al., 2014). Further, a relatively large proportion of bloom events were initiated during the MLD shoaling phase (39% principal blooms and 60% all events), sometimes specifically during the upwelling-favourable period (May-September; Relvas et al., 2007; 14% principal blooms and 35% all events). These results are probably a reflection of reduced I_m values, due to higher turbidity (see Krug et al., 2017b, 2018), and increased nutrient availability due to the influence of continental sources (e.g., riverine discharge: Caballero et al., 2014; Krug et al., 2018; submarine groundwater discharges: Piló et al., 2018 and references therein) and upwelling events (Krug et al., 2017b, 2018).

In contrast to previous phenoregions, over the Upwelling-influenced region, Chl-a presented a bimodal annual cycle (Fig. 4E) and this region showed the highest mean number of bloom events per year (4.4 events year^{-1}). Frequent phytoplankton blooms, associated with enhanced nutrient availability driven by upwelling, have also been reported for western Iberia (e.g., Moita, 2001; Picado et al., 2014; Bode et al., 2015; Krug et al., 2017b) and other coastal upwelling systems (e.g., Carr and Kearns, 2003; Foukal and Thomas, 2014; Corredor-Acosta et al., 2015). In contrast to classic sustained phytoplankton blooms, in coastal upwelling systems, diatom blooms usually occur as a series of separate, recurrent short blooms, separated by upwelling-relaxation periods, when dinoflagellates often bloom (Pitcher et al., 2010; Smayda and Trainer, 2010). Over the Upwelling-influenced phenoregion, a large fraction of bloom events were initiated during the MLD shoaling phase (72% principal blooms and 80% all events), specifically during the upwelling-favourable period (33% principal blooms and 61% all events). Phenological studies addressing coastal upwelling systems have also reported a close linkage between phytoplankton phenology and upwelling intensity and patterns, with blooms mostly initiating during the upwelling active period (Henson and Thomas, 2007; Foukal and Thomas, 2014; see next section).

Over the River-influenced phenoregion, phytoplankton presented a unimodal annual cycle and, as for the other coastal phenoregions, multiple short bloom events along the year (up to 6 bloom events year^{-1}). This phenoregion receives multiple freshwater discharges, from the Guadiana and Guadalquivir rivers, coastal wetlands and lagoons (Ria Formosa and Doñana park), and small estuarine systems and rivers, including Piedras, Tinto-Odiel (northeastern GoC), Oued Loukkos and Sebou (southeastern GoC). Over this turbid Case-II water masses, satellite-derived Chl-a retrievals could represent an overestimate, especially during high discharge periods (IOCCG, 2000; Caballero et al., 2014; Picado et al., 2014). However a direct relationship between river discharge and Chl-a was previously reported for this area (coastal northeastern GoC), using both OCRS (Navarro and Ruiz, 2006; Caballero et al., 2014; Krug et

al., 2017b; Sala et al., 2018) and *in situ* collected data (Prieto et al., 2009; Huertas et al., 2006). In comparison with the other coastal phenoregions, most bloom events initiated earlier, during the MLD deepening phase (as for open ocean regions), and a smaller fraction initiated during the MLD shoaling phase (33% principal blooms and 54% all events). Mechanisms underlying the positive effects of riverine discharge include its influence as a nutrient source (Cravo et al., 2006; Reul et al., 2006), and its role as a promoter of water column stratification. Despite high turbidity (Caballero et al., 2014), due to salinity stratification, MLD shoaling could be anticipated within the area of influence of riverine plumes (Barbosa and Chícharo, 2011), thereby enabling earlier bloom initiation, in respect with the Coastal-Slope phenoregion.

4.3 Phytoplankton phenology off SW Iberia: interannual patterns and environmental drivers

During the 18-year study period, significant interannual trends in putative phytoplankton drivers, previously reported by others, included a linear intensification of wind speed over all regions (see Fig. S21 in González Taboada and Anadón, 2014), an increase in northerly winds and upwelling intensity over the Upwelling-influenced region, a complex non-linear pattern in riverine discharge and an increase in MLD over the coastal phenoregions (see Krug et al., 2017b and references therein). Despite the generalized ocean warming observed and anticipated for the study area (Krug et al., 2017b; Baptista et al., 2017), no significant trends in SST were detected during our study period. Furthermore, unreported trends over the SWIP area were also detected, including linearly increasing delays in MLD deepening (over open ocean phenoregions) and shoaling onsets (except SW Oceanic), monotonic increases in PAR over all phenoregions, and linear increases in NO_3 over all except the Upwelling-influenced region. Notwithstanding the significant trends identified in individual environmental variables, strong interannual variability patterns in phenological indices were not detected. This could be associated with the resilience of phytoplankton to environmental variability. Moreover,

phytoplankton act as an integrator of alterations in multiple drivers, some with opposing effects, potentially showing slower rates of change than their drivers (Henson et al., 2017).

Taking into consideration the region-specific linkages between Chl-a and these environmental variables over SWIP (see Krug et al., 2017b and references therein), alterations in phytoplankton phenological indices are expected to occur during the study period, and vary among phenoregions. Indeed, GAM analyses revealed across-region differences in interannual patterns of phenological indices and their linkages with large-scale climate indices, local-scale hydrological processes and ocean abiotic variables. Yet, as pointed by Krug et al. (2017b), significant associations between phenological indices and environmental variables (predictors) may not necessarily represent causation, and should be interpreted with caution, even when plausible mechanistic relationships are proposed. The inclusion of other potential drivers of phytoplankton phenology, such as abiotic environmental variables (e.g., heat fluxes, eddy kinetic energy; Yamada and Ishizaka, 2006; Song et al., 2010, 2011; Zhao et al., 2013; Cole et al., 2015; Lacour et al., 2015), as well as top-down controls (e.g., grazing, viral lyses, sedimentation; e.g., Behrenfeld, 2014; Friedland et al., 2016; Martinez et al., 2016; Zarubin et al., 2017), would likely promote a more robust understanding of phytoplankton phenology and controls over the SWIP region.

4.3.1 Open Ocean phenoregions

GAMM analysis identified complex non-linear interannual patterns in bloom peak timing and duration, more notable for the duration of the accumulation phase, over the SW Oceanic region, and no significant trends over the Oceanic region (Fig. S4). Previous studies, based on linear analysis, a stiffer approach, reported no significant trends in spring bloom duration, magnitude and initiation timing over the SWIP region (Racault et al., 2012; Land et al., 2014).

Yet, Kahru et al. (2010) detected a linearly increasing delay in bloom peak timing over this region. Further, other studies (González Taboada and Anadón, 2014; Zhang et al., 2017; Friedland et al., 2018) also reported significant but spatially variable, in some cases contrasting, linear trends, for both bloom magnitude, timing and duration over the SWIP area, thus supporting the relevance of a phenoregion-based analysis. Over the oceanic regions, timing of bloom initiation and bloom duration were not correlated, in contrast with previous studies referring that early blooms tend to last longer (e.g., Racault et al., 2012; González Taboada and Anadón, 2014; Friedland et al., 2016, 2018).

Phenological variability over the oceanic phenoregions was related with multiple large-scale climate indices, MLD values, and pre-bloom conditions. The interpretation of phenology-climate linkages is not simple since climate indices can affect, directly and indirectly, multiple phytoplankton drivers including bottom-up and top-down controls (e.g., Friedland et al., 2016; Martinez et al., 2016). Further, their effects on specific drivers can vary, depending on season, geographic location and local atmospheric forcing, and interact (see Krug et al., 2017b). Over the two oceanic phenoregions, high magnitude blooms were strongly associated with high negative EA_W years. EA represents the second prominent mode of inter-annual variability over the North Atlantic/Europe. This index, particularly important over southern Europe and correlated with SST off west Iberia (Santos et al., 2011), was previously associated with Chl-a variability over SWIP coast and slope regions (Krug et al., 2017b). The stimulation of bloom magnitude (i.e., Chl-a peak value) under negative EA_W years could probably reflect an indirect beneficial effect of increased mixing intensity, during low SST years.

Over the SW Oceanic region, prolonged blooms were detected during high negative AMO_Y and low MEI ($-0.5 < MEI_Y < 0.5$) years. High negative AMO periods are usually associated with a reduction in water column stratification and SST over the North Atlantic (Martinez et al., 2009), also off Iberia (Santos et al., 2011). Therefore, enhanced vertical advection of nutrients

into the euphotic zone during these years probably supported longer bloom events over this relatively oligotrophic nutrient-limited phenoregion (Krug et al., 2018). AMO variability was also negatively associated with Chl-a over the SWIP open ocean domain (see Krug et al., 2017b), and considered a relevant driver of phytoplankton biomass (Martinez et al., 2009) and phenology over the North Atlantic basin (D'Ortenzio et al., 2012; Martinez et al., 2016). The SW Oceanic phenoregion was the only region depicting significant relationships between MEI and phytoplankton phenology. ENSO patterns and MEI have been referred as strong determinants of interannual variability in phytoplankton biomass and phenology over tropical regions, namely in the Pacific Ocean (Yoo et al., 2008; Boyce et al., 2010; D'Ortenzio et al., 2012; Racault et al., 2012; Foukal and Thomas, 2014; Corredor-Acosta et al., 2015). However, recent studies also reported significant MEI effects, at a global scale, on Chl-a (von Schuckmann et al., 2017) and phytoplankton phenology (Racault et al., 2017), sometimes with opposing regional effects. For non-tropical sectors of North Atlantic, positive MEI periods were associated with intensified winds, decreased light availability, and reduced and delayed phytoplankton growth. Yet, weaker and spatially variable linkages between MEI and phytoplankton phenology were detected over the SWIP area (Racault et al., 2017).

In contrast to previous studies, no significant relationships between phenological indices and NAO variability were detected over the oceanic regions. For most of the eastern-central North Atlantic, shorter blooms (Racault et al., 2012), with earlier initiation (Ueyama and Monger, 2005; Friedland et al., 2016) have been observed during high negative NAO periods, and usually associated with decreased (western) wind-induced vertical mixing and higher I_m. However, over the SWIP oceanic phenoregions, this NAO effect does not necessarily apply due to a relatively stronger nutrient limitation (see Krug et al., 2017b, 2018). In fact, the lack of significant relationships between NAO and bloom initiation timing was also reported for the the subtropical North Atlantic (Henson et al., 2009).

Environmental conditions preceding bloom initiation and MLD annual maximum (MLD_{Max}), mean annual (MLD_Y) and mean winter (MLD_W) values were also significant predictors of phytoplankton phenology over the SWIP oceanic phenoregions, reinforcing the relevance of vertical mixing and nutrient limitation over these regions (Krug et al., 2017b, 2018). NO_3 conditions preceding bloom initiation were generally related with phenology over both oceanic regions. Over SW Oceanic phenoregion, high NO_3 values were positively and linearly associated with bloom magnitude (i.e., Chl-a peak value), a signature of intensified oligotrophic conditions over this oceanic region (Krug et al., 2018). Over the SW Oceanic region, MLD_{Max} higher than ca. 200 m showed a negative influence on bloom magnitude, probably a result of dilution caused by the entrainment of phytoplankton-free deep water; yet, values between 160 m and 200 m showed a positive influence on bloom magnitude. For the Oceanic region, high MLD values prior to bloom initiation were related with longer bloom events. These influences of MLD on phenological indices can be probably explained by increased nutrient fluxes into the euphotic zone, under higher mixing conditions, but also by a decline in phytoplankton grazing-induced mortality (see Behrenfeld and Boss, 2014). Previous studies have also reported strong linkages between phytoplankton phenology and MLD or its timing metrics (e.g., initiation of mixed layer shoaling), in some cases mediated by wind forcing (Ueyama and Monger, 2005; Yamada and Ishizaka, 2006; Henson et al., 2006; Martinez et al., 2011; González Taboada and Anadón, 2014). These linkages were detected over North Atlantic (e.g., Follows and Dutkiewicz, 2002; Siegel et al., 2002; Henson et al., 2009; Martinez et al., 2011; Zhai et al., 2011; Lavigne et al., 2013; Zhao et al., 2013; Ferreira et al., 2015; Lacour et al., 2015) and other marine domains (e.g., Yamada and Ishizaka, 2006; Yoo et al., 2008; Chiswell et al., 2013; Lavigne et al., 2013; Shiozaki et al., 2014), with usually positive effects in subtropical (nutrient limited) and negative effects in temperate-polar (light limited) areas.

4.3.2 Coastal phenoregions

Interannual patterns in phenological indices varied across the three coastal phenoregions, reflecting the higher complexity of environmental forces driving phytoplankton biomass and phenology over SWIP coastal areas (see Krug et al., 2017b, and references therein). GAMM analysis identified an increasingly delay in the timings of bloom initiation and termination for the River-influenced region, and linear increases in bloom duration and its deceleration phase for the Coastal-Slope and Upwelling-influenced regions, respectively (see Fig. S4). Phenological studies addressing the SWIP region generally used global or large scale spatial coverages (Kahru et al., 2010; Racault et al., 2012; González Taboada and Anadón, 2014; Land et al., 2014; Zhang et al., 2017), thus not allowing the inspection of trends in phenology over specific SWIP coastal domains. The interannual variability patterns in phytoplankton phenology and underlying environmental drivers reported for other coastal systems are extremely variable, depending on ecosystem properties, environmental alterations and phytoplankton controls, being further affected by variable methodological approaches (e.g., North Sea: Edwards and Richmond, 2004; Wiltshire and Manly, 2004; Wiltshire et al., 2008; Kromkamp and van Engeland, 2010; Baltic Sea: Groetsch et al., 2016; Kahru et al., 2015; Northwest Atlantic shelves: Song et al., 2010; Zhao et al., 2013). As example, variable interannual patterns in phenological indices and multiple environmental drivers have been reported for different areas within the upwelling-influenced California Current System (Kim et al., 2009; Henson and Thomas, 2007; Foukal and Thomas, 2014), supporting the need for region-oriented analyses of phytoplankton phenology over coastal domains (Foukal and Thomas, 2014).

Over the Coastal-Slope SWIP phenoregion, NAO and/or wind speed (W) prior to bloom initiation, not influential over the oceanic regions, were the most significant predictors of all phenological indices. High negative NAO years were associated with a reduction in bloom frequency per year, higher Chl-a peak values and antecipated bloom initiation. NAO variability

has been associated with changes in several coastal variables and processes over SWIP and adjacent areas, and is positively correlated with SST and upwelling intensity over the west Iberia (deCastro et al., 2006; Santos et al., 2011; Pardo et al., 2011; Krug et al., 2017b), and negatively related to zonal westerly winds, wave height (Kumar et al., 2016), storminess (Plomaritis et al., 2015), precipitation (Martin-Vide and Lopez-Bustins, 2006), and riverine discharge over the SWIP area (Krug et al., 2017b). Thus, during negative NAO periods, increased availability of nutrients derived from intensified wind-induced mixing and riverine discharges, could partially support high magnitude blooms and earlier bloom initiation.

For the Coastal-Slope phenoregion, high W values prior to principal bloom initiation were associated with a reduction in the number of bloom events per year, but stronger, earlier and longer principal blooms. These positive influences of wind speed could represent their effects on water column mixing and nutrient availability, potentially more effective over this relatively shallower SWIP domain, in comparison with oceanic phenoregions. Longer blooms could be associated with a relative depletion in nutrient availability and increase in predator density, pre-conditioning the success of subsequent phytoplankton blooms and, therefore, reducing bloom frequency. Over this phenoregion, bloom initiation timing and duration were significantly related, as reported in previous studies (Racault et al., 2012; González Taboada and Anadón, 2014; Friedland et al., 2016, 2018), and blooms that initiated earlier lasted longer ($p<0.001$). This relationship has been explained by decreased phytoplankton mortality during anticipated bloom events (Racault et al., 2012; Friedland et al., 2016, 2018). Prolonged periods of high nutrient availability for earlier blooms, which initiated mostly during the MLD deepening phase, could further explain the negative association between bloom initiation and duration. Over this phenoregion, riverine discharge was also an influential predictor of bloom magnitude, with high Chl-a peak values associated with high Gdn_W years. High Gdq discharge periods are associated with extended turbid river plumes, thus affecting adjacent coastal areas (Caballero et al., 2014) within this phenoregion (Fig. 4A), and potentially increasing nutrient

availability (see Krug et al., 2018). Yet, these optically complex Case-II water masses could be associated with an overestimation of Chl-a (e.g., Caballero et al., 2014; IOCCG, 2000; Picado et al., 2014), partially affecting our estimates of bloom magnitude.

Over the River-influenced phenoregion, GAM analysis identified riverine discharge as an influential predictor of bloom frequency, intensity and duration. High river discharge years were generally associated with high magnitude blooms, and a high number of blooms per year. Gdq_W values up to ca. 750 m^3 s^{-1} showed also positive effects on bloom duration. Despite increased turbidity (Caballero et al., 2014), riverine-driven inputs in dissolved inorganic nutrients (Cravo et al., 2006; Reul et al., 2006) possibly sustained multiple events and intensified principal blooms, during high discharge years (see Krug et al., 2017b).

Over the Upwelling-influenced region, high mean annual MLD values were associated with fewer but stronger blooms per year, probably reflecting the stimulatory effects of increased nutrient availability on primary blooms (Krug et al., 2018). Moreover, upwelling intensity was also an influential predictor of other phenological indices. High upwelling intensities (i.e., high negative $CSET_S$) and low SST values prior to the principal bloom initiation were associated with high magnitude principal blooms, and intermediate $CSET_Y$ and low SST were also related with prolonged blooms. Indeed, the longest bloom event detected over this phenoregion (18 weeks; May 2002 – Sep 2003; see Fig. S3) was associated with a period of persistently strong upwelling intensity over the west Portuguese coast (Fig. S6). These results probably reflected the effects of increased nutrient availability, associated with intense upwelling events (see Krug et al., 2017b, 2018). Positive effects of upwelling patterns and intensity on bloom timing and magnitude were reported for other coastal upwelling systems (Henson and Thomas, 2007; Foukal and Thomas, 2014; Corredor-Acosta et al., 2015). However, no significant relationships between upwelling-associated abiotic variables (e.g., SST, wind, upwelling intensity) and phytoplankton phenology were detected in some systems (Kim et al., 2009). In our study,

interestingly, no apparent additional positive effects of upwelling on phenological indices were detected for very high annual mean upwelling intensities ($CSET_Y$ < ca. -500 m^3 s^{-1} km^{-1} coastline). This could be partially explained by the increased offshore horizontal advection of coastal phytoplankton during very strong upwelling events (e.g., Pitcher et al., 2010; Foukal and Thomas, 2014; Palma et al., 2010). Under these conditions, Chl-a rich mesoscale upwelling filaments, eddies and meanders could be advected beyond the 1000 m isobath (Souza and Bricaud, 1992; Peliz et al., 2004; Sánchez et al., 2008; Krug et al., 2017b, 2018). In fact, increased advection of phytoplankton could also explain the reduction in bloom frequency under strong northerly winds (negative V) and low SST, both indicators of strong upwelling intensity. Furthermore, higher nutrient availability could also sustain prolonged blooms, resulting progressively in fewer events per year.

5 - Conclusions

An 18-year time series of satellite-derived Chl-a was used to explore phytoplankton phenology, and phenological indices were directly used for objectively partitioning the heterogeneous SWIP area. Our analysis identified five spatially coeherent phenoregions, including two open ocean and three coastal regions, with similar phenological patterns. Over the open ocean phenoregions, a single, long, low magnitude bloom per year typically initiated around November. Bloom initiation occurred during the MLD deepening phase, reflecting the relevance of nutrient limitation over these regions. Coastal phenoregions presented multiple (up to six), short bloom events throughout the year, higher intra-annual variability, and more complex linkages with environmental drivers. A significant proportion of the blooms over the Coastal-Slope phenoregion initiated during the early-MLD shoaling phase, indicating the increased relevance of light limitation, whereas over the Upwelling-influenced region, a higher fraction of blooms initiated later, during the upwelling favourable period.

Interannual patterns in phenological indices and the underlying effects of physical-chemical, coastal hydrodynamic variables, and regional and basin-scale climate indices varied across phenoregions. Despite significant interannual trends detected for multiple environmental variables, phenological indices did not exhibit strong interannual variability patterns. This could be associated with the resilience of phytoplankton to environmental variability and/or the neutralization of opposing effects of individual drivers, acting simultaneously on phytoplankton.

Overall, for the SW Oceanic and Oceanic phenoregions, large-scale climate indices (EA, AMO), along with MLD and NO_3 values preceding primary bloom events, were relevant predictors of phytoplankton phenological indices (bloom magnitude, duration and timing), supporting the relevance of nutrient limitation. Over the Coastal-Slope phenoregion, NAO and W were the most relevant predictors of phenology (bloom frequency, magnitude, duration and timing). Further, primary bloom duration was best predicted by bloom onset timing, earlier blooms lasted longer, and bloom magnitude was also positively influenced by riverine discharge. The later was the most influential predictor of phenology over the River-influenced phenoregion, affecting bloom frequency, magnitude and duration. For the Upwelling-influenced region, upwelling intensity and mean annual MLD showed stronger partial effects on phytoplankton phenology, affecting all indices.

Our results reinforce the advantage of a proper geographic partition for the analysis of phytoplankton dynamics and phenology, namely over coastal areas. The occurrence of complex, non-linear interannual patterns and linkages between environmental drivers and phenological indices, highlight the need for flexible statistical approaches, not limited to linear analyses. Globally, our phenology-based unsupervised approach promoted a biologically-relevant partition, which improved our current knowledge of phytoplankton variability patterns and controls over a complex marine domain, potentially supporting the prediction of phytoplankton responses to future environmental changes.

Acknowledgements

The authors wish to express their gratitude to Ocean Colour Climate Change Initiative (ESA), OceanColor (NASA), Copernicus Marine Environment Monitoring Service, Ocean Productivity (Oregon University) and every group that works hard to provide free and high quality products for a data-thirsty ocean science community, and to the Jawaharlal Nehru Science Fellowship to TP. This research was supported by the combination of three funding sources: PhD scholarship to LAK from the Programme Science without Borders (Conselho Nacional de Desenvolvimento Científico e Tecnológico, of the Ministry of Science, Technology and Innovation of Brazil – 237998/2012-2); training fellowship grant to LAK by the Partnership for Observation of the Global Oceans and the Scientific Committee on Oceanic Research (POGO-SCOR) Programme; and research project "Remote sensing of phytoplankton variability off South-Western Iberia: a sentinel for climate change?" - PHYTOCLIMA, funded by the Portuguese Foundation for Science and Technology (FCT, reference PTDC/AAC-CLI/114512/2009). This work is also a contribution to the activities of the National Centre for Earth Observations, of the Natural Environment Research Council of the United Kingdom.

References

Alvarez, I., Gomez-Gesteira, M., deCastro, M., Lorenzo, M. N., Crespo, A. J. C., Dias, J. M., 2011. Comparative analysis of upwelling influence between the western and northern coast of the Iberian Peninsula. Continental Shelf Research, Volume 31, Issue 5, Pages 388-399, DOI 10.1016/j.csr.2010.07.009.

Ardyna, M., Babin, M., Gosselin, M., Devred, E., Rainville, L., Tremblay, J-É., 2014. Recent Artic Ocean sea ice loss triggers novel fall phytoplankton blooms. Geophysical Research Letters, Volume 41, Pages 6207-6212, DOI 10.1002/2014GL061047

Ardyna, M., Claustre, H., Sallée, J.-B., D'Ovidio, F., Gentili, B., van Dijken, G., D'Ortenzio, F., Arrigo, K. R., 2017. Delineating environmental control of phytoplankton biomass and phenology in the Southern Ocean, Geophysical Research Letters, Volume 44, DOI 10.1002/2016GL072428.

Bakun, A., 1973. Coastal upwelling indices, west coast of North America, 1946-1971. US Dept. Commerce NOAA Technical Report NMFS-SSRF 671, pp. 1-103.

Baptista, V., Silva, P.L., Relvas, P., Teodósio, A., Leitão, F., 2017. Sea surface temperature variability along the Portuguese coast since 1950. International Journal of Climatology, DOI 10.1002/joc.5231.

Barbosa, A. B., Chícharo, M. A., 2011. Hydrology and Biota Interactions as Driving Forces for Ecosystem Functioning, in: Wolanski, E., McLusky, D. S. (Eds.) Treatise on Estuarine and Coastal Science, Volume 10, Ecohydrology and Restoration, Elsevier, pp. 7-47, DOI 10.1016/B978-0-12-374711-2.01002-0.

Barth, J.A., Menge, B.A., Lubchenco, J., Chan, F., Bane, J.M., Kirincich, A.R., McManus, M.A., Nielsen, K.J., Pierce, S.D., Washburn, L., 2007. Delayed upwelling alters nearshore coastal ocean ecosystems in the northern California current. Proceedings of the National Academy of Sciences of the United States of America, Volume 104, Issue 10, Pages 3719-3724, DOI 10.1073/pnas.0700462104

Behrenfeld, M.J., Boss, E.S., 2014. Resurrecting the ecological underpinnings of ocean plankton blooms. Annual Review of Marine Science, Volume 6, Pages 167–194, DOI 10.1146/annurev-marine-052913-021325

Behrenfeld, M.J., Doney, S.C., Lima, I., Boss, E.S., Siegel, D.A., 2013. Annual cycles of ecological disturbance and recovery underlying the subarctic Atlantic spring plankton bloom. Global Biogeochemical Cycles, Volume 27, Pages 1-15, DOI 10.1002/gbc.20050

Behrenfeld, M. J., 2010. Abandoning Sverdrup's Critical Depth hypothesis on phytoplankton blooms. Ecology, Volume 91, Issue 4, Pages 977-989, DOI 10.1890/09-1207.1.

Behrenfeld, M. J., 2014. Climate-mediated dance of the plankton. Nature Climate Change, Volume 4, Pages 880-887, DOI 10.1038/nclimate2349.

Bode, A., Estévez, M. G., Varela, M., Vilar, J. A., 2015. Annual trend patterns of phytoplankton species abundance belie homogeneous taxonomical group responses to climate in the NE Atlantic upwelling. Marine Environmental Research, Volume 110, Pages 81-91, DOI 10.1016/j.marenvres.2015.07.017.

Boss, E., Behrenfeld, M.J., 2010. In situ evaluation of the initiation of the North Atlantic phytoplankton bloom. Geophysical Research Letters, Volume 37, L18603, DOI 10.1029/2010GL044174

Boyce, D.G., Lewis, M.R., Worm, B., 2010. Global phytoplankton decline over the past century. Nature, Volume 466, Pages 591-596, DOI 1 0.1038/nature09268.

Brody, S.R., Lozier, M.S., Dunne, J.P., 2013. A comparison of methods to determine phytoplankton bloom initiation. Journal of Geophysical Research Oceans, Volume 118, Pages 1-13, DOI 10.1002/jgrc.20167, 2013

Bruno, M., Chioua, J., Romero, J., Vázquez, A., Macías, D., Dastis, C., Ramírez-Romero, E., Echevarria, F., Reyes, J., García, C. M., 2013. The importance of sub-mesoscale processes for the exchange of properties through the Strait of Gibraltar. Progress in Oceanography, Volume 116, Pages 66-79, DOI 10.1016/j.pocean.2013.06.006.

Caballero, I., Morris, E., Pietro, L., Navarro, G., 2014. The influence of the Guadalquivir river on spatio-temporal variability in the pelagic ecosystem of the eastern Gulf of Cádiz, Mediterranean Marine Science, Volume 15, Issue 4, Pages 721-738, DOI 10.12681/mms.844.

Cabré, A., Shields, D., Marinov, I., Kostadinov, T.S., 2016. Phenology of size-partitioned phytoplankton carbon-biomass from Ocean Color Remote Sensing and CMIP5 models. Frontiers in Marine Science, Volume 3, Article 39, DOI 10.3389/fmars.2016.00039

Carr, M-.E., Kearns, E. J., 2003. Production regimes in four Eastern Boundary Current systems. Deep-Sea Research II, Volume 50, Issues 22-26, Pages 3199-3221, DOI 10.1016/j.dsr2.2003.07.015.

Carstensen, J., Klais, R., Cloern, J. E., 2015. Phytoplankton blooms in estuarine and coastal waters: Seasonal patterns and key species. Estuarine, Coastal and Shelf Science. Volume 162, Pages 98-109, DOI 10.1016/j.ecss.2015.05.005

Castelle, B., Dodet, G. Masselink, G., Scott, T., 2017. A new climate index controlling winter wave activity along the Atlantic coast of Europe: The West Europe Pressure Anomaly. Geophysical Research Letters. Volume 44, DOI 10.1002/2016GL072379

Cermeño, P., Dutkiewicz, S., Harris, R. P., Follows, M., Schofield, O., Falkowski, P.G., 2008. The role of nutricline depth in regulating the ocean carbon cycle. PNAS, Volume 105, Issue 51, Pages 20344-20349, DOI 10.1073/pnas.0811302106

Chiswell, S.M., Bradford-Grieve, J., Hadfield, M.G., Kennan, S.C., 2013. Climatology of surface chlorophylla, autumn-winter and spring blooms in the southwest Pacific Ocean. Journal of Geophysical Research Oceans, Volume 118, Pages 1003-1018, DOI 10.1002/jgrc.20088

Chiswell, S.M., Calil, P.H.R., Boyd, P.W., 2015. Spring blooms and annual cycles of phytoplankton: a unified perspective. Journal of Plankton Research, Volume 37, Issue 3, Pages 500-508, DOI 10.1093/plankt/fbv021

Cloern, J. E., Dufford, R., 2005. Phytoplankton community ecology - Principles applied in San Francisco Bay. Marine Ecology Progress Series, Volume 285, Pages 11-28, DOI 10.3354/meps285011.

Cloern, J.E., Jassby, A.D., 2008. Complex seasonal patterns of primary producers at the land-sea interface. Ecology Letters, 11 (12), 1294-1303, DOI 10.1111/j.1461-0248.2008.01244.x.

Cloern, J.E., Abreu, P.C., Carstensen, J., Chauvaud, L., Grall, J., Greening, H., Johansson, R.J.O., Kahru, M., Sherwood, E.T., Xu, J.I.E., Yin, K., 2016. Human activities and climate variability drive fast-paced change across the world's estuarine-coastal ecosystems. Global Change Biology, 22(2), 513-529, DOI 10.1111/gcb.13059.

Cole, H., Henson, S., Martin, A., Yool, A., 2012. Mind the gap: the impact of missing data on the calculation of phytoplankton phenology metrics. Journal of Geophysical Research, Volume 117, C08030, DOI 10.1029/2012JC008249

Cole, H., Henson, S., Martin, A.P., Yool, A., 2015. Basin-wide mechanisms for spring bloom initiation: how typical is the North Atlantic? ICES Journal of Marine Science, Volume 72, Issue 6, Pages 2029-2040, DOI 10.1093/icesjms/fsu239

Corredor-Acosta, A., Morales, C.E., Hormazabal, S., Andrade, I., Correa-Ramirez, M.A., 2015. Phytoplankton phenology in the coastal upwelling region off central-southern Chile (35°S–38°S): Time-space variability, coupling to environmental factors, and sources of uncertainty in the estimates. Journal of Geophysical Research Oceans, Volume 120, Issue 2, Pages 813-831, DOI 10.1002/ 2014JC010330

Cravo, A., Madureira, M., Felícia, H., Rita, F., Bebianno, M. J., 2006. Impact of outflow from the Guadiana River on the distribution of suspended particulate matter and nutrients in the adjacent coastal zone. Estuarine, Coastal and Shelf Science, Volume 70, Issues 1-2, Pages 63-75, DOI 10.1016/j.ecss.2006.05.034.

Criado-Aldeanueva, F., García-Lafuente, J., Navarro, G., Ruiz, J., 2009. Seasonal and interannual variability of the surface circulation in the eastern Gulf of Cadiz (SW Iberia). Journal of Geophysical Research, Volume 114, C01011, DOI 10.1029/2008JC005069.

Cristina, S., Moore, G. F., Goela, P. R. F. C., Icely, J. D., Newton, A., 2014. In situ validation of MERIS marine reflectance off the southwest Iberian Peninsula: assessment of vicarious adjustment and corrections for near-land adjacency. International Journal of Remote Sensing, Volume 35, Issue 6, Pages 2347-2377, DOI 10.1080/01431161.2014.894657.

Cristina, S., Icely, J., Goela, P. C., DelValls, T. A., Newton, A., 2015. Using remote sensing as a support to the implementation of the European Marine Strategy Framework Directive in SW Portugal. Continental Shelf Research, Volume 108, Pages 169-177, DOI 10.1016/j.csr.2015.03.011.

Cristina, S., Cordeiro, C., Lavender, S., Goela, P. C., Icely, J. D., Newton, A., 2016a. MERIS phytoplankton time series products from the SW Iberian Peninsula (Sagres) using seasonal-trend decomposition based on Loess. Remote Sensing, Volume 8, Issue 6, 449, DOI 10.3390/rs8060449.

Cristina, S., D'Alimonte, D., Goela, P. C., Kajiyama, T., Icely, J., Moore, G., Fragoso, B., Newton, A., 2016b. Standard and regional bio-optical algorithms for chlorophyll a estimates in the Atlantic off the southwestern Iberian Peninsula. IEEE Geoscience and Remote Sensing Letters, Volume 13, Issue 6, Pages 757-761, DOI 10.1109/LGRS.2016.2529182.

D'Ortenzio, F., d'Alcalà, M.R., 2009. On the trophic regimes of the Mediterranean Sea: a satellite analysis. Biogeosciences, 6 (2), 139-148, DOI 10.5194/bg-6-139-2009.

D'Ortenzio, F., Antoine, D., Martinez, E., Ribera d'Alcalà, M., 2012. Phenological changes of oceanic phytoplankton in the 1980s and 2000s as revealed by remotely sensed ocean-color observations. Global Biogeochemical Cycles, Volume 26, GB4003, DOI 10.1029/2011GB004269.

Dabrowski, T., Reffray, G., Perruche, C., Gutknecht, E., 2016. Quality Information Document for IBI Biogeochemical Analysis Product IBI_Reanalysis_BIO_005_003.Issue 2.1.http://cmems-resources.cls.fr/documents/QUID/CMEMS-IBI-QUID-005-003.pdf (accessed 22.11.17).

deCastro, M., Lorenzo, N., Taboada, J. J., Sarmiento, M., Alvarez, I., Gomez-Gesteira, M., 2006. Influence of teleconnection patterns on precipitation variability and on river flow regimes in the Miño River basin (NW Iberian Peninsula). Climate Research, Volume 32, Issue 1, Pages 63-73, DOI 10.3354/cr032063.

Demarcq, H., Reygondeau, G., Alvain, S., Vantrepotte, V., 2012. Monitoring marine phytoplankton seasonality from space. Remote Sensing of Environment, Volume 117, Pages 211-222, DOI 10.1016/j.rse.2011.09.019

Dormann, C. F., Elith, J., Bacher, S., Buchmann, C., Carl, G., Carré, G., Marquéz, J. R. G., Grube, B., Lafourcade, B., Leitão, P. J., Münkemüller, T., McClean, C., Osborne, P. E., Reineking, B., Schröder, B., Skidmore, A. K., Zurell, D., Lautenbach, S., 2013. Collinearity: a review of methods to deal with it and a simulation study evaluating their performance. Ecography, Volume 36, Issue 1, Pages 27-46, DOI 10.1111/j.1600-0587.2012.07348.x.

Edwards, M., Richardson, A. J., 2004. Impact of climate change on marine pelagic phenology and trophic mismatch. Nature, Volume 430, Pages 881–884, DOI 10.1038/nature02808.

Eliasen, S.K., Hátún, H., Larsen, K.M.H., Hansen, B., Rasmussen, T.A.S., 2017. Phenologically distinct phytoplankton regions on the Faroe Shelf - identified by satellite data, observations and model. Journal of Marine Systems, Volume 169, Pages 99-110, DOI 10.1016/j.jmarsys.2017.01.015

Elsberry, R.L., Camp, N.T., 1978. Oceanic thermal response to strong atmospheric forcing. I. Characteristics of forcing events. Journal of Physical Oceanography, Volume 8, Issue 2, Pages 206-214, DOI 10.1175/1520-0485(1978)008<0206:OTRTSA>2.0.CO;2.

Fendereski, F., Vogt, M., Payne, M.R., Lachkar, Z., Gruber, N., Salmanmahiny, A., Hosseini, S.A., 2014. Bio-geographic classification of the Caspian Sea. Biogeosciences, Volume 11, Issue 22, Pages 6451-6470, DOI 10.5194/bg-11-6451-2014.

Ferreira, A. S., Visser, A.W., MacKenzie, B.R., Payne, M.R., 2014. Accuracy and precision in the calculation of phenology metrics. Journal of Geophysical Research Oceans, Volume 119, Pages 8438-8453, DOI 10.1002/2014JC010323.

Ferreira, A. S.A., Hátún, H., Counillon, F., Payne, M. R., Visser, A. W., 2015. Synoptic-scale analysis of mechanisms driving surface chlorophyll dynamics in the North Atlantic. Biogeosciences, Volume 12, Pages 3641-3653, DOI 10.5194/bg-12-3641-2015

Field, C. B., Behrenfeld, M. J., Randerson, J. T., Falkowski, P., 1998. Primary production of the biosphere: Integrating terrestrial and oceanic components. Science, Volume 281, Pages 237-240, DOI 10.1126/science.281.5374.237.

Fischer, A.D., Moberg, E.A., Alexander, H., Brownlee, E.F., Hunter-Cevera, K.R., Pitz, K.J., Rosengard, S.Z., Sosik, H.M., 2014. Sixty years of Sverdrup: A retrospective of progress in the study of phytoplankton blooms. Oceanography, Volume 27, Issue 1, Pages 222-235, DOI 10..5670/oceanog.2014.26

Follows, M., Dutkiewicz, S., 2002. Meteorological modulation of the North Atlantic spring bloom. Deep Sea Research Part II: Topical Studies in Oceanography, Volume 49, Issues 1–3, Pages 321-344, DOI 10.1016/S0967-0645(01)00105-9.

Foukal, N.P., Thomas, A.C., 2014. Biogeography and phenology of satellite-measured phytoplankton seasonality in the California current. Deep Sea Research Part I: Oceanographic Research Papers, 92, 11-25, DOI 10.1016/j.dsr.2014.06.008.

Franks, P.J.S., 2014. Has Sverdrup's critical depth hypothesis been tested? Mixed layers vs. turbulent layers. ICES Journal of Marine Science, Volume 72, Issue 6, Pages 1897-1907, DOI 10.1093/icesjms/fsu175

Friedland, K. D., Record, N. R., Asch, R. G., Kristiansen, T., Saba, V. S., Drinkwater, K. F., Henson, S., Leaf, R. T., Morse, R. E., Johns, D. G., Large, S. I., Hjøllo, S. S., Nye, J. A., Alexander, M. A., Ji, R., 2016. Seasonal phytoplankton blooms in the North Atlantic linked to the overwintering strategies of copepods. Elementa: Science of the Anthropocene, Volume 4, Pages 1-19, DOI 10.12952/journal.elementa.000099.

Friedland, K.D., Mouw, C.B., Asch, R.G., Ferreira, A.S.A., Henson, S., Hyde, K.J.W., Morse, R.E., Thomas, A.C., Brady, D.C., 2018. Phenology and time series trends of the dominant seasonal phytoplankton bloom across global scales. Global Ecology and Biogeography, Pages 1-19, DOI 10.1111/geb.12717.

Fuentes-Yaco, C., Koeller, P.A., Sathyendranath, S., Platt, T., 2007. Shrimp (*Pandalus borealis*) growth and timing of the spring phytoplankton bloom on the Newfoundland–Labrador Shelf. Fisheries Oceanography, Volume 16, Issue 2, Pages 116-129, DOI 10.1111/j.1365-2419.2006.00402.x

Gamito, R., Pita, C., Teixeira, C., Costa, M. J., Cabral, H. N., 2016. Trends in landings and vulnerability to climate change in different fleet components in the Portuguese coast. Fisheries Research, Volume 181, Pages 93-101, DOI 10.1016/j.fishres.2016.04.008.

García-Lafuente, J., Delgado, J., Criado-Aldeanueva, F., Bruno, M., del Río, J., Vargas, J.M., 2006. Water mass circulation on the continental shelf of the Gulf of Cádiz. Deep Sea Research II, Volume 53, Issues 11-13, Pages 1182–1197, DOI 10.1016/j.dsr2.2006.04.011.

García-Lafuente, J., Ruiz, J., 2007. The Gulf of Cádiz pelagic ecosystem: A review. Progress in Oceanography, Volume 74, Issues 2-3, Pages 228-251, DOI 10.1016/j.pocean.2007.04.001.

Goela, P.C., Icely, J., Cristina, S., Newton, A., Moore, G., Cordeiro, C., 2013. Specific absorption coefficient of phytoplankton off the Southwest coast of the Iberian Peninsula: A contribution to algorithm development for ocean colour remote sensing. Continental Shelf Research, 52 (1), 119-132, DOI 10.1016/j.csr.2012.11.009.

Goela, P.C., Danchenko, S., Icely, J.D., Lubian, L.M., Cristina, S., Newton, A., 2014. Using CHEMTAX to evaluate seasonal and interannual dynamics of the phytoplankton community off the South-west coast of Portugal. Estuarine, Coastal and Shelf Science, Volume 151, Pages 112-123, DOI 10.1016/j.ecss.2014.10.001.

Goela, P. C., Cordeiro, C., Danchenko, S., Icely, J., Cristina, S., Newton, A., 2016a. Time series analysis of data for sea surface temperature and upwelling components from the southwest coast of Portugal. Journal of Marine Systems, Volume 163, Pages 12-22, DOI 10.1016/j.jmarsys.2016.06.002.

Goela, P., Cristina, S., Kajiyama, T., Icely, J., Moore, G., Fragoso, B., Newton, A., 2016b. Technical note: Algal Pigment Index 2 in the Atlantic off the southwest Iberian Peninsula:

standard and regional algorithms. Ocean Science, Volume 23, Pages 1279-1288, DOI 10.5194/os-12-1279-2016.

González Taboada, F.G., Anadón, R., 2014. Seasonality of North Atlantic phytoplankton from space: impact of environmental forcing on a changing phenology (1998–2012). Global Change biology, Volume 20, Issue 3, Pages 698-712, DOI 10.1111/gcb.12352

Gregg, W. W., Conkright, M. E., Ginoux, P., O'Reilly, J. E., Casey, N. W., 2003. Ocean primary production and climate: Global decadal changes. Geophysical Research Letters, Volume 30, Issue 15, 1809, DOI 10.1029/2003GL016889.

Groetsch, P.M.M., Simis, S.G.H., Eleveld, M.A., Peters, S.W.M., 2016. Spring blooms in the Baltic Sea have weakened but lengthened from 2000 to 2014. Biogeosciences, Volume 13, Pages 4959-4973, DOI 10.5194/bg-13-4959-2016

Harrison, W.G., Børsheim, K.Y., Li, W.K.W., Maillet, G.L., Pepin, P., Sakshaug, E., Skogen, M.D., Yeats, P.A., 2013. Phytoplankton production and growth regulation in the Subarctic North Atlantic: A comparative study of the Labrador Sea-Labrador/Newfoundland shelves and Barents/Norwegian/Greenland seas and shelves. Progress in Oceanography, Volume 114, Pages 26-45, DOI 10.1016/j.pocean.2013.05.003

Hauke, J., Kossowski, T., 2011. Comparison of values of Pearson's and Spearman's correlation coefficient on the same sets of data. Quaestiones Geographicae, Volume 30, Issue 2, Pages 87-93, DOI 10.2478/v10117-011-0021-1.

Henson, S.A., Thomas, A.C., 2007. Interannual variability in timing of bloom initiation in the California Current System. Journal of Geophysical Research, Volume 112, C08007, DOI 10.1029/2006JC003960

Henson,S.A.,Robinson,I., Allen,J.T., Waniek, J.J., 2006. Effect of meteorological conditions on interannual variability in timing and magnitude of the spring bloom in the Irminger Basin, North Atlantic. Deep Research Part I Oceanographic Research Papers. Volume 53, Issue 10, Pages 1601-1615, DOI 10.1016/j.dsr.2006.07.009

Henson, S.A., Dunne, J.P., Sarmiento, J.L., 2009. Decadal variability in North Atlantic phytoplankton blooms. Journal of Geophysical Research, Volume 114, C04013, DOI 10.1029/2008JC005139

Henson, S.A., Sarmiento, J.L., Dunne, J.P., Bopp, L., Lima, I., Doney, S.C., John, J., Beaulieu, C., 2010. Detection of anthropogenic climate change in satellite records of ocean chlorophyll and productivity. Biogeosciences, Volume 7, Pages 621-640, DOI 10.5194/bg-7-621-2010

Henson, S. A., Beaulieu, C., Lampitt, R., 2016. Observing climate change trends in ocean biogeochemistry: when and where. Global Change Biology, Volume 22, Issue 4, Pages 1561-1571, DOI 10.1111/gcb.13152.

Henson, S.A., Beaulieu, C., Ilyina, T., John, J.G., Long, M., Séférian, R., Tjiputra, J., Sarmiento, J.L., 2017. Rapid emergence of climate change in environmental drivers of marine ecosystems. Nature Communications, Volume 8, 14682, Pages 1-9, DOI 10.1038/ncomms14682.

Henson, S.A., Cole, H.S., Hopkin, J., Martin, A.P., Yool, A., 2018. Detection of climate change-driven trends in phytoplankton phenology. Global Change Biology, Volume 24, Issue 1, Pages e101-e111, DOI 10.1111/gcb.13886.

Hoepffner, N., Dowell, M.D., 2005. Assessing the dynamics of ecological provinces in European Seas, European Commission, EUR 21514 EN, Ispra, pp. 1-43.

Horta e Costa, B., Assis, J., Franco, G., Erzini, K., Henriques, M., Gonçalves, E. J., Caselle, J. E., 2014. Tropicalization of fish assemblages in temperate biogeographic transition zones. Marine Ecology Progress Series, Volume 504, Pages 241-252, DOI 10.3354/meps10749.

Huertas, I. E., Navarro, G., Rodríguez-Gálvez, S., Lubián, L. M., 2006. Temporal patterns of carbon dioxide in relation to hydrological conditions and primary production in the northeastern shelf of the Gulf of Cadiz (SW Spain). Deep Sea Research Part II: Topical Studies in Oceanography, Volume 53, Issues 11-13, Pages 1344-1362, DOI 0.1016/j.dsr2.2006.03.010.

Huisman, J., van Oostveen, P., Weissing, F.J., 1999. Critical depth and critical turbulence: Two different mechanisms for the development of phytoplankton blooms. Limnology and Oceanography, Volume 44, Pages 1781-1787, DOI 10.4319/lo.1999.44.7.1781

Hurrell, J.W., 1995. Decadal Trends in the North Atlantic Oscillation: Regional Temperatures and Precipitation. Science, Volume 269, Issue 5224, Pages 676-679, DOI 10.1126/science.269.5224.676.

Hurrell, J. W., Kushnir, Y., Ottersen, G., Visbeck, M., 2003. The North Atlantic Oscillation: Climatic significance and environmental impact. Book Series: Geophysical Monograph Series, John Wiley & Sons, DOI 10.1029/GM134.

IOC, IHO and BODC, 2003. Centenary Edition of the GEBCO Digital Atlas, published on CD-ROM on behalf of the Intergovernmental Oceanographic Commission and the International Hydrographic Organization as part of the General Bathymetric Chart of the Oceans, British Oceanographic Data Centre, Liverpool.

International Ocean Colour Coordinating Group (IOCCG), 2000. Remote Sensing of Ocean Colour in Coastal, and Other Optically-Complex, Waters. Sathyendranath, S. (Ed.), Reports and Monographs of the International Ocean-Colour Coordinating Group (IOCCG), Volume 3, IOCCG, Dartmouth, p. 140.

International Ocean Colour Coordinating Group (IOCCG), 2009. Partition of the ocean into ecological provinces: Role of ocean-colour radiometry. Dowell, M. Platt, T., Stuart, V. (Eds) Reports and Monographs of the International Ocean-Colour Coordinating Group (IOCCG), Volume 9, Dartmouth, p. 98.

Itoh, S., Yasuda, I., Saito, H., Tsuda, A., Komatsu, K., 2015. Mixed layer depth and chlorophyll a: Profiling float observations in the Kuroshio–Oyashio Extension region. Journal of Marine Systems, Volume 151, Pages 1-14, DOI 10.1016/j.jmarsys.2015.06.004

Ji, R., Edwards, M., Mackas, D.L., Runge, J.A., Thomas, A.C., 2010. Marine plankton phenology and life history in a changing climate: current research and future directions. Journal of Plankton Research. Volume 32, Pages 1355–1368, DOI 10.1093/plankt/fbq062

Kahru, M., Brotas, V., Manzano-Sarabia, M., Mitchell, B.G., 2010. Are phytoplankton blooms occurring earlier in the Arctic? Global Change Biology, Volume 17, Issue 4, Pages 1733-1739, DOI 10.1111/j.1365-2486.2010.02312.x

Kahru, M., Elmgren, R., Savchuk, O.P., 2015. Changing seasonality of the Baltic Sea. Biogeosciences Discussions, Volume 12, Pages 18855-18882, DOI 10.5194/bgd-12-18855-2015

Kaplan, A., Cane, M. A., Kushnir, Y., Clement, A. C., Blumenthal, M. B., Rajagopalan, B., 1998. Analyses of global sea surface temperature 1856-1991. Journal of Geophysical Research, 103 (C9), 18,567-18,589, 1998, DOI 10.1029/97JC01736

Kim, H.-J., Miller, A.J., McGowan, J., Carter, M.L., 2009. Coastal phytoplankton blooms in the Southern California Bight. Progress in Oceanography, Volume 82, Pages 137-147, DOI 10.1016/j.pocean.2009.05.002

Kirk, J.T.O., 1986. Light and photosynthesis in aquatic ecosystems, Cambridge University Press, Cambridge.

Koeller, P., Fuentes-Yaco, C., Platt, T., Sathyendranath, S., Richards, A., Ouellet, P., Orr, D., Skúladóttir, U., Wieland, K., Savard, L., Aschan, M., 2009. Basin-scale coherence in phenology of shrimps and phytoplankton in the North Atlantic Ocean. Science, Volume 324, Issue 5928, Pages 791-793, DOI 10.1126/science.1170987

Kostadinov, T.S., Cabré, A., Vedantham, H., Marinov, I., Bracher, A., Brewin, R.J.W., Bricaud, A., Hirata, T., Hirawake, T., Hardman-Mountford, N.J., Mouw, C., Roy, S., Uitz, J., 2017. Inter-comparison of phytoplankton functional type phenology metrics derived from ocean color algorithms and Earth System Models. Remote Sensing of Environment, Volume 190, Pages 162-177, DOI 10.1016/j.rse.2016.11.014

Kovats, R.S., Valentini, R., Bouwer, L.M., Georgopoulou, E., Jacob, D., Martin, E., Rounsevell, M., Soussana, J. -F., 2014. in: Barros, V.R., Field, C.B., Dokken, D.J., Mastrandrea, M.D., Mach, K.J., Bilir, T.E., Chatterjee, M., Ebi, K. L., Estrada, Y. O., Genova, R. C., Girma, B., Kissel, E. S., Levy, A.N., MacCracken, S., Mastrandrea, P. R., White, L. L. (Eds.) Climate Change 2014: Impacts, Adaptation, and Vulnerability. Part B: Regional Aspects. Contribution of Working Group II to the Fifth Assessment Report of the Intergovernmental Panel on Climate Change. Cambridge University Press, Cambridge, United Kingdom and New York, NY, USA, pp. 1267-1326.

Kromkamp, J.C, van Engeland, T., 2010. Changes in Phytoplankton Biomass in the Western Scheldt Estuary During the Period 1978–2006. Estuaries and Coasts, Volume 33, Pages 270-285, DOI 10.1007/s12237-009-9215-3

Krug, L. A., Platt, T., Sathyendranath, S., Barbosa, A. B., 2017a. Ocean surface partitioning strategies using Ocean Colour Remote Sensing: a review. Progress in Oceanography, Volume 155, Pages 41-53, DOI 10.1016/j.pocean.2017.05.013.

Krug, L. A., Platt, T., Sathyendranath, S., Barbosa, A. B., 2017b. Unravelling region-specific environmental drivers of phytoplankton across a complex marine domain (off SW Iberia), Remote Sensing of Environment, Volume 203, Pages 162-184, DOI 10.1016/j.rse.2017.05.029.

Krug, L.A., Platt,T., Barbosa, A.B., 2018. Delineation of ocean surface provinces over a complex marine domain (off SW Iberia): an objective abiotic-based approach. Regional Studies in Marine Science, Volume 18, Pages 80-96, DOI 10.1016/j.rsma.2018.01.003.

Kumar, P., Min, S., Weller, E., Lee, H., Wang, X., 2016. Influence of climate variability on extreme ocean surface wave heights assessed from ERA-Interim and ERA-20C. Journal of Climate, Volume 29, Issue 11, Pages 4031-4046, DOI 10.1175/JCLI-D-15-0580.1.

Lacour, L., Claustre, H., Prieur, L., D'Ortenzio, F., 2015. Phytoplankton biomass cycles in the North Atlantic subpolar gyre: A similar mechanism for two different blooms in the Labrador Sea. Geophysical Research Letters. Volume 42, Pages 5403–5410,DOI 10.1002/2015GL064540.

Land, P.E., Shutler, J.D., Platt, T., Racault, M.F., 2014. A novel method to retrieve oceanic phytoplankton phenology fromsatellite data in the presence of data gaps. Ecological Indicators. Volume 37, Pages 67-80, DOI 10.1016/j.ecolind.2013.10.008

Lavigne, H., D'Ortenzio, F., Migon, C., Claustre, H., Testor, P., d'Alcalá, M.R., Lavezza, R., Houpert, L., Prieur, L., 2013. Enhancing the comprehension of mixed layer depth control on the Mediterranean phytoplankton phenology. Journal of Geophysical Research Oceans, Volume 118, Pages 1-15, DOI 10.1002/jgrc.20251

Liu, F., Su, J., Moll, A., Krasemann, H., Chen, X., Pohlmann, T., Wirtz, K., 2014. Assessment of the summer–autumn bloom in the Bohai Sea using satellite images to identify the roles of wind mixing and light conditions. Journal of Marine Systems, Volume 129, Pages 303-317, DOI 10.1016/j.jmarsys.2013.07.007

Longhurst, A., 2007. Ecological geography of the sea, second ed. Academic Press, Burlington.

Lutz, M.J., Caldeira, K., Dunbar, R.B., Behrenfeld, M.J., 2007. Seasonal rhythms of net primary production and particulate organic carbon flux to depth describe the efficiency of biological pump in the global ocean. Journal of Geohysical Research, Volume 112, C10011, DOI 10.1029/2006JC003706

Mahadevan, A., D'asaro, E., Lee, C., Perry, M.J., 2012. Eddy-driven stratification initiates North Atlantic spring phytoplankton blooms. Science, Volume 337, Pages 54-58, DOI 10.1126/science.1218740

Malick, M.J., Cox, S.P., Mueter, F.J., Peterman, R.M., 2015. Linking phytoplankton phenology to salmon productivity along a north/south gradient in the Northeast Pacific Ocean. Canadian Journal of Fisheries and Aquatic Sciences, Volume 72, Issue 5, Pages 697-708, DOI 10.1139/cjfas-2014-0298

Martin-Vide J., Lopez-Bustins J.A., 2006. The Western Mediterranean Oscillation and Iberian Peninsula Rainfall. International Journal of Climatology, Volume 26, Issue 11, Pages 1455-1475, DOI 10.1002/joc.1388.

Martinez, E., Antoine, D., D'Ortenzio, F., Gentili, B., 2009. Climate-driven basin-scale decadal oscillations of oceanic phytoplankton. Science, Volume 326, Pages 1253-1256, DOI: 10.1126/science.1177012.

Martinez, E., Antoine, D., D'Ortenzio, F., Montégut, C. B., 2011. Phytoplankton spring and fall blooms in the North Atlantic in the 1980s and 2000s. Journal of Geophysical Research, Volume 116, C11029, DOI 10.1029/2010JC006836.

Martinez, E., Raitsos, D.E., Antoine, D., 2016. Warmer, deeper, and greener mixed layers in the North Atlantic subpolar gyre over the last 50 years. Global Change Biology, Volume 22, Pages 604-612, DOI 10.1111/gcb.13100

Mayot, N., D'Ortenzio, F., d'Alcalá, M.R., Lavigne, H., Claustre, H., 2015. Interannual variability of the Mediterranean trophic regimes from ocean color satellites. Biogeosciences Discussions, 12, 14941-14980, DOI 10.5194/bgd-12-14941-2015.

Moita, M. T., 2001. Estrutura, variabilidade e dinâmica do fitoplâncton na costa de Portugal continental. PhD dissertation, University of Lisbon, Lisbon. https://www.ipma.pt/resources.www/docs/publicacoes.site/teses/Teresa_Moita-thesis.pdf (accessed 09.08.16).

Muñoz, M., Reul, A., Plaza, F., Gómez-Moreno, M.-L., Vargas-Yañez, M., Rodríguez, V., Rodríguez, J., 2015. Implication of regionalization and connectivity analysis for marine spatial planning and coastal management in the Gulf of Cadiz and Alboran Sea. Ocean & Coastal Management, 118, Part A, 60-74, DOI 10.1016/j.ocecoaman.2015.04.011.

Navarro, G., Ruiz, J., 2006. Spatial and temporal variability of phytoplankton in the Gulf of Cádiz through remote sensing images, Deep Sea Research Part II: Topical Studies in Oceanography, Volume 53, Issues 11–13, Pages 1241-1260, DOI 10.1016/j.dsr2.2006.04.014.

Navarro, G., Caballero, I., Prieto, L., Vázquez, A., Flecha, S., Huertas, I. E., Ruiz, J., 2012. Seasonal-to-interannual variability of chlorophyll-a bloom timing associated with physical forcing in the Gulf of Cádiz. Advances in Space Research, Volume 50, Issue 8, Pages 1164-1172, DOI 10.1016/j.asr.2011.11.034.

Nechad, B., Ruddick, K., Schroeder, T., Oubelkheir, K., Blondeau-Patissier, D., Cherukuru, N., Brando, V., Dekker, A., Clementson, L., Banks, A. C., Maritorena, S., Werdell, J., Sá, C., Brotas, V., Caballero de Frutos, I., Ahn, Y.-H., Salama, S., Tilstone, G., Martinez-Vicente, V., Foley, D., McKibben, M., Nahorniak, J., Peterson, T., Siliò-Calzada, A., Röttgers, R., Lee, Z., Peters, M., Brockmann, C., 2015. CoastColour Round Robin datasets: a database to evaluate the performance of algorithms for the retrieval of water quality parameters in coastal waters. Earth System Science Data, Volume 7, Pages 173-258, DOI 10.5194/essd-7-319-2015

Nixon, S.W., Fulweiler, R.W., Buckley, B.A., Granger, S.L., Nowicki, B.L., Henry, K.M., 2009. The impact of changing climate on phenology, productivity, and benthic–pelagic coupling in Narragansett Bay. Estuarine, Coastal and Shelf Science, Volume 82, Pages 1-18, DOI 10.1016/j.ecss.2008.12.016

Oliver, M.J., Glenn, S., Kohut, J.T., Irwin, A.J., Schofield, O.M., 2004. Bioinformatic approaches for objective detection of water masses on continental shelves. Journal of Geophysical Research, 109 (C07S04), DOI 10.1029/2003JC002072.

Oziel, L., Neukermans, G., Ardyna, M., Lancelot, C., Tison, J-L., Wassmann, P., Sirven, J., Ruiz-Pino, D., Gascard, J-C., 2017. Role for Atlantic inflows and sea ice loss on shifting

phytoplankton blooms in the Barents Sea. Journal of Geophysical Research Oceans, Volume 122, Pages 5121–5139, DOI 10.1002/2016JC012582

Palma, S., Mouriño, H., Silva, A., Barão, M.I., Moita, M.T., 2010. Can *Pseudo-nitzschia* blooms be modeled by coastal upwelling in Lisbon Bay? Harmful Algae, Volume 9, Issue 3, Pages 294-303, DOI 10.1016/j.hal.2009.11.006.

Pardo, P.C., Padín, X.A., Gilcoto, M., Farina-Busto, L., Pérez, F.F., 2011. Evolution of upwelling systems coupled to the long-term variability in sea surface temperature and Ekman transport. Climate Research, Volume 48, Pages 231-246, DOI 10.3354/cr00989.

Peliz, Á., Santos, A. M. P., Oliveira, P. B., Dubert, J., 2004. Extreme cross-shelf transport induced by eddy interactions southwest of Iberia in winter 2001. Geophysical Research Letters, Volume 31, L08301, DOI 10.1029/2004GL019618.

Picado, A., Alvarez, I., Vaz, N., Varela, R., Gomez-Gesteira, M., Dias, J. M., 2014. Assessment of chlorophyll variability along the northwestern coast of Iberian Peninsula. Journal of Sea Research, Volume 93, Pages 2-11, DOI 10.1016/j.seares.2014.01.008.

Piló, D., Barbosa, A., Teodósio, M., Encarnação, J., Leitão, F., Range, P., Krug, L.A., Cruz, J., Chicharo, L., 2018. Are submarine groundwater discharges affecting the structure and physiological status of rocky intertidal communities? Marine Environmental Research, Volume 136, Pages 158-173, DOI 10.1016/j.marenvres.2018.02.013.

Pitcher, G.C., Figueiras, F.G., Hickey, B.M., Moita, M.T., 2010. The physical oceanography of upwelling systems and the development of harmful algal blooms. Progress in Oceanography, Volume 85, Pages 5-32, DOI 10.1016/j.pocean.2010.02.002

Platt, T., Sathyendranath, S., 2008. Ecological indicators for the pelagic zone of the ocean from remote sensing. Remote Sensing of Environment, Volume 112, Issue 8, Pages 3426–3436, DOI 10.1016/j.rse.2007.10.016.

Platt, T., Fuentes-Yaco, C., Frank, K.T., 2003. Spring algal bloom and larval fish survival. Nature 423, 398-399, DOI 10.1038/423398b.

Platt, T., White III, G.N., Zhai, L., Sathyendranath, S., Roy, S., 2009. The phenology of phytoplankton blooms: Ecosystem indicators from remote sensing. Ecological Modelling, Volume 220, Issue 21, Pages 3057-3069, DOI 10.1016/j.ecolmodel.2008.11.022

Platt, T., Sathyendranath, S., White III, G.N., Fuentes-Yaco, C., Zhai, L., Devred, E., Tang, C. 2010. Diagnostic properties of phytoplankton time series from remote sensing. Estuaries and Coasts, Volume 33, Pages 428-439, DOI 10.1007/s12237-009-9161-0.

Plomaritis, T. A., Benavente, J., Laiz, I., Del Río, L., 2015. Variability in storm climate along the Gulf of Cadiz: the role of large scale atmospheric forcing and implications to coastal hazards. Climate Dynamics, Volume 45, Issue 9-10, Pages 2499-2514, DOI 10.1007/s00382-015-2486-4.

Prieto, L., Navarro, G., Rodríguez-Gálvez, S., Huertas, I. E., Naranjo, J. M., Ruiz, J., 2009. Oceanographic and meteorological forcing of the pelagic ecosystem on the Gulf of Cadiz shelf (SW Iberian Peninsula). Continental Shelf Research, Volume 29, Issue 17, Pages 2132-2137, DOI 10.1016/j.csr.2009.08.007.

R Core Team, 2016. R: A language and environment for statistical computing. R Foundation for Statistical Computing, Vienna, Austria. http://www.R-project.org/ (accessed 24.03.17).

Racault, M.F., Le Quéré, C., Buitenhuis, E., Sathyendranath, S., Platt, T., 2012. Phytoplankton phenology in the global ocean. Ecological Indicators. Volume 14, Pages 152-163, DOI 10.1016/j.ecolind.2011.07.010

Racault, M., Platt, T., Sathyendranath, S., Ağirbaş, E., Vicente, V.M., Brewin, R., 2014a. Plankton indicators and ocean observing systems: support to the marine ecosystem state assessment. Journal of Plankton Research, 36 (3), 621-629, DOI 10.1093/plankt/fbu016

Racault, M., Sathyendranath, S. Platt, T., 2014b. Impact of missing data on the estimation of ecological indicators from satellite ocean-colour time-series. Remote Sensing of Environment, Volume 152, Pages 15-28, DOI 10.1016/j.rse.2014.05.016.

Racault, M.F., Raitsos, D.E., Berumen, M.L., Brewin, R.J.W., Platt, T., Sathyendranath, S., Hoteit, I., 2015. Phytoplankton phenology indices in coral reef ecosystems: Application to ocean-color observations in the Red Sea. Remote Sensing of Environment, Volume 160, Pages 222-234, DOI 10.1016/j.rse.2015.01.019.

Racault, M.F., Sathyendranath, S., Menon, N., Platt, T., 2017. Phenological responses to ENSO in the global oceans. Surveys in Geophysics, Volume 38, Issue 1, Pages 277-293, DOI 10.1007/s10712-016-9391-1

Relvas, P., Barton, E.D., Dubert, J., Oliveira, P. B., Peliz, A., da Silva, J. C. B., Santos, A. M. P., 2007. Physical oceanography of the western Iberia ecosystem: Latest views and challenges, Progress in Oceanography, Volume 74, Issues 2-3, Pages 149-173, DOI 10.1016/j.pocean.2007.04.021.

Reul A., Muñoz, M., Criado-Aldeanueva, F., Rodríguez, V., 2006. Spatial distribution of phytoplankton <13 µm in the Gulf of Cádiz in relation to water masses and circulation pattern under westerly and easterly wind regimes. Deep Sea Research Part II: Topical Studies in Oceanography, 53 (11-13), 1294-1313, DOI 10.1016/j.dsr2.2006.04.008.

Rochford, P. A., Kara, A. B., Wallcraft, A. J., Arnone, R. A., 2001. Importance of solar subsurface heating in ocean general circulation models. Journal of Geophysical Research - Oceans, Volume 106, Issue C12, Pages 30923-30938, DOI 10.1029/2000JC000355.

Sá, C., D'Alimonte, D., Brito, A. C., Kajiyama, T., Mendes, C. R., Vitorino, J., Oliveira, P. B., da Silva, J. C. B., Brotas, V., 2015. Validation of standard and alternative satellite ocean-color chlorophyll products off Western Iberia. Remote Sensing of Environment, Volume 168, Pages 403-419, DOI 10.1016/j.rse.2015.07.018.

Sala, I., Navarro, G., Bolado-Penagos, M., Echevarría, C.M., 2018. High-Chlorophyll-Area assessment based on remote sensing observations: the case study of Cape Trafalgar. Remote Sensing, Volume 10, Issue 2, 165, DOI 10.3390/rs10020165.

Sallée, J-B., Llort, J., Tagliabue, A., Lévy, M., 2015. Characterization of distinct bloom phenology regimes in the Southern Ocean. ICES Journal of Marine Science, Volume 72, Issue 6, Pages 1985-1998, DOI 10.1093/icesjms/fsv069

Sánchez, R. F., Relvas, P., Martinho, A., Miller, P., 2008. Physical description of an upwelling filament west of Cape St. Vincent in late October 2004. Journal of Geophysical Research, Volume 113, C07044, DOI 10.1029/2007JC004430.

Santos, F., Gesteira, M. G., deCastro, M., 2011. Coastal and oceanic SST variability along the western Iberian Peninsula. Continental Shelf Research, Volume 31, Pages 2012-2017, DOI 10.1016/j.csr.2011.10.005.

Sapiano, M.R.P., Brown, C.W., Uz, S.S.,Vargas, M., 2012. Establishing a global climatology of marine phytoplankton phenological characteristics. Journal of Geophysical Research, Volume 117, C08026, DOI 10.1029/2012JC007958

Sasaoka, K., Chiba, S., Saino, T., 2011. Climatic forcing and phytoplankton phenology over the subarctic North Pacific from 1998 to 2006, as observed from ocean color data. Geophysical Research Letters, Volume 38, L15609, 10.1029/2011GL048299

Sathyendranath, S., Brewin, R.J.W., Jackson, T., Mélin, F., Platt, T., 2017. Ocean-colour products for climate-change studies: what are their ideal characteristics? Remote Sensing of Environment, Volume 203, Pages 125-138, DOI 10.1016/j.rse.2017.04.017.

Sathyendranath, S., Groom, S., Grant, M., Brewin, R.J.W., Thompson, A., Chuprin, A., Horseman, A., Jackson, T., Martinez Vicente , V., Platt, T., Brockmann, C., Zühlke, M., Doerffer, R., Valente, A., Brotas, V., Krasemann, H., Müller, D., Dowell, M., Mélin, F., Swinton, J., Farman, A., Lavender, S., Moore, T.S., Regner, P., Roy, S., Steinmetz, F., Mazeran, C., Brando, V.E., Taberner, M., Antoine, D., Arnone, R., Balch, W.M., Barker, K., Barlow, R., Bélanger, S., Berthon, J., Beşiktepe, Ş., Canuti, E., Chavez, F., Claustre, H., Crout, R., Frouin, R., García-Soto, C., Gibb, S.W., Gould, R., Hooker, S., Kahru, M., Klein, H., Kratzer, S., Loisel, H., McKee, D., Mitchell, B.G., Moisan, T., Feldman, G., Franz, B., Muller-Karger, F., O'Dowd, L., Ondrusek, M., Poulton, A.J., Repecaud, M., Smyth, T., Sosik, H.M., Twardowski, M., Voss, K., Werdell, J., Wernand, M., Zibordi, G., 2016. ESA Ocean Colour Climate Change Initiative (Ocean_Colour_cci): Version 2.0 Data. Centre for Environmental Data Analysis. DOI 10.5285/b0d6b9c5-14ba-499f-87c9-66416cd9a1dc

Scheffers, B.R., Meester, L.D., Bridge, T.C.L., Hoffmann, A.A., Pandolfi, J.M., Corlett, R.T., Butchart, S.H.M., Pearce-Kelly, P., Kovacs, K.M., Dudgeon, D., Pacifici, M., Rondinini, C., Foden, W.B., Martin, T.G., Mora, C., Bickford, D., Watson, J.E.M., 2016. The broad footprint of climate change from genes to biomes to people. Science, 354(6313), 1-11, DOI 10.1126/science.aaf7671.

Schwartz, M.D., 2003. Chapter 1.1 Introduction. In: Phenology: an integrative environmental science, Ed.: M.D.Schartw, Springer, Netherlands. 3-7 pp

Sherman, K., 1994. Sustainability, biomass yields, and health of coastal ecosystems: an ecological perspective. Marine Ecology Progress Series, 112, 277-301.

Shiozaki, T., Ito, S-I., Takahashi, K., Saito, H., Nagata, T., Furuya, K., 2014. Regional variability of factors controlling the onset timing and magnitude of spring algal blooms in the northwestern North Pacific. Journal of Geophysical Research Oceans, Volume 119, Pages 253-265, 10.1002/2013JC009187

Siegel, D.A., Doney, S.C., Yoder, J.A., 2002. The North Atlantic spring phytoplankton bloom and Sverdrup's critical depth hypothesis. Science, Volume 296, Pages 730-733, DOI 10.1126/science.1069174

Smayda, T.J., Trainer, V.L., 2010. Dinoflagellate blooms in upwelling systems: Seeding, variability, and contrasts with diatom bloom behaviour. Progress in Oceanography, Volume 85, Issues 1-2, Pages 92-107, DOI 10.1016/j.pocean.2010.02.006

Song, H., Ji, R., Stock, C., Wang, Z., 2010. Phenology of phytoplankton blooms in the Nova Scotian Shelf–Gulf of Maine region: remote sensing and modeling analysis. Journal of Plankton Research, Volume 32, Issue 11, Pages 1485-1499, DOI 10.1093/plankt/fbq086

Song, H., Ji, R., Stock, C., Kearney, K., Wang, Z., 2011. Interannual variability in phytoplankton blooms and plankton productivity over the Nova Scotian Shelf and in the Gulf of Maine. Marine Ecology Progress Series, Volume 426, Pages 105-118, DOI 10.3354/meps09002

Soppa, M.A., Völker C., Bracher, A., 2016. Diatom phenology in the Southern Ocean: mean patterns, trends and the role of climate oscillations. Remote Sensing, Volume 8, 420, DOI 10.3390/rs8050420

Souza, F. M., Bricaud, A., 1992. Satellite-derived phytoplankton pigment structures in the Portuguese upwelling area. Journal of Geophysical Research - Oceans, Volume 97, Issue C7, Pages 22343-11356, DOI 10.1029/92JC00786.

Spalding, M.D., Agostini, V.N., Rice, J., Grant, S.M., 2012. Pelagic provinces of the world: A biogeographic classification of the world's surface pelagic waters. Ocean & Coastal Management, 60, 19-30, DOI 10.1016/j.ocecoaman.2011.12.016.

Spalding, M.D., Fox, H.E., Allen, G.R., Davidson, N., Ferdaña, Z.A., Finlayson, M., Halpern, B.S., Jorge, M.A., Lombana, A., Lourie, S.A., Martin, K.D., McManus, E., Molnar, J., Recchia, C.A., Robertson, J., 2007. Marine Ecoregions of the World: A Bioregionalization of Coastal and Shelf Areas. BioScience, 57 (7), 573-583, DOI 10.1641/B570707.

Sverdrup, H. U., 1953. On conditions for the vernal blooming of phytoplankton. Journal du Conseil International pour l'Exploration de la Mer, Volume 18, Issue 3, Pages 287-295, DOI 10.1093/icesjms/18.3.287.

Teira, E., Mouriño, B., Marañón, E., Pérez, V., Pazó, M. J., Serret, P., de Armas, D., Escánez, J., Woodward, E. M. S., Fernández, E., 2005. Variability of chlorophyll and primary production in the Eastern North Atlantic Subtropical Gyre: potential factors affecting phytoplankton activity. Deep Sea Research Part I: Oceanographic Research Papers, Volume 52, Issue 4, Pages 569-588, DOI 10.1016/j.dsr.2004.11.007.

Tilstone, G., Mallor-Hoya, S., Gohin, F., Couto, A.B., Sá, C., Goela, P., Cristina, S., Airs, R., Icely, J., Zühlke, M., Groom, S., 2017. Which ocean colour algorithm for MERIS in NorthWest European waters? Remote Sensing of Environment, Volume 189, Pages 132-151, DOI 10.1016/j.rse.2016.11.012.

Trigo, I.F, 2006. Climatology and interannual variability of storm-tracks in the Euro-Atlantic sector: a comparison between ERA-40 and NCEP/NCAR reanalyses. Climate Dynamics, Volume 26, Issue 2, Pages 127-143, DOI 10.1007/s00382-005-0065-9.

Ueyama, R., Monger, B. C., 2005. Wind-induced modulation of seasonal phytoplankton blooms in the North Atlantic derived from satellite observations. Limnology and Oceanography, Volume 50, Issue 6, Pages 1820-1829, DOI 10.4319/lo.2005.50.6.1820.

Varela, R., Álvarez, I., Santos, F., deCastro, M., Gómez-Gesteira, M., 2015. Has upwelling strengthened along worldwide coasts over 1982-2010? Scientific Reports, Volume 5, 10016, DOI 10.1038/srep10016.

Vargas, J.M., García-Lafuente, J., Delgado, J., Criado, F., 2003. Seasonal and wind-induced variability of Sea Surface Temperature patterns in the Gulf of Cádiz. Journal of Marine Systems, Volume 38, Issues 3-4, Pages 205-219, DOI 10.1016/S0924-7963(02)00240-3.

Vargas, M., Brown, C.W., Sapiano, M.R.P., 2009. Phenology of marine phytoplankton from satellite ocean color measurements. Geophysical Research Letters, Volume 36, L01608, DOI 10.1029/2008GL036006.

von Schuckmann, K., Le Traon, P., Alvarez-Fanjul, E., Axell, L., Balmaseda, M., Breivik, L., Brewin, R. J. W., Bricaud, C., Drevillon, M., Drillet, Y., Dubois, C., Embury, O., Etienne, H., Sotillo, M. G., Garric, G., Gasparin, F., Gutknecht, E., Guinehut, S., Hernandez, F., Juza, M., Karlson, B., Korres, G., Legeais, J., Levier, B., Lien, V. S., Morrow, R., Notarstefano, G., Parent, L., Pascual, A., Pérez-Gómez, B., Perruche, C., Pinardi, N., Pisano, A., Poulain, P., Pujol, I. M., Raj, R. P., Raudsepp, U., Roquet, H., Samuelsen, A., Sathyendranath, S., She, J., Simoncelli, S., Solidoro, C., Tinker, J., Tintoré, J., Viktorsson, L., Ablain, M., Almroth-Rosell, E., Bonaduce, A., Clementi, E., Cossarini, G., Dagneaux, Q., Desportes, C., Dye, S., Fratianni, C., Good, S., Greiner, E., Gourrion, J., Hamon, M., Holt, J., Hyder, P., Kennedy, J., Manzano-Muñoz, F., Melet, A., Meyssignac, B., Mulet, S., Nardelli, B. B., O'Dea, E., Olason, E., Paulmier, A., Pérez-González, I., Reid, R., Racault, M., Raitsos, D. E., Ramos, A., Sykes, P., Szekely, T., Verbrugge, N., 2017. The Copernicus Marine Environment Monitoring Service Ocean State Report. Journal of Operational Oceanography, Volume 9, Pages s235-s320, DOI 10.1080/1755876X.2016.1273446.

Ward, J.H., 1963. Hierarchical grouping to optimize an objective function. Journal of the American Statistical Association, 58 (301), 236-244, DOI 10.1080/01621459.1963.10500845.

Wilks, D. S., 2006. Statistical Methods in the Atmospheric Sciences, second ed. Academic Press, London.

Wiltshire, K.H., Malzahn, A.M., Wirtz, K., Greve, W., Janisch, S., Mangelsdorf, P., Manly, B.F.J., Boersma, M., 2008. Resilience of North Sea phytoplankton spring bloom dynamics: An analysis of long-term data at Helgoland Roads. Limnology and Oceanography, Volume 53, Issue, 4, Pages 1294-1302, DOI 10.4319/lo.2008.53.4.1294

Wilsthire, K.H., Manly, B.F.J., 2004. The warming trend at Helgoland Roads, North Sea: phytoplankton response. Helgoland Marine Research, Volume 58, Issue 4, Pages 269-273, DOI 10.1007/s10152-004-0196-0.

Winder, M., Cloern, J.E., 2010. The annual cycles of phytoplankton biomass. Philosophical Transactions of the Royal Society B-Biological Sciences, 365, 3215-3226, DOI 10.1098/rstb.2010.0125.

Wolter, K., Timlin, M. S., 2011. El Niño/Southern Oscillation behaviour since 1871 as diagnosed in an extended multivariate ENSO index (MEI.ext). International Journal of Climatology, Volume 31, Issue 7, Pages 1074-1087, DOI 10.1002/joc.2336.

Wood S.N., 2006. Generalized additive models: an introduction with R. Chapman & Hall/CRC, Boca Raton.

Xu, Y., Ishizaka, J., Yamaguchi, H., Siswanto, E., Wang, S., 2013. Relationships of interannual variability in SST and phytoplankton blooms with giantjellyfish (Nemopilema nomurai) outbreaks in the Yellow Sea and East China Sea. Journal of Oceanography, Volume 69, Issue 5, Pages 511-526, DOI 10.1007/s10872-013-0189-1

Yamada, K., Ishizaka, J., 2006. Estimation of interdecadal change of spring bloom timing, in the case of the Japan Sea. Geophysical Research Letters, Volume 33, L02608, DOI 10.1029/2005GL024792

Yoo, S., Batchelder, H.P., Peterson, W.T., Sydeman, W.J., 2008. Seasonal, interannual and event scale variation in North Pacific ecosystems. Progress in Oceanography, Volume 77, Pages 155-181, DOI 10.1016/j.pocean.2008.03.013

Zarubin, M., Lindermann, Y., Genin, A., 2017. The dispersion-confinement mechanism: Phytoplankton dynamics and the spring bloom in a deeply-mixing subtropical sea. Progress in Oceanography, Volume 155, Pages 13-27, DOI 10.1016/j.pocean.2017.05.005

Zhai, L., Platt, T., Tang, C., Sathyendranath, S., Walls, R.H., 2011. Phytoplankton phenology on the Scotian Shelf. ICES Journal of Marine Science, Volume 68, Issue 4, Pages 781-791, DOI 10.1093/icesjms/fsq175

Zhai, L., Platt, T., Tang, C., Sathyendranath, S., Walne, A., 2013. The response of phytoplankton to climate variability associated with the North Atlantic Oscillation. Deep-Sea Research II, Volume 93, Pages 159-168, DOI 10.1016/j.dsr2.2013.04.009

Zhang, H.-M., Bates, J.J., Reynolds, R.W., 2006. Assessment of composite global sampling: Sea surface wind speed. Geophysical Research Letters, Volume 33, L17714, DOI 10.1029/2006GL027086.

Zhang, M., Zhang, Y., Qiao, F., Deng, J., Wang, G., 2017. Shifting trends in bimodal phytoplankton blooms in the North Pacific and North Atlantic Oceans from space with the Holo-Hilbert spectral analysis. Journal of Selected Topics in Applied Earth Observations and Remote Sensing, Volume 10, Issue 1, Pages 57-64, DOI 10.1109/JSTARS.2016.2625813

Zhao, H., Han, G., Wang, D., 2013. Timing and magnitude of spring bloom and effects of physical environments over the Grand Banks of Newfoundland. Journal of Geophysical Research Biogeosciences, Volume 118, Pages 1385-1396, DOI 10.1002/jgrg.20102

Highlights:

- Phytoplankton phenology is derived from ocean colour remote sensing imagery
- Phenological indices are used for an unsupervised partition of the surface ocean
- Region-specific phenology patterns and environmental drivers are evaluated

Patterns and drivers of phytoplankton phenology off SW Iberia: a phenoregion based perspective

Lilian Anne Krug[a *], Trevor Platt [b], Shubha Sathyendranath[c], Ana B. Barbosa[a]

Electronic supplementary material

Table S1- Summary of results from the generalized additive mixed models (GAMM) used to model interannual variability for SW Oceanic, Oceanic, Coastal-Slope and River-influenced phenoregions off South West Iberia Peninsula (1997 - 2015). Information includes model adjusted coefficient of determination (R^2_a), equivalent to total explained deviance, parametric coefficients (intercept ± 1 Standard Error), estimated degrees of freedom (edf) and approximate significance level (p-value) for the model covariates. Smoothing functions are referred to as s(Month/Time). Values of edf equal to 1 imply a linear effect and values higher than 1 indicate progressively stronger nonlinear effects. Symbols ', *, **, *** indicate p-value <0.10, <0.05, <0.01 and <0.001, respectively.

SW Oceanic phenoregion		
Duration of principal bloom event		
Intercept	**SE**	**p-value**
20.944	0.2167	$<2e^{-16}$ ***
Smooth terms	**Edf**	**p-value**
s (Year)	6.710	0.06'
		$R^2_{adj.}$ = 0.54; n = 18
Duration of principal bloom accumulation phase		
Intercept	**SE**	**p-value**
14.678	0.2018	$3.4e^{-16}$***
Smooth terms	**Edf**	**p-value**
s (Year)	5.927	$9.34e^{-5}$ ***
		$R^2_{adj.}$ = 0.42; n = 18
Principal bloom timing of peak		
Intercept	**SE**	**p-value**
24.731	0.2477	$<2e^{-16}$ ***
Smooth terms	**edf**	**p-value**
s (Year)	5.091	$7.75e^{-4}$***
		$R^2_{adj.}$ = 0.41; n = 18
Coastal-Slope phenoregion		
Total duration of bloom events		
Intercept	**SE**	**p-value**
23.160	0.7017	$3.8e^{-16}$***
Smooth terms	**edf**	**p-value**
s (Year)	1.000	0.09'
		$R^2_{adj.}$ = 0.12; n = 18
Duration of principal bloom event		
Intercept	**SE**	**p-value**
13.708	1.021	$3.95e^{-10}$***
Smooth terms	**edf**	**p-value**
s (Year)	1.000	0.06'
		$R^2_{adj.}$ = 0.10; n = 18

Upwelling-influenced phenoregion		
Duration of principal bloom deceleration phase		
Intercept	**SE**	**p-value**
3.993	0.350	$4.26e^{-9}$***
Smooth terms	**edf**	**p-value**
s (Year)	1.000	$9.02e^{-4}$***
		$R^2_{adj.}$ = 0.22; n = 18
River-influenced phenoregion		
Total duration of bloom events		
Intercept	**SE**	**p-value**
21.8910	0.5499	$2.27e^{-16}$ ***
Smooth terms	**edf**	**p-value**
s (Year)	2.317	0.07'
		$R^2_{adj.}$ = 0.32; n =18
Principal bloom timing of initiation		
Intercept	**SE**	**p-value**
12.048	1.583	$1.05e^{-6}$ ***
Smooth terms	**edf**	**p-value**
s (Year)	1.000	0.09'
		$R^2_{adj.}$ = 0.12; n = 18
Principal bloom timing of peak		
Intercept	**SE**	**p-value**
16.798	1.355	$2.5e^{-9}$***
Smooth terms	**Edf**	**p-value**
s (Year)	1.872	0.03*
		$R^2_{adj.}$ = 0.26; n = 18
Principal bloom timing of termination		
Intercept	**SE**	**p-value**
23.445	1.705	$2.78e^{-10}$ ***
Smooth terms	**Edf**	**p-value**
s (Year)	1.00	0.06'
		$R^2_{adj.}$ = 0.04; n = 18

Table S2 – Summary results of the best-performing generalized additive models (GAM) used to model region-specific phenological indices off SW Iberia (period: 1997 - 2015) as a function of multiple environmental covariates (predictors). Note that only statistically significant covariates were retained in the models. Information includes: model adjusted coefficient of determination (R^2_{adj}), equivalent to total explained deviance; Akaike's Information Criteria (AIC); parametric coefficients (intercept ± 1 Standard Error); and estimated degrees of freedom (edf) and approximate significance level (p-value) for the model covariates.

Smoothing functions are referred to as s(i), where i indicates the covariates including large-scale climate indices (NAO – North Atlantic Oscillation; AMO – Atlantic Multidecadal Oscillation; EA – Eastern Atlantic Pattern; MEI – Multivariate ENSO Index; WeMO – Western Mediterranean Oscillation), local hydrodynamic variables (CSET - cross shore Ekman transport off the western Portuguese coast; Gdn – Guadiana river discharge; Gdq – Guadalquivir river discharge), MLD_Y – annual average of mixed layer depth; MLD_{Max} – maximum annual value of mixed layer depth, and average environmental conditions preceding the initiation of the principal bloom for MLD – mixed layer depth; PAR – surface photosynthetically available radiation; NO_3 – nitrate concentration averaged within the first layer; SST – sea surface temperature; W – wind speed; V – meridional wind speed. Subscripts Y, W and S associated to predictors indicate annual, winter and upwelling-season (May-September) averages, respectively. Symbols ‘, *, **, *** indicate p-value <0.10, <0.05, <0.01 and <0.001, respectively.

SW Oceanic phenoregion

Ch-a peak value

Intercept	SE	p-value
0.4092	0.0117	$3.55e^{-6}$***
Smooth terms	**edf**	**p-value**
s (EA_W)	1.426	0.009**
s (MLD_{Max})	2.528	0.036*
s (NO_3)	1.000	0.018*
s (V)	3.000	0.078‘

$R^2_{adj.}$ = 0.90; AIC = -40.71; n = 13

Principal bloom duration

Intercept	SE	p-value
20.9231	0.2003	$6.03e^{-14}$***
Smooth terms	**edf**	**p-value**
s (AMO_Y)	1.000	0.004**
s (MEI_Y)	1.916	0.031*
s (NO_3)	1.000	0.048*

$R^2_{adj.}$ = 0.63; AIC = 34.08; n = 13

Principal bloom timing of initiation

Intercept	SE	p-value
11.0556	0.1008	$<2e^{-16}$***
Smooth terms	**edf**	**p-value**
s (PAR)	2.160	0.032*

$R^2_{adj.}$ = 0.38; AIC = 25.36; n = 18

Principal bloom peak timing

Intercept	SE	p-value
24.6667	0.3061	$<2e^{-16}$***
Smooth terms	**edf**	**p-value**
s (SST)	2.902	0.002**
s (W)	1.000	0.046*

$R^2_{adj.}$ = 0.70; AIC = 66.58; n = 18

Oceanic phenoregion

Ch-a peak value

Intercept	SE	p-value
0.5623	0.020	$7.14e^{-9}$***
Smooth terms	**edf**	**p-value**
s (EA_W)	2.256	0.006**
s (NO_3)	2.053	0.011*

$R^2_{adj.}$ = 0.86; AIC = -24.42; n = 13

Principal bloom duration

Intercept	SE	p-value
19.7692	0.1648	$5.74e^{-13}$***
Smooth terms	**edf**	**p-value**
s (NO_3)	2.819	0.007**
s (MLD)	2.107	0.062‘

$R^2_{adj.}$ = 0.95; AIC = 29.29; n = 13

Principal bloom timing of initiation

Intercept	SE	p-value
12.7692	0.1667	$5.81e^{-12}$***
Smooth terms	**edf**	**p-value**
s (NO_3)	2.874	$57.62e^{-9}$***
s (MLD)	1.000	0.007**
s (EA_Y)	1.000	0.023*

$R^2_{adj.}$ = 0.98; AIC = 29.54; n = 13

Principal bloom peak timing

Intercept	SE	p-value
25.0000	0.2107	$8.84e^{-15}$***
Smooth terms	**edf**	**p-value**
s (MLD_W)	8.644	0.004**

$R^2_{adj.}$ = 0.77; AIC = 54.52; n = 18

Coastal-Slope phenoregion

Number of blooms per year

Intercept	SE	p-value
3.500	0.2347	$5.27e^{-10}$***
Smooth terms	**edf**	**p-value**
s (W)	1.000	0.006**
s (NAO_W)	1.956	0.045*

$R^2_{adj.}$ = 0.58; AIC = 56.38; n = 18

Ch-a peak value

Intercept	SE	p-value
0.8944	0.0235	$5.56e^{-13}$***
Smooth terms	**edf**	**p-value**
s (NAO_Y)	1.000	0.006**
s (Gdn_W)	1.000	0.009**
s (W)	2.058	0.061‘

$R^2_{adj.}$ = 0.73; AIC = -24.24; n = 16

Principal bloom duration – M1

Intercept	SE	p-value
13.7778	0.7469	$2.03e^{-11}$***
Smooth terms	**edf**	**p-value**
s (SST)	1.606	0.002**
s (W)	1.000	0.004**

$R^2_{adj.}$ = 0.65; AIC = 10.04; n = 18

Principal bloom duration – M2

Intercept	SE	p-value
13.7778	0.6998	$4e^{-12}$***
Smooth terms	**edf**	**p-value**
s (Initiation)	2.008	$6.47e^{-5}$***

$R^2_{adj.}$ = 0.69; AIC = 94.98; n = 18

Principal bloom timing of initiation

Intercept	SE	p-value
20.2780	1.391	$2.89e^{-10}$***
Smooth terms	**edf**	**p-value**
s (NAO_Y)	1.000	0.031*
s (W)	1.000	0.040*

$R^2_{adj.}$ = 0.47; AIC = 119.70; n = 18

Principal bloom peak timing

Intercept	SE	p-value
24.0556	0.5936	$9.42e^{-11}$***
Smooth terms	**Edf**	**p-value**
s (W)	8.786	$2e^{-4}$***

$R^2_{adj.}$ = 0.86; AIC = 91.78; n = 18

Upwelling-influenced phenoregion

Number of blooms per year

Intercept	SE	p-value
4.3889	0.1547	$1.69e^{-12}$***
Smooth terms	**Edf**	**p-value**
s (MLD_Y)	1.000	0.001**
s (V)	1.000	0.003**
s (SST)	2.821	0.006**

$R^2_{adj.}$ = 0.83; AIC = 42.52; n = 18

Ch-a peak value

Intercept	SE	p-value
1.1550	0.0289	$1.31e^{-13}$***
Smooth terms	**Edf**	**p-value**
s (MLD_Y)	2.823	$7.86e^{-4}$***
s (SST)	1.765	0.003**
s ($CSET_S$)	1.000	0.009**

$R^2_{adj.}$ = 0.73; AIC = --17.34; n = 18

Principal bloom duration

Intercept	SE	p-value
8.3333	0.6652	$6.32e^{-9}$***
Smooth terms	**edf**	**p-value**
s ($CSET_Y$)	2.195	0.011*
s (SST)	1.000	0.011*

$R^2_{adj.}$ = 0.57; AIC = 94.05; n = 18

Principal bloom timing of initiation

Intercept	SE	p-value
27.0000	1.753	$1.2e^{-10}$***
Smooth terms	**edf**	**p-value**
s ($CSET_Y$)	1.892	0.037*

$R^2_{adj.}$ = 0.30; AIC = 127.95; n = 18

Principal bloom peak timing

Intercept	SE	p-value
31.389	1.669	$1.74e^{-11}$***
Smooth terms	**edf**	**p-value**
s ($CSET_Y$)	2.702	0.015*

$R^2_{adj.}$ = 0.50; AIC = 126.80; n = 18

River-Influenced phenoregion

Number of blooms per year

Intercept	SE	p-value
3.5294	0.1729	$1.07e^{-8}$***
Smooth terms	**edf**	**p-value**
s (NAO_W)	1.000	$2.78e^{-4}$***
s (Gdn_Y)	2.423	0.012*
s (MLD_Y)	1.000	0.045*
s ($WeMO_W$)	1.000	0.072’

$R^2_{adj.}$ = 0.79; AIC = 43.9; n = 17

Ch-a peak value

Intercept	SE	p-value
2.3824	0.1091	$9.31e^{-12}$***
Smooth terms	**edf**	**p-value**
s (Gdq_W)	1.7870	0.006**
s (PAR)	1.000	0.038*

$R^2_{adj.}$ = 0.71; AIC = 26.4; n = 17

Principal bloom duration

Intercept	SE	p-value
12.7647	0.5643	$4.84e^{-10}$***
Smooth terms	**edf**	**p-value**
s (Gdq_W)	2.815	$1.04e^{-4}$***
s (MLD_Y)	3.000	0.009**

$R^2_{adj.}$ = 0.83; AIC = 83.88; n = 17

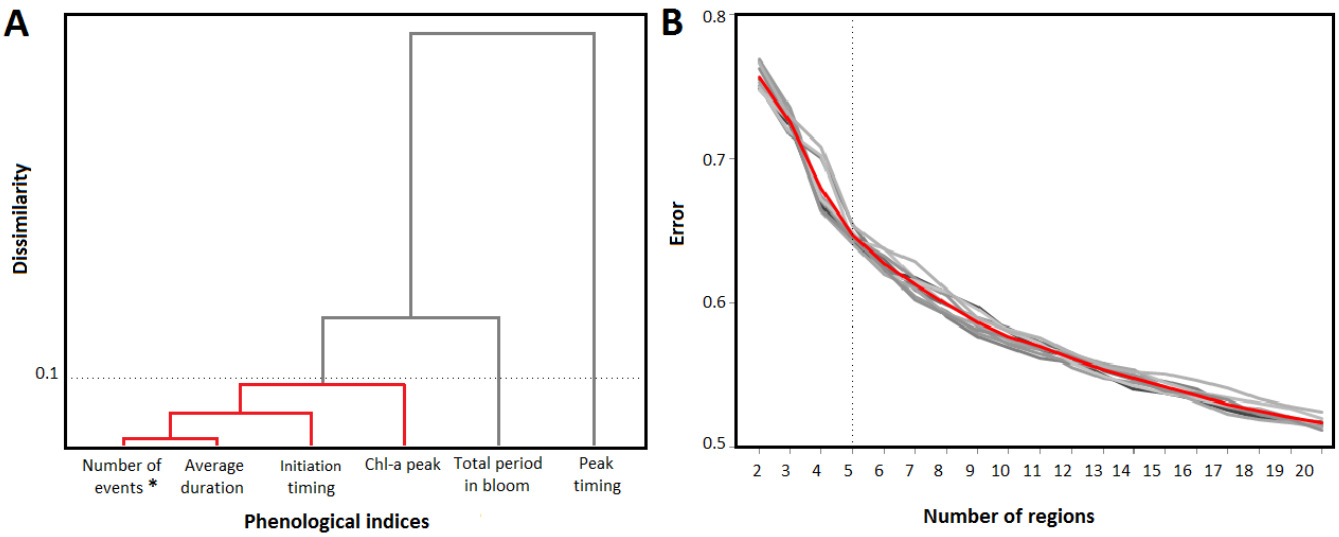

Figure S1 – A) Dissimilarity analysis based on phenological indices averages off SW Iberia, during the 1997-2015 period. Red nodes indicate the group with dissimilarity values below the defined threshold (0.1), and the asterisk symbol denotes the index selected to represent it. B) Average error (red line) of cross-validations (grey lines) as a function of number of regions and the vertical dashed line indicate the threshold defining the optimal number of regions.

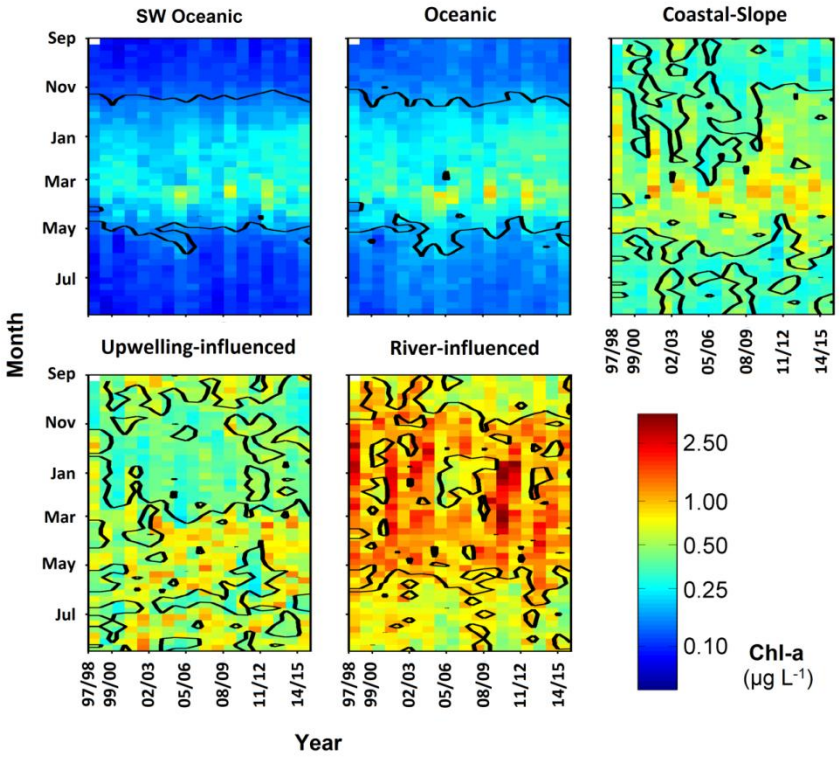

Figure S2 – Weekly Chl-a values for each phenological region between 1997 and 2015. Black lines represent the annual threshold limit and periods delimited represent a bloom situation (see Fig. 4 for region location).

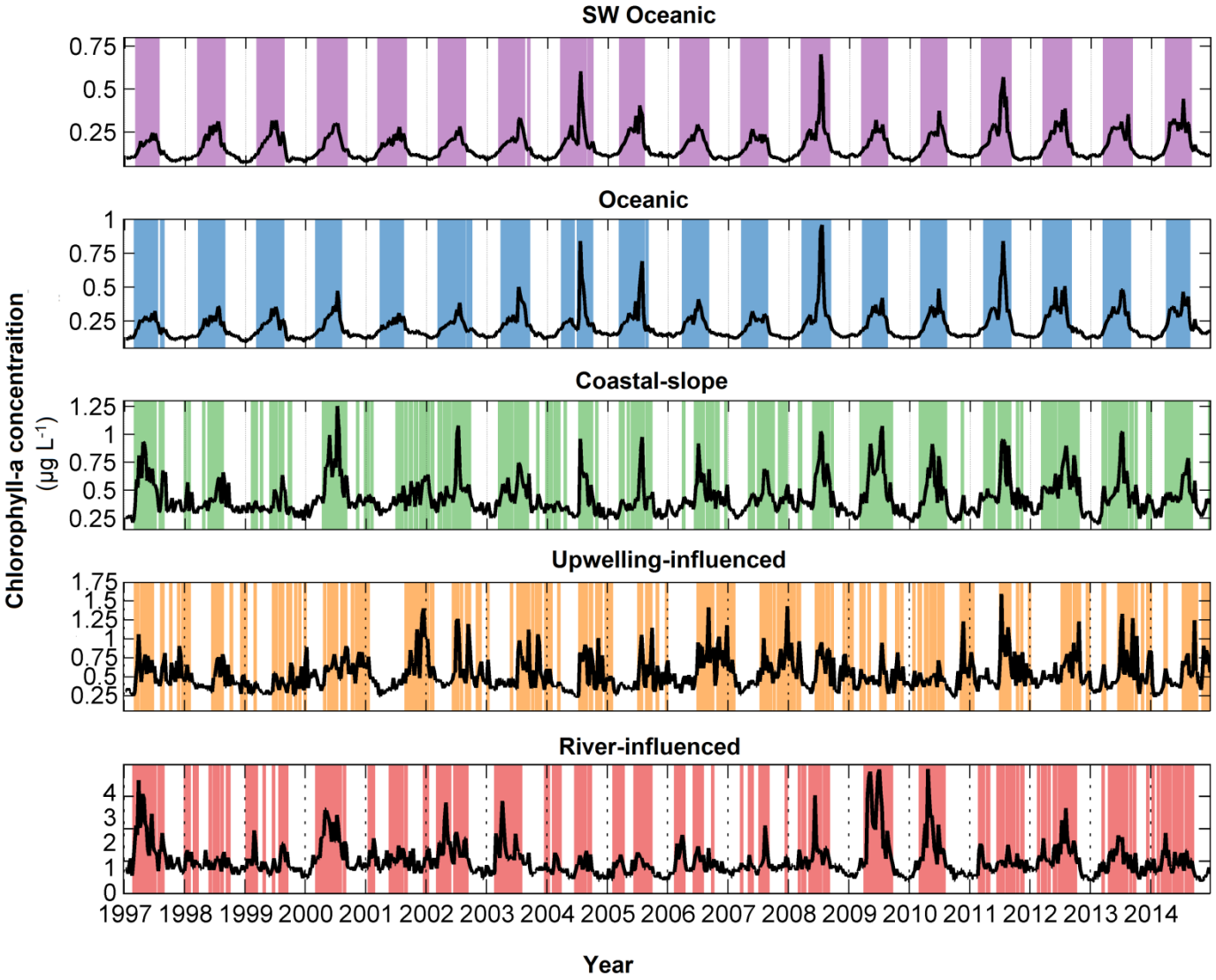

Figure S3 - Time series of chlorophyll-a (Chl-a; black lines; note different y-scales) and bloom periods (coloured-shaded columns) for each phenoregion off SW Iberian Peninsula (see Fig. 4 for region location and colour code). Vertical dashed lines indicate the first week of September of the respective year.

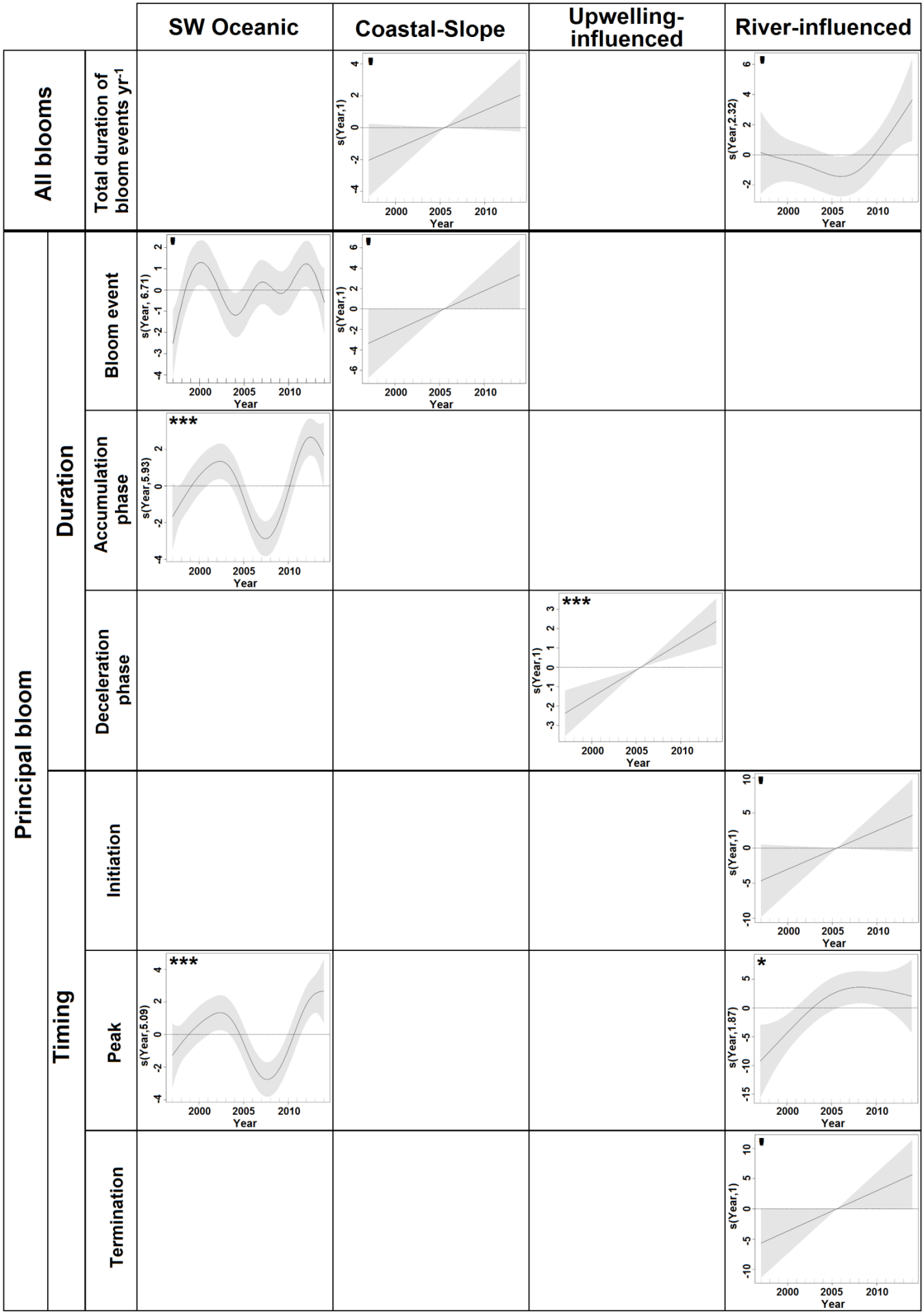

Figure S4 - Partial effects of significant interannual variability (expressed as year) of the SW Oceanic, Coastal-Slope, Upwelling and River-influenced phenoregions off Southwest Iberia Peninsula (period: 1997-2015; see Fig. 4 for region location), derived from generalized additive mixed models (GAMMs). Model explanatory power (as % explained variance) is shown on the top left

with the significance level (p-value; in parenthesis) of the predictor (year), denoted by asterisk symbols, where ‘, *, **, *** indicate p-value <0.10, 0.05, <0.01 and <0.001, respectively. For each plot, years are represented on the x-axis, while values on the y-axis represent the partial effects of the specific predictor. Numbers in parentheses on the y-axis represent the effective degrees of freedom (edf), indicative of the smoothness of each function; values of edf equal to 1 represent a linear effect of the predictor, and values higher than 1 indicate progressively stronger non-linear effects. Solid lines indicate the smoothed non-parametric trends, and grey shaded areas designate the point-wise 95% confidence intervals. Regions where the 95% CI bands enclose the x-axis line indicate no significant effects of the prediction (see Table S1 for detailed statistics).

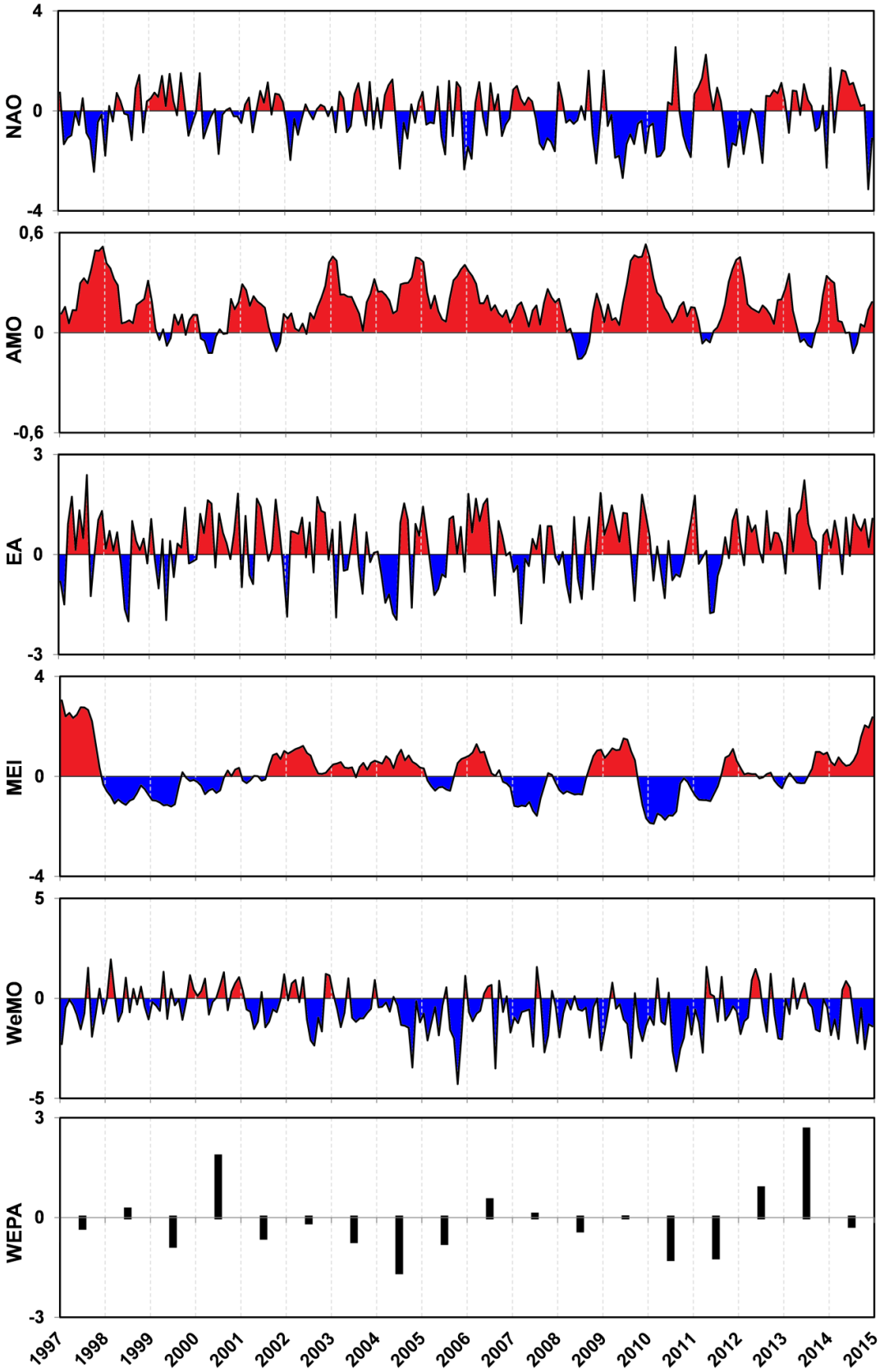

Figure S5– Temporal variability of climate indices during the period 1997 to 2015 based on monthly values of North Atlantic Oscillation index (NAO); Atlantic Multidecadal Oscillation index (AMO); East Atlantic pattern index (EA); Multivariate ENSO

Index (MEI); Western Mediterranean Oscillation index (WeMO) and winter-averaged (December-March) West Europe Pressure Anomaly (WEPA). Vertical dashed lines signalize the month of September of the respective year.

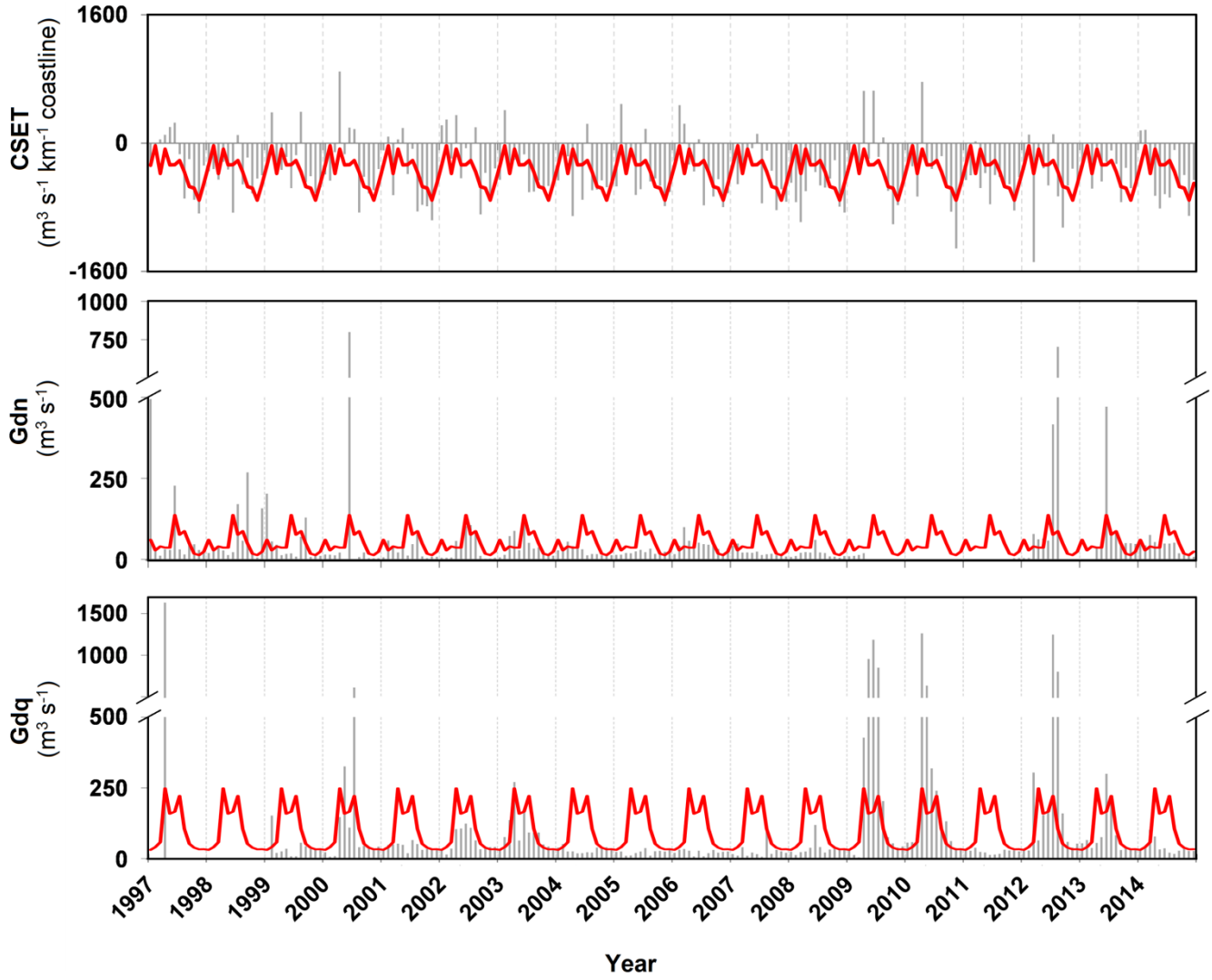

Figure S6 - Temporal variability of upwelling intensity and river discharge over the southwest area off the Iberian Peninsula (SWIP), during the period 1997 to 2015. Cross-shore Ekman transport, a wind-based upwelling index, for the west Portuguese coast (CSET); negative (positive) values indicate upwelling-favourable (upwelling-unfavourable) conditions. Guadiana (Gdn) and Guadalquivir (Gdq) river discharge. Red lines represent monthly climatologies for the study period and grey vertical dashed lines signalize the month of September of the respective year